LBNL-38839
UC-401

Lawrence Berkeley Laboratory

UNIVERSITY OF CALIFORNIA

CHEMICAL SCIENCES DIVISION

Reaction Mechanism Studies of Unsaturated Molecules Using Photofragment Translational Spectroscopy

C.A. Longfellow
(Ph.D. Thesis)

May 1996

Prepared for the U.S. Department of Energy under Contract Number DE-AC03-76SF00098

LBNL-38839
UC-401

Reaction Mechanism Studies of Unsaturated Molecules Using Photofragment Translational Spectroscopy

Cheryl Ann Longfellow
Ph.D. Thesis

Department of Chemistry
University of California, Berkeley

and

Chemical Sciences Division
Ernest Orlando Lawrence Berkeley National Laboratory
University of California
Berkeley, California 94720

May 1996

This work was supported by the Director, Office of Energy Research, Office of Basic Energy Sciences, Chemical Sciences Division, of the U.S. Department of Energy under Contract No. DE-AC03-76SF00098.

Reaction Mechanism Studies of Unsaturated Molecules Using Photofragment Translational Spectroscopy

by

Cheryl Ann Longfellow

B.S. (Lewis and Clark College) 1991

A thesis submitted in partial satisfaction of the requirements for the degree of

Doctor of Philosophy

in

Chemistry

in the

GRADUATE DIVISION

of the

UNIVERSITY of CALIFORNIA at BERKELEY

Committee in charge:

Professor Yuan T. Lee, Chair
Professor Daniel M. Neumark
Professor Y. Ron Shen

1996

Abstract

Reaction Mechanism Studies of Unsaturated Molecules Using Photofragment Translational Spectroscopy

by

Cheryl Ann Longfellow

Doctor of Philosophy in Chemistry

University of California, Berkeley

Professor Yuan T. Lee, Chair

A number of molecules have been studied using the technique of photofragment translational spectroscopy. In Chapter One a brief introduction to the experimental technique is given. The focus is on the type of information that can be obtained, which includes product identities, translational energy distributions, and angular distributions, and how this information can be used to predict reaction mechanisms. The relevance of these studies to bulk experiments is also addressed.

In Chapter Two the infrared multiphoton dissociation (IRMPD) of acetic acid is discussed. Carbon dioxide and methane were observed for the first time as products from dissociation under collisionless conditions. The product translational energy distribution peaks well away from zero, which supports a four-center transition state. A previously observed channel, resulting in the formation of water and ketene, was verified. With a laser fluence of 12 J/cm^2, decarboxylation accounts for roughly 35% of the total dissociation yield.

Chapter Three relates an IRMPD experiment of hexafluoropropene. Two primary channels and one secondary channel were identified. The predominant channel produces $CFCF_3$ or C_2F_4 and CF_2, with the heavier species undergoing further dissociation to two CF_2 fragments. A number of dissociation mechanisms are proposed for the elimination of CF_2, including direct cleavage of the carbon-carbon double bond. In the second primary channel, a simple bond rupture reaction produces CF_3 and C_2F_3. The activation energy for this simple bond rupture is estimated to be 100-105 kcal/mol. The branching ratio between the two primary pathways is 4.0 ± 1.0.

In Chapter Four the ultraviolet (UV) dissociation of hexafluoropropene is investigated. At 193 nm one primary channel results in the loss of a fluorine atom; from the maximum translational energy release, a value of 121 kcal/mol was found for the C-F bond dissociation energy. The two other channels are CF_2 and CF_3 loss as observed in the IRMPD experiments. A simultaneous excitation to two electronic states is suggested based on the observed anisotropy parameters. It is proposed that one electronic state results in F atom and C_3F_5 formation, while the other electronic state undergoes rapid internal conversion to produce the ground state products CF_3, C_2F_3, CF_2, and C_2F_4.

Chapter Five explores the IRMPD of octafluoro-1-butene and octafluoro-2-butene. The predominant reaction in octafluoro-1-butene at moderate laser fluences is cleavage of a carbon-carbon single bond to give the products CF_3 and C_3F_5. In octafluoro-2-butene CF_2 loss and cleavage of the carbon-carbon double bond compete with CF_3 loss. A branching ratio, CF_3:CF_2:C_2F_4, of 1.0:0.8:0.6 is found at a fluence of 60 J/cm^2. Dissociation of octafluoro-1-butene to the resonance stabilized perfluoroallyl radical is

suggested to account for the observation of signal at much lower fluences than in octafluoro-2-butene.

Table of Contents

Acknowledgments

I first met Prof. Yuan T. Lee as a perspective graduate student. His enthusiasm for science certainly influenced my decision to come to Berkeley, and I have never regretted that choice. Over the years I have been continually amazed at his chemical knowledge and intuition. Five minutes with him will change your whole outlook on your experiment. His suggestions on everything from which molecules to study to detector electronics settings to fits to the data were all exceptionally helpful. In addition, I am exceedingly grateful to him for the opportunity to undertake experiments in Taiwan. A major plus of this six month stay was that I was able to discuss my experiments with Yuan almost every week; I believe this accelerated my graduation date greatly.

My first exposure to molecular beam machines, lasers, and all the trimmings came from working with Simon North on the B machine. He was a patient teacher and I enjoyed working on the azomethane experiments with him. The wealth of experience in the Lee group in the form of other graduate students was very beneficial later on in my graduate career. Arthur Suits, our group leader in Yuan's absence, suggested many useful experimental improvements and was always willing to take the time to discuss the latest results. Tzong-Tsong Miau knows these machines like very few people do. I can distinctly remember a few times where I should have talked with him before cutting a certain wire or struggling with interference effects; I would have saved myself a lot of grief. He is also an excellent cook and good friend. Hongtao Hou was always around and willing to offer sound advice. His constant good cheer in spite of any difficulty was an inspiration to me. I've enjoyed the last year I've spent working with Cindy Berrie on

the rotating source machine. I wish her much continued success with the acetone and hexafluoroacetone experiments.

Doo Wan Boo was helpful when I began to set up the CO_2 laser that had not been used in our group for a couple years. Jim Myers and Floyd Davis always did their best to answer any questions I had and continued to do so via e-mail once they had graduated. James Chesko's wild enthusiasm for any and every project led to some interesting and fruitful discussions. Dr. Mimmo Stranges introduced me to the Berkeley rotating source machine. The succession of post-docs I shared my office with from Albert Stolow and Deon Anex to Jinchun Xie and K. T. Lu were always kind enough to discuss any subject. I especially want to thank Lu for the work she did calculating minimum energy pathways for various fluorocarbons. Her work forced me to think seriously about various aspects of our experiment.

The support our group receives from the machine shop here is unparalleled. Chuck Gemmell and later Eric Granlund made sure we received all our requested pieces in a timely manner. The intricate machining of Hans Graetsch was always appreciated as was the friendliness and helpfulness of Bob Dunn. Tom Lawhead in the glass shop was always sure to fix our bubblers with a smile. These people, along with those in the electronics shop and the wood shop, made our experiments possible. I truly felt bereft when our group secretary, Ann Lawhead, left. She was a good source of useful information and had a way of ensuring that our purchase requests would make it through the LBL bureaucracy. I've appreciated the competent and friendly help of Daina Tekorius and Marian Grebanier in the last few years.

I owe an enormous debt of gratitude to Prof. S. M. Lin at the Institute of Atomic and Molecular Sciences in Taipei, Taiwan. He was generous enough to offer two graduate students, Laura Smoliar and myself, six months of experimental time on his rotating source machine. Plus he put himself, his post-doc, and an assistant at our disposal to help in any way they could. I value the time I spent in his lab greatly. I learned much about Chinese customs and culture; plus, the stay resulted in the experiments described in Chapters 3 and 4. I was constantly in awe of Dr. Ya-Rong Lee, the post-doc, who managed a one year old child, a 2-3 hour commute, and was an excellent experimentalist. The assistant, Chen-Ying Yeh, was an invaluable help during the experiments and translated for us when we had to talk with various bureaucrats. She also took me on a daring ride through the streets of Taipei on a scooter in search of chocolate. Visit Taipei, you'll understand why it was daring. The Institute had a very good machinist, Mr. Hou, who amazingly enough spoke English. Prof. Lee's secretary, Mrs. Shaw, helped us in many ways, including always scheduling us in to visit with Yuan even when various political bigwigs wanted to meet with him. The time that I spent working with Laura Smoliar was extremely productive. I admire her experimental know-how and willingness to work hard. Prof. Fanao Kong of the Institute of Chemistry in China was kind enough to invite us to visit his lab in Beijing. The interconnectedness of the international science community never fails to amaze me.

Michael Morgen helped to keep me sane during much of my time spent here at Berkeley. Besides proofreading my thesis (the whole thing!), he also kept me from being

too much of a stick-in-the-mud. I had great fun on our adventures. Warning - don't ever forget to drink water if you hike down into the Grand Canyon in July.

After a horrible and boring high school chemistry class I decided to "get it out of the way" early in college. My advisor at Lewis and Clark College, Dr. Janis Lochner, is responsible for peaking my interest and encouraging me to continue with chemistry. The challenges of quantum as taught by Dr. Richard Bettega convinced me that I wanted to be a physical chemist. I appreciate the love and support of my family. My mother's return to school after having four kids to earn a bachelors and an MBA has always seemed a tremendous accomplishment to me. My belief in the importance of education stems from that time. I will be happy, however, that the annual Christmas question, "Are you still in school?" can finally be answered in the negative.

Chapter One

Laser Induced Dissociations

1.1. Introduction to Experimental Techniques

Early chemical kinetics experiments were often extremely difficult to interpret because of the secondary collisions which occurred. These collisions obscured the identity of the primary products; especially radical species, which could rapidly react with any other species present in these bulk experiments. In addition, using heat or a Hg lamp to decompose molecules limited the amount of quantitative information that could be obtained. These complications have decreased with the widespread use of vacuum chambers, molecular beam sources, and lasers which allow elegant studies of single molecule-single molecule or single molecule-photon reactions. The availability of these techniques has spurred the growth of the extensive field of molecular reaction dynamics. This field is complementary to the study of macroscopic kinetics events, but focused on quantities such as exit barriers on potential energy surfaces, transition state structures and lifetimes, and energy deposition in the products. In this chapter a brief introduction to the technique of photofragment translation spectroscopy is given along with a short summary of the types of molecules investigated using this technique.

1.1.1. Photofragment Translational Spectroscopy

The first photofragment translational spectroscopy experiments were performed by Wilson and co-workers.[1] In these experiments a molecular beam source intersected a 1 Hz ultraviolet (UV) laser at 90°. Detection of the products was performed with a

quadrupole mass spectrometer located only a few centimeters from the interaction region. The advantage of a molecular beam is that it produces molecules that are internally cold and have relatively monoenergetic (5-10% spread) translational energy distributions. Once the molecular beam has expanded into the vacuum region, interactions within the beam do not take place. By crossing this molecular beam with a laser the products of dissociation can be detected without the occurrence of secondary reactions. The use of the quadrupole mass spectrometer as the detector allows the detection of any product produced.

The second generation molecular beam machines included a rotatable detector.[2] This allowed angular distributions of all the product fragments to be collected. In a photodissociation experiment the angular distribution gives information on the polarization dependence of a molecule, allowing predictions of the electric dipole direction, the lifetimes of the highly excited intermediate species, and reaction mechanisms. A machine built in this lab and subsequently copied in many other laboratories contains a rotatable source and a fixed detector.[3] All of the experiments in this thesis were carried out on this type of rotating source machine, the schematic of which is shown in Figure 1-1.

Besides obtaining the mass and angular distribution of the products it is also possible to obtain their translational energy distribution. This is done as a function of the time it takes the fragments to travel from the interaction region to the detector (a distance of 36.7 cm). The detector consists of a Brink type ionizer[4], quadrupole mass spectrometer, Daly type detector[5] and a photomultiplier tube. The flight time of the ion through the detector

is subtracted to give the flight time of the neutral fragment from the interaction region to the ionizer. As this distance is accurately known, the velocity and therefore the translational energy of the fragments can be obtained. The translational energy is a measure of the energy disposal in the products and can lend insight into the dynamics of the dissociation.

1.1.2. Infrared Multiphoton Dissociation

The technique of infrared multiphoton dissociation (IRMPD) has been used quite extensively in the past 20 years to investigate molecular dissociation. IRMPD was sparked by the development of high powered CO_2 lasers, specifically TEA or Transversely Excited Atmospheric pressure lasers.[6] The possibility of infrared photons inducing dissociations was first discussed in the early 1970's.[7] In 1975 two groups used infrared lasers to demonstrate isotopic selection on SF_6.[8] It is interesting to note that these papers (one Russian and one American) appeared only months apart during the height of the Cold War. It is almost certain that the real interest in this technique was not in separating isotopes of SF_6.

Initially, it was suggested that IRMPD actually bypassed the normal thermal decomposition pathways. The suggestion of mode selective behavior caused great excitement in the chemistry community. The idea was proposed that different products could be obtained depending on which vibrational mode was excited. A noted example was the decomposition of SF_6 to SF_4 and F_2 instead of the lowest thermodynamically allowed pathway of $SF_5 + F$.[9] Detailed experimental work in our lab and confirmed by Zare's group at Stanford showed these results were wrong.[10] The mechanism of infrared

multiphoton absorption has now been extensively detailed.[11] IRMPD is selective for the initial absorption of photons, and this allows for its isotopic selectivity A molecule must have an absorption at the wavelength used, although both power broadening and rotational excitation can increase the absorption probability of these first few photons. Absorption in the discrete states is followed by absorption through the quasicontinuum. It is in the quasicontinuum where energy is randomized among all the modes, destroying the possibility of mode selective chemistry. Further absorption of photons results in excitation into the continuum. From there competition between further excitation and decomposition takes place.

The vibrational population distribution created by infrared multiphoton excitation is not identical to a thermal heating process.[12] Essentially the distribution of the IR excited molecule is slightly narrower. When IMRPD is coupled with photofragment translation spectroscopy, the primary processes of a thermal decomposition can be unraveled without the secondary collisions commonly found in a typical bulb experiment. A number of molecules have been investigated in this manner, including SF_6,[10] CH_3NO_2,[13] and RDX.[14] Typically reactions which do not involve exit barriers can be described using the well-known Rice-Ramsperger-Kassel-Marcus (RRKM) statistical theory.[15] It is possible to obtain activation energies from photofragment translational energy experiments by using RRKM theory and modeling the IRMPD process.[16] This will be discussed in more detail in Chapter Three.

1.1.3. UV Photolysis

The use of an UV laser coupled with photofragment translational spectroscopy has some useful applications. First, as opposed to an IR laser, it is possible to access excited electronic states and probe their dissociation products. Also, because a known amount of energy (193 nm or 248 kcal/mol using an ArF excimer laser) is placed in the molecule via a one-photon process, it is possible to obtain bond dissociation energies. Equation 1-1 represents how conservation of energy is used to find a bond dissociation energy.

$$E_{int}(\text{reactant}) + E_{h\nu} = D^{o} + E_{T} + E_{int}(\text{products}) \qquad (1\text{-}1)$$

This will be discussed further in Chapter 4.

It is also possible to investigate the effects of the laser polarization on the angular distribution. These effects are described by the electric dipole expression[17] given in Equation 1-2.

$$I(\theta) = (1/4\pi)[1 + \beta P_2(\cos\theta)] \qquad (1\text{-}2)$$

The β parameter ranges from 2 to -1 predicting either a parallel or perpendicular dissociation, respectively. A pure parallel dissociation can result when the electric vector of the laser light lies along the electric dipole of the molecule and the fragments recoil axially. Observation of a strong anisotropy effect indicates dissociation from a repulsive electronic surface and a lifetime less than the rotational period of the parent molecule. A slight polarization effect, β equals 0.4 rather than 2, indicates possible predissociation and/or a longer lived intermediate. A null polarization effect could indicate that internal

conversion to the ground state followed by dissociation occurs, although a more complicated excitation scheme is possible.

An example of using UV excitation to probe the lifetime of a dissociating complex is the photolysis of azomethane at 351 nm.[18] No evidence of the methyl diazenyl intermediate was observed (reaction 1-3). However, the methyl time-of-flight spectrum indicated the presence of two different types of methyl radicals.

$$CH_3N_2CH_3 \rightarrow CH_3N_2 + CH_3 \rightarrow 2CH_3 + N_2 \qquad (1\text{-}3)$$

In this case no laser polarization effect was observed, but it was necessary to use an anisotropic secondary angular distribution to explain the reaction products. Because of this anisotropic secondary angular distribution, a limiting lifetime could be placed on the methyl diazenyl radical of less than 1 ps. This was in stark contrast to earlier work where a 5 ns lifetime was suggested.[19]

1.2. Molecules of Interest

Section 1.1 of this thesis has served to reiterate the powers of the photofragment translational spectroscopy technique which have been discussed in many previous papers.[20] There are a few limitations to this technique which should be mentioned. The background counts at certain masses (N_2, CO_2, H_2O) is quite high. The background counts from nitrogen, the most abundant background species, is typically 1×10^5 counts/second. Because of this high background long hours of signal averaging may be necessary if this happens to be the mass of interest. Extensive fragmentation of products in the electron impact ionizer can lead to many products appearing at the same mass. For

example, C_3F_6 can fragment to C_3F_5, C_3F_4, C_2F_4, CF_3, CF_2 and other species. This limitation can be overcome by using the Advanced Light Source as a tunable VUV ionization source. In addition, although it is possible to obtain the partitioning between translation and internal energy the partitioning between vibration and rotation can not be examined.

There exists the possibility to study many molecules by either IRMPD or UV photodissociation. This has caused an explosion of such experiments in the past 20 years. Many molecules have been investigated more than once, including azomethane,[18,19] acetone,[21,22] OClO,[23,24] and acetylene[3,25] to mention a few. Obviously, although dissociation experiments can be readily attempted, interpretations of experimental results can lead to widely different results. In the next few sections the motivation behind the investigations undertaken in this thesis will be given.

1.2.1. Acetic Acid

The decomposition of acetic acid has been extensively studied since the 1960's. Even with a multitude of published experiments some questions remain about its dissociation process. The products observed in pyrolysis and in previous IRMPD experiments are not the same. Based on the theory of multiphoton absorption discussed in Section 1.1.2 the products from IRMPD and pyrolysis should be the same. Pyrolysis experiments observe competition between dehydration and decarboxylation while the IMRPD experiments observe only dehydration. In Chapter Two the discrepancies between these two types of experiments will be addressed.

1.2.2. Fluorocarbons

The following fluorocarbons were investigated: hexafluoropropene, perfluoro-1-butene and perfluoro-2-butene. The interest in these compounds stems initially from the explosive polymerization and decomposition of C_2F_4, which in the absence of air, results in the formation of CF_4 and carbon.[26] As this reaction cannot be unimolecular, it was suggested that recombination followed by dissociation can explain the presence of CF_4. Figure 1-2 shows a possible reaction pathway whereby two C_2F_4 molecules could recombine and lead to the formation of higher molecular weight fluorocarbons. The elimination of CF_4 from a higher molecular weight fluorocarbon is then possible, providing the activation energy is not much greater for this process than for other decomposition processes.

Although hexafluoropropene had been previously investigated using IRMPD, these earlier experiments were performed in a photolysis cell where collisions could hinder the observation of the primary products. The reinvestigation of hexafluoropropene reported in Chapter Three concentrated on measuring all the primary products of the dissociation process. Hexafluoropropene also has a reasonable absorption cross section at 193 nm and Chapter Four discusses its UV dissociation. These experiments present the possibility to obtain previously unknown bond dissociation energies.

Prior to the study described in Chapter Five no experimental IRMPD work has been done on either octafluoro-1-butene or octafluoro-2-butene. Primarily these species have been identified as products in tetrafluoroethylene pyrolysis. These IRMPD experiments

represent the first effort to fully understand the dissociation pathways of these perfluorobutenes. Although these molecules test the limits of photofragment translational spectroscopy owing to their size and extensive fragmentation, Chapter Five discusses the various dissociation pathways observed.

References and Notes

[1] G. E. Busch, R. T. Mahoney, R. I. Morse, and K. R. Wilson, J. Chem. Phys. **51**, 449 (1969) and G. Hancock and K. R. Wilson, in Proceedings, IVth International Symposium on Molecular Beams, Cannes, France, 1973.

[2] Y. T. Lee, J. D. McDonald, P. R. LeBreton, and D. R. Herschbach, Rev. Sci. Instrum. **40**, 1402 (1969).

[3] A. M. Wodtke and Y. T. Lee, J. Phys. Chem. **89**, 4744 (1985).

[4] G. O. Brink, Rev. Sci. Instrum. **37**, 857 (1966).

[5] N. R. Daly, Rev. Sci. Instrum. **31**, 264 (1960).

[6] J. A. Beaulieu, App. Phys. Lett. **16**, 504 (1970).

[7] N. R. Isenor and M. C. Richardson, App. Phy. Lett. **18**, 224 (1971).

[8] R. V. Ambartsumyan, Y. A. Gorokhov, V. S. Letokhov, and G. N. Makarov, JETP Lett. **21**, 171 (1975); J. L. Lyman, R. J. Jensen, J. Rink, C. P. Robinson, and S. D. Rockwood, App. Phys. Lett. **27**, 87 (1975).

[9] K. L. Kompa, In *Tunable Lasers and Applications*, A. Mooradian, T. Jaeger and P. Stokseth, Eds; Berlin: Springer; pp 177-89; 1976.

[10] M. J. Coggiola, P. A. Schulz, Y. T. Lee, and Y. R. Shen, Phy. Rev. Lett, **38**, 17 (1977); G. J. Diebold, F. Engelke, D. M. Lubman, J. C. Whitehead, and R. N. Zare, J.Chem. Phys. **67**, 6408 (1977).

[11] P. A. Schulz, Aa. Sudbo, D. J. Krajnovich, H. S. Kwok, Y. R. Shen, and Y. T. Lee, Ann. Rev. Phys. Chem. **30**, 379 (1979) and references therein.

[12] E. R. Grant, P. A. Schulz, Aa. S. Sudbo, Y. R. Shen, and Y. T. Lee, Phy. Rev. Let. **40**, 115 (1978).

[13] A. M. Wodtke, E. J. Hintsa, and Y. T. Lee, J. Chem. Phys. **84**, 1044 (1986).

[14] X. Zhao, E. J. Hintsa, and Y. T. Lee, J. Chem. Phys. **88**, 801 (1988).

[15] P. J. Robinson and K. A. Holbrook, *Unimolecular Reactions*; Wiley: London, 1972; W. Forst, *Theory of Unimolecular Reactions*; Academic Press: New York, 1973.

[16] A. M. Wodtke, E. J. Hintsa, and Y. T. Lee, J. Phys. Chem. **90**, 3459 (1986); E. J. Hintsa, A. M. Wodtke, and Y. T. Lee, J. Phys. Chem. **92**, 5379 (1988).

[17] R. N. Zare, Mol. Photochem. **4**, 1 (1972).

[18] S. W. North, C. A. Longfellow, and Y. T. Lee, J. Chem. Phys. **99**, 4423 (1993).

[19] B. K. Andrews, K. A. Burton, and R. B. Weisman, J. Chem. Phys. **96**, 1111 (1992).

[20] A. M. Wodtke and Y. T. Lee, In *Advances in Gas Phase Photochemistry and Kinetics*, M. N. R. Ashfold and J. E. Baggott, Eds.; Royal Society of Chemistry: London; 1987.

[21] S. W. North, D. A. Blank, J. D. Gezelter, C. A. Longfellow, and Y. T. Lee, J. Chem. Phys., **102**, 4447 (1995).

[22] K. A. Trentelman, S. H. Kable, D. B. Moss, and P. L. Houston, J. Chem. Phys. **91**, 7498 (1989).

[23] H. F. Davis and Y. T. Lee, J. Phys. Chem. **96**, 5681 (1992).

[24] E. Bishenden, J. Haddock, and D. J. Donaldson, J. Phys. Chem. **95**, 2113 (1991).

[25] B. A. Balko, J. Zhang, and Y. T. Lee, J. Chem. Phys. **94**, 7958 (1991).

[26] Y. I . Babenko, Y. A. Lisochkin, and U. I. Poznyak, Combustion Explosion and Shock Waves **29**, 603 (1993).

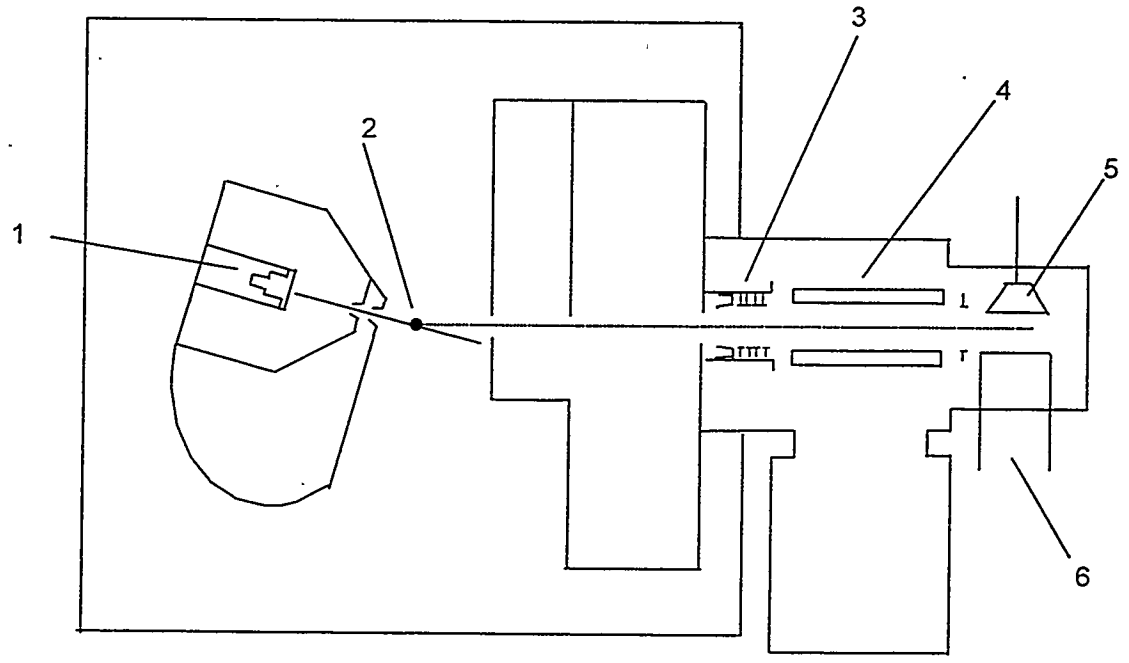

Figure 1-1. The rotating source machine. (1) Pulsed valve source. (2) Interaction region. (3) Electron impact ionizer and focusing elements. (4) Quadrupole mass filter. (5) Daly doorknob. (6) Photomultiplier tube.

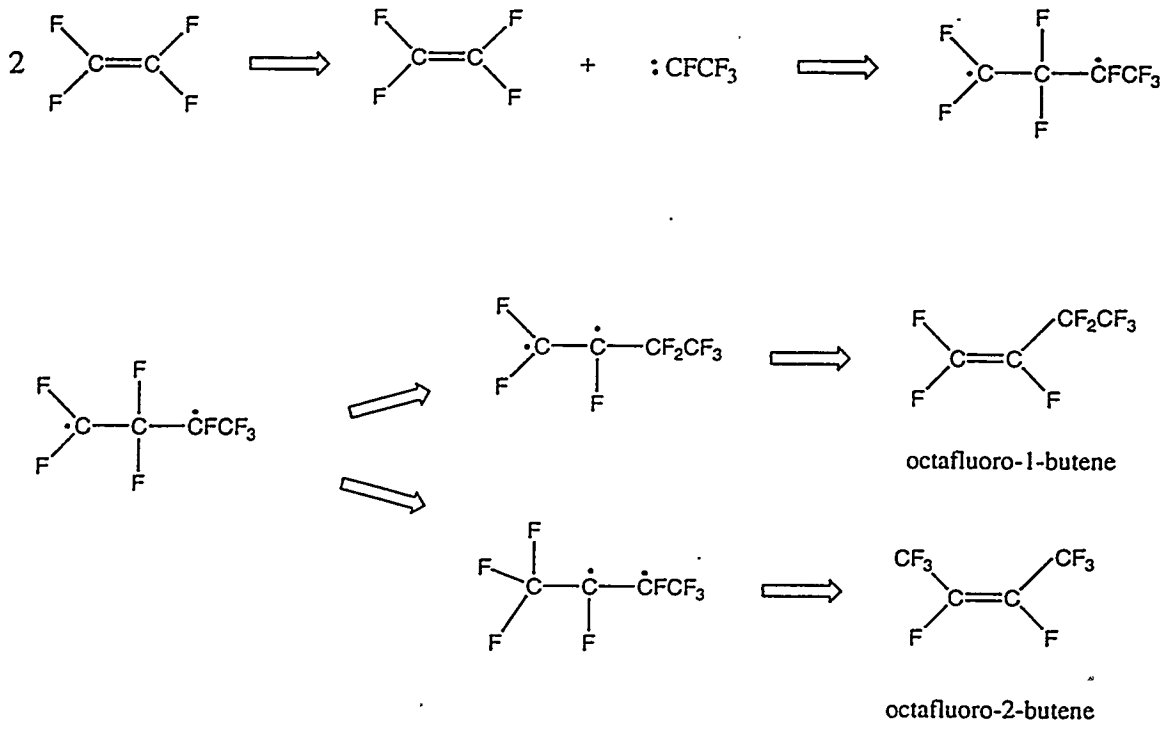

Figure 1-2. Reaction mechanism scheme for the formation of a perfluorobutene from two tetrafluoroethylene molecules. One tetrafluoroethylene molecule must have a fluorine migration to form a carbene which can then add to a tetrafluoroethylene double bond. Depending on the direction of a second fluorine migration either octafluoro-1-butene or octafluoro-2-butene can be formed.

Chapter Two

Methane Loss in the Infrared Multiphoton Dissociation of Acetic Acid

2.1. Introduction

It is well-known that the deposition of a large amount of energy in a polyatomic molecule can lead to unimolecular reactions. The thermal decomposition of many molecules has been successfully described by statistical theories such as RRKM.[1] However, to reiterate the points made in Chapter 1, results from thermal experiments are often difficult to interpret owing to multiple collisions, which can lead to further reactions and obscure the true primary products. By using molecular beam techniques with laser excitation these complications can be eliminated. Extensive experiments have shown that the primary products in an infrared multiphoton dissociation (IRMPD) experiment are identical to those in a thermal decomposition.[2] The absorption of multiple infrared photons results in highly vibrationally excited molecules, wherein intramolecular vibrational redistribution (IVR) takes place rapidly before dissociation occurs. In this manner it is possible to study "thermal" decompositions under collision free conditions.

Insight into the dissociation dynamics of a reaction can be obtained by directly measuring the translational energy release of the products. Translational energy distributions for a simple bond rupture reaction will typically peak at zero while in the case of a concerted reaction with an exit barrier the distribution will be peaked away from zero. For simple bond rupture reactions it is straightforward to extend RRKM theory to predict the translational energy distributions based on the available excess energy.[3] Far more interesting dynamics are exhibited by those reactions in which an exit barrier is involved and the translational energy distributions cannot be readily predicted using RRKM theory. For example, a transition state structure can be proposed or confirmed based on the shape of the translational energy distribution. Also, in these reactions the

partitioning between product kinetic energy and internal excitation will lend insight to the type of repulsion being felt by the products. As is shown in Figure 2-1,[4] the decomposition of acetic acid offers the prospect of observing direct competition between two such channels.

Early studies investigating the thermal decomposition of acetic acid identified two molecular elimination pathways:[5,6]

$$CH_3COOH \rightarrow CH_4 + CO_2 \qquad (2\text{-}1)$$

$$CH_3COOH \rightarrow CH_2CO + H_2O \qquad (2\text{-}2)$$

A shock tube study suggests the products of reaction 2-1 and reaction 2-2 are produced in approximately equal amounts.[7] Identical activation energies and A factors were obtained for the two reactions. A more recent shock tube study found that at lower acetic acid densities reaction 2-2 begins to dominate.[8] The activation energies measured in the above-mentioned experiments range from 62 - 72.5 kcal/mol for reaction 2-1 and 65 - 72.5 kcal/mol for reaction 2-2, as shown in Figure 2-1.

With the availability of high power, pulsed CO_2 lasers, IRMPD studies of acetic acid have become feasible. An initial study in a photolysis cell used laser induced fluorescence (LIF) as the detection technique.[9] The results of this experiment suggest that the dehydration of acetic acid (2-2) competes with the simple bond rupture reaction (2-3) which produces hydroxyl and acetyl radicals.

$$CH_3COOH \rightarrow CH_3CO + OH \qquad (2\text{-}3)$$

The fluences used in this experiment were on the order of 40 J/cm^2. Another experiment, using comparable fluences, investigated the decomposition of acetic acid produced initially from the IRMPD of acetic anhydride.[10] The formation of CH_3, detected by VUV photoionization, was attributed to the decomposition of acetyl radical formed in the simple bond rupture reaction (2-3). This was the only channel observed which could be assigned unambiguously to acetic acid decomposition. In this research group the secondary dissociation of acetic acid, produced from the IRMPD of ethyl acetate, was

investigated with photofragment translational spectroscopy.[11,12] Using a fluence of 40 J/cm^2, the decomposition of ethyl acetate resulted in 97% formation of acetic acid and ethylene. Two-thirds of the acetic acid then underwent secondary decomposition to give the products ketene and water with a large translational energy release averaging 23.7 kcal/mole. No other species were identified as decomposition products of acetic acid.

Besides the extensive experimental work, there have been a number of theoretical studies on acetic acid decomposition. It is the transition states of the decarboxylation (2-1) and dehydration (2-2) reactions that have been the focus of theoretical work as the interpretation of the simple bond rupture reaction (2-3) is expected to be quite straightforward. The transition states for reactions 2-1 and 2-2 were first proposed by Blake and co-workers.[6] Figure 2-2a shows the four-center transition state in the decarboxylation reaction (2-1). It involves the transfer of a hydrogen atom to an already saturated carbon, and this results in a highly unusual pentavalent carbon atom. Conversely, the dehydration four-center transition state, Figure 2-2b, resulting in the transfer of a methyl hydrogen atom to an oxygen atom, does not require expanded valences.

Initial calculations[13] associated with the transition states shown in Figures 2-2a and 2-2b found activation energies of 77.3 kcal/mole (decarboxylation) and 76.0 kcal/mole (dehydration). These calculations were later found to be flawed and an alternative dissociation mechanism involving a rearrangement to 1,1-dihydroxyethylene (2-4) followed by a concerted elimination (2-5) to give the products ketene and water was proposed.[14]

$$CH_3COOH \rightarrow CH_2C(OH)_2 \qquad (2\text{-}4)$$

$$CH_2C(OH)_2 \rightarrow CH_2CO + H_2O \qquad (2\text{-}5)$$

This transition state is shown in Figure 2-2c and differs from the originally proposed transition state in that a hydrogen is now being transferred between two oxygen atoms. A second group performed ab initio MO calculations to investigate the plausibility of the

transition states suggested in Figures 2a and 2c.[15] Activation energies of 77.7 kcal/mole and 86.0 kcal/mole were found for reactions 2-1 and 2-4. The second step in the dehydration (2-5) was found to be exothermic and therefore does not contribute to the overall activation energy of this reaction. Very recent calculations found the activation energies of reactions 2-1, 2-2 and 2-4 to be 71.8, 76.4 and 73.1 kcal/mole, respectively.[16]

Both theoretical and experimental studies agree that dehydration occurs in the thermal unimolecular decomposition of acetic acid, although the exact mechanism is presently uncertain. Whereas the decarboxylation reaction (2-1) was observed in bulk experimental studies, it was not identified in any of the IRMPD studies. In addition, the transition state involving a pentavalent carbon atom has been questioned (Figure 2-2a), leading to the reinterpretation of one of the shock tube studies.[17] It was found that a methyl radical chain reaction can satisfactorily explain the formation of methane. The 107 kcal/mole[18] needed for acetic acid to undergo simple bond rupture is significantly higher than the experimentally determined activation energies for the dehydration and decarboxylation pathways. However, this channel was observed in one of the IRMPD studies.

As the activation energies of the two channels are similar, both the decarboxylation and the dehydration channels should occur. In practice, however, the two products of the decarboxylation channel, carbon dioxide and methane, are often difficult to detect. Because one of the IRMPD studies used LIF as its detection method it was not sensitive to these two molecular products.[9] In the study by Welge and co-workers the VUV at 118 nm was below the photoionization threshold for both CO_2 and CH_4.[10] In the previous photofragment translational spectroscopy experiment in this laboratory the occurrence of a second primary channel in ethyl acetate decomposition could have obscured these products.[11]

The most recent theoretical studies mentioned above predict that the decarboxylation channel has the lowest activation energy. It should be of some concern to

experimentalists and theorists alike that this reaction has not been observed in IRMPD studies. The present study of the primary decomposition of acetic acid was undertaken to resolve whether decarboxylation is a primary dissociation channel, and if it can effectively compete with dehydration and simple bond rupture channels.

2.2. Experimental Section

These experiments were primarily performed on a rotating source molecular beam machine which has been described in Chapter One of this thesis. Briefly, helium was bubbled through glacial acetic acid at room temperature and passed through a pulsed valve[19] with a .020" diameter nozzle, operating at 20 Hz. Since acetic acid at standard conditions is 97% in its dimer form,[20] heating of the nozzle was required. In order to heat the piezoelectric pulsed valve, the tip was water cooled and a copper extension with an orifice of 0.040" was electrically heated with thermocoaxial wire. This source is shown in Figure 2-3. The design of this source allows it to fit in a key such as commonly used on a fixed source rotating detector machine. Initial acetic acid IRMPD experiments on the B-machine and the observation of extensive dimer formation led to the development of this source.

The optimum nozzle temperature at which signal owing to dimer dissociation could be suppressed and the acetic acid dissociation signal observed was 340 - 350°C. A stagnation pressure of 635 torr was used to create a supersonic expansion of approximately 5% acetic acid in He. The molecular beam had a mean velocity of 2050 m/s and a full width at half-maximum (FWHM) spread of 10%. The velocity distribution of molecules in the pulsed beam was measured using standard time-of-flight techniques with a spinning slotted wheel.[21]

The molecular beam was collimated with one skimmer resulting in an angular divergence on the order of 4 degrees. With a second skimmer in place the signal-to-noise ratio was significantly decreased and no additional structure resolved. A Lumonics TEA-

820 pulsed CO_2 laser was tuned to the R(20) line of the 9.6-μm branch (1079 cm^{-1}) and crossed the molecular beam at the interaction region. The laser beam was focused to a 2 × 2.5 mm^2 spot resulting in a laser fluence of 12 J/cm^2. The fragments created by IRMPD traveled 36.7 cm to the detector, which consisted of the standard electron impact ionizer, quadrupole mass filter and Daly type ion detector as shown in Figure 1-1. A multichannel scaler triggered by the laser collected the ion counts as a function of flight time from the interaction region to the detector.

2.3. Results and Analysis

Measurements were taken at detector to source angles of 20, 30, 40, and 50 degrees. The IRMPD mass spectrum of acetic acid at 20° is shown in Table 2-1. Dissociation signal was observed at m/e ratios 44, 42-40, 29-28, and 18-13. Laser correlated dissociation signal was observed at the parent masses of the CO_2 (m/e = 44) and CH_2CO (m/e = 42) products. This is unambiguous evidence of the decarboxylation (2-1) and dehydration (2-2) reactions. No signal was observed at m/e = 43, CH_3CO, indicating the simple bond rupture reaction (2-3) is not taking place under these conditions. Additionally, at m/e = 17, OH, only the fragmentation of H_2O caused by electron bombardment in the ionizer is observed.

The resulting data from acetic acid was analyzed using standard forward convolution techniques.[22] A center-of-mass translational energy distribution is assumed and yields a simulated time-of-flight spectrum in the lab frame, which is averaged over apparatus functions, such as the ionizer width. This spectrum is then compared to the experimental time-of-flight spectrum, and the translational energy distribution is modified until the two match. In principle, for each dissociation channel it is necessary to measure only one of the dissociating fragments to obtain the center-of-mass translational energy distribution. The corresponding velocity of the other fragment is obtained using the conservation of linear momentum. In practice the time-of-flight spectra of all fragments are measured

and the conservation of linear momentum is used to identify which products belong to the same channel.

2.3.1. Decarboxylation Channel. This channel, leading to CO_2 and CH_4, has not been observed previously from dissociation under collisionless conditions. The time-of-flight data at m/e = 44 and m/e = 15 at 20° and 40° are shown in Figure 2-4. These time-of-flight spectra are unambiguous evidence that in the unimolecular decomposition of acetic acid decarboxylation occurs. The dissociation signal for methane is measured at m/e = 15 due to the interference of water from the dehydration channel which can also fragment to m/e = 16. By tuning the quadrupole mass filter to m/e = 15, methane can be observed without any such interference.

The second, slower peak in the m/e = 15 spectra does not momentum match to any other species observed. It is attributed to the dissociation of residual dimers or higher order clusters in the molecular beam. In order to decrease the signal due to acetic acid dimers the source was heated. Table 2-2 shows the ratio of the dimer to monomer signal at three temperatures. The contribution to the methane (m/e =15) time-of-flight spectra from monomer and dimer (slow peak) dissociation signal at a lab angle of 20° are compared. As the acetic acid source nozzle temperature is increased, the cluster signal becomes less intense relative to the monomer dissociation signal. Since the dimer signal does not overlap with the relevant dissociation signal, further efforts to increase the source temperature and completely eliminate the dimers were not taken.

Figure 2-5a shows the center-of-mass translational energy distribution for this channel. It is derived from the momentum matched fragments at m/e = 15 and m/e = 44, and has an average translational energy release of 26.4 ± 2 kcal/mole that peaks at 25 kcal/mole. This large translational energy release, E_{max} ~ 50 kcal/mole, indicates a significant exit barrier as previously suggested by thermal studies.[5-8]

2.3.2. Dehydration Channel. As expected the signal at m/e 18 (H_2O) is momentum matched to that at m/e = 42 (CH_2CO) providing further evidence of reaction 2-2. The

time-of-flight spectra obtained from m/e = 42 and m/e = 18 at 20° and 40° are shown in Figure 2-6. The resulting center-of-mass translational energy distribution, shown in Fig. 2-5b, has an average translational energy release of 18.7 ± 2 kcal/mole, peaked at 17 kcal/mole. These products has been observed previously in the secondary decomposition of ethyl acetate.[11] In that study an average translational energy release of 23.7 kcal/mole peaked at 25 kcal/mole was obtained. The results from a secondary dissociation are inherently less certain than from a primary dissociation experiment owing to the necessity of extensive averaging over both the beam velocity distribution and the primary translational energy distribution.[22] That the average translational energy release in the primary dissociation is lower than the previous results is not surprising. Acetic acid formed in the dissociation of ethyl acetate is internally hot. Therefore, subsequent dissociation of acetic acid occurs from a higher range of internal energy levels than in the primary dissociation study.

2.3.3. Branching ratio.[23] Of fundamental chemical interest is the relative ratio of the dissociation products produced. In order to calculate the branching ratio the relative yield for each product is determined by summing over all parent and daughter masses and dividing by the total yield. The ionization cross section for each fragment is taken into account to give the relative yield of each fragment. The difficulties in determining ionization cross sections are discussed in detail elsewhere.[24] Here we use the relatively straightforward method of Fitch and Sauter[25] to obtain the ionization cross sections. The uncertainties in the ionization cross section values obtained by this method may be as high as 25%.[24]

The branching ratio, $[CO_2]/[H_2O]$, is 0.54 ± 0.1. A major portion of the uncertainty results from predicting the ionization cross sections. Furthermore, as illustrated in Table 1, it is not possible to assign the dissociation signal at m/e = 28 unambiguously. This is because CO, m/e = 28, can result from either CH_2CO or CO_2 fragmenting in the ionizer. The resolution in this experiment is not high enough to separate these two processes.

This same difficulty is encountered again at m/e = 16 where the water and methane signal is indistinguishable. Although the uncertainty in the branching ratio is large, the emphasis should be on the significant amount of methane and carbon dioxide products that are observed, roughly 35%, under collisionless conditions.

2.4. Discussion

In this experiment the decarboxylation channel (2-1), has been shown to occur under collisionless conditions. This substantiates the results of thermal experiments[5-8] and verifies that decarboxylation is a primary decomposition product in the unimolecular dissociation of acetic acid. Competition between the decarboxylation channel and the dehydration channel (2-2) was observed. A comparison of the translational energy releases in these two reactions should help elucidate the dissociation dynamics occurring. The simple bond rupture reaction (2-3) was not detected.

2.4.1. Methane Production. Questions have been raised as to whether CH_4 is produced in the unimolecular primary decomposition of acetic acid. The only previous experiments which observed the decarboxylation channel of acetic acid were performed under conditions in which collisions might obscure the results. In addition, the pentavalent carbon transition state (Figure 2-2a) was not readily accepted as high activation energies must be involved when the carbon valence shell is expanded.[26] One study proposed that the CH_3 radical is produced and then participates in a chain reaction to produce methane.[17] It has not been possible until now to definitively attribute the formation of methane to a unimolecular decomposition. Also, the translational energy distribution obtained in the present experiment supports this unusual pentavalent transition state. In this transition state a hydrogen migration from an oxygen atom to a fully saturated carbon takes place. Although intramolecular hydrogen shifts have been readily observed under collisionless conditions,[11,27] these situations typically involve a more electronegative atom as the hydrogen receptor. The observation of the

decarboxylation of acetic acid is the first time, to our knowledge, that a hydrogen atom transfer has occurred from a more electronegative atom, oxygen, to a saturated carbon atom under collisionless conditions.

2.4.2. Translational Energy Release. The maximum translational energy released in these two primary decomposition channels lends insight into the nature of the transition states. The decarboxylation channel has a maximum of 50 kcal/mole released to translation while the dehydration channel shows a maximum of 40 kcal/mole. Since the heats of formation differ greatly with the dehydration products being higher in energy by 42.7 kcal/mole (see Figure 2-1), it might be expected that the maximum translational energy release of the decarboxylation channel would extend well beyond that of the dehydration channel. However, only a 10 kcal/mole difference is observed.

Although all the proposed transition states are similar in that they involve concerted four-center eliminations, the partitioning between internal and translational energy is not necessarily similar for the different transition states.[27] For example, in the case of the four-center HCl elimination from 1,1,1-trichloroethane, it is known that the transition state is extremely distorted and much of the excess energy becomes internal excitation as the products rearrange to their equilibrium bond lengths and angles.[28] In contrast, the three-center elimination of H_2 from formaldehyde leads to a much larger fraction of excess energy being converted to translational energy.[29] When the transition state geometry is closer to the geometry of the products, the repulsion between the two molecular products H_2 and CO leads to a large translational energy release.

These results imply that in the decarboxylation of acetic acid the structure of the transition state must be far away from the product equilibrium bond distances and angles, resulting in high internal excitation of the products. In the case of dehydration, it is the repulsion between the molecular products, H_2O and CH_2CO, which results in the large translational energy release. This interpretation of the maximum translational energy release was first suggested by reaction path calculations.[30] These calculations showed

that the energy partitioning is quite different for the two channels, with significant exit channel coupling between vibrational modes in the case of decarboxylation.

2.4.3. Dehydration Mechanism. Two dissociation mechanisms have been discussed for the dehydration reaction. Direct elimination of water from a four-center transition state, Figure 2-2b, analogous to the decarboxylation of acetic acid has been predicted by many groups.[6,8,11] The alternative dissociation mechanism proposes a rearrangement (2-4) followed by decomposition (2-5) from a different four-center transition state, Figure 2-2c.[14,15,16] In both cases the same products are formed through a concerted molecular elimination with a large exit barrier Similarly, both mechanisms would be expected to exhibit similar dynamics with a large translational energy release, as observed in this experiment. Therefore, our experiment does not provide any evidence as to which of the decomposition mechanisms is occurring.

2.4.4. Comparison with Previous Experiments. The decarboxylation channel was not observed in previous IRMPD experiments. This is in contrast to theoretical calculations which have predicted its existence and thermal experiments which have measured the products from this channel. This channel may not have been observed previously because of limitations in the detection schemes used as discussed earlier. Recent discussions over the observation of methane have led to a reexamination of the results from the secondary dissociation of ethyl acetate performed in our group.[31] In reference 11 the time-of-flight spectrum for m/e = 44 has an anomalous fast edge. This fast edge is now believed to be evidence for the decarboxylation channel from the secondary dissociation of acetic acid.

Another factor to consider is the high fluences used in the previous experiments (~40 J/cm^2), which may have played a role in obscuring this channel. In this experiment a relatively low fluence of 12 J/cm^2 was utilized. It is well-known that the fluence can affect the branching ratio when either the preexponential factors or activation energies of the two channels are different.[2] For example, in the IRMPD of CF_2Cl_2, the molecular

elimination of Cl_2 was seen to decrease within the relatively small fluence range of 0.3-8 J/cm^2 as compared to chlorine atom loss.[32] Because the decarboxylation channel was observed only at low laser fluences this suggests it has a lower activation energy as well as a lower A factor compared with the dehydration reaction. At higher fluences the decarboxylation channel may be produced with such a low yield that it is extremely difficult to detect the products, methane and carbon dioxide. Also, the low fluence used may explain why the simple bond rupture reaction was not observed.

The favoring of the dehydration channel, $[CO_2]/[H_2O] = 0.54$, found in the present work was also observed in a shock tube study.[8] In the shock tube study it was found that at low acetic acid densities the branching ratio decreased from 1 to 0.6. Theoretical branching ratios have been calculated showing the dehydration reaction is favored at higher temperatures owing to a larger A factor.[16] Transition state theory predicts a branching ratio of 1.6 at 900 K, while at 1500 K a value of 0.7 was determined. The higher temperature value is in reasonable agreement with our experimental results. In addition, a recent theoretical paper also predicts that the loss of water dominates by a factor ranging from 2 to 9.[33]

A very recent experimental paper has also examined the unimolecular decomposition of acetic acid.[34] The products of chemically activate acetic acid were detected by Fourier transform infrared (FTIR) spectroscopy. These experiments were performed in a fast flow reactor with 0.8 Torr of Ar gas. The products detected were H_2O and CO_2. Although these experiments were not performed under collisionless conditions, these molecular products from acetic acid decomposition should not react further. As infrared chemiluminescence is used to detect the products it is not possible to measure the ground state populations. Without correcting for the ground state populations the branching ratio, $[CO_2]/[H_2O]$, is approximately 1. However, owing to geometrical considerations, 80% of H_2O is thought to be in its ground vibrational state while only 50% of the CO_2 molecules are vibrationally unexcited. This leads to an estimate of the branching fraction

of the dehydration channel as ~ 2 times larger than the decarboxylation channel, $[CO_2]/H_2O] = 0.4$. This is in good agreement with our results, $[CO_2]/[H_2O] = 0.54$. Furthermore, these FTIR results predict that the decarboxylation channel leads to greater internal excitation as is also suggested by our measured translational energy release.

2.5. Conclusions

Observation of decarboxylation in the IRMPD of acetic acid confirmed it is a unimolecular process. The large translational energy release observed supports the existence of a strained transition state in which a hydrogen is transferred to a saturated carbon. Decarboxylation competes with dehydration and the branching ratio of 0.54, favoring dehydration, agrees with theoretical calculations. Despite the differences in the products' heats of formation similar maximum translational energy releases were obtained in both cases. This indicates that a higher percentage of available energy becomes internal excitation in the case of decarboxylation as compared to dehydration. Simple bond rupture does not compete with molecular elimination at the relatively low levels of excitation used in this experiment.

References and Notes

[1] P. J. Robinson and K. A. Holbrook, *Unimolecular Reactions*; Wiley: London, 1972; W. Forst, *Theory of Unimolecular Reactions*; Academic Press: New York, 1973.

[2] P. A. Schulz, Aa. S. Sudbo, D. J. Krajnovich, H. S. Kwok, Y. R. Shen, and Y. T. Lee, Ann. Rev. Phys. Chem. **30**, 379 (1979); Aa. S. Sudbo, P. A. Schulz, Y. R. Shen, and Y. T. Lee, In *Multiple-Photon Excitation and Dissociation of Polyatomic Molecules*, Cantrell, C. D. Ed., Springer-Verlag: Berlin; New York, 1986; Chapter 3.

[3] S. A. Safron, N. D. Weinstein, D. R. Herschbach, and J. C. Tully, Chem. Phys. Lett. **12**, 564 (1972).

[4] The heat of formations for these molecules at 298 K were obtained from the following sources: CH_3COOH: J. Chao and B. J. Zwolinski, J. Phys. Chem. Ref. Data, **7**, 363 (1978). CH_3CO: D. F. McMillan and D. M. Golden, Ann. Rev. Phys. Chem. **33**, 493 (1982). CH_2CO: S. W. Benson, *Thermochemical Kinetics*, 2nd ed.; Wiley: New York, 1976. OH, H_20, CH_4 and CO_2: D. R. Stull, and H. Prophet, *JANAF Thermochemical Tables*, Natl. Stand. Ref. Data Sr. U.S. Natl. Bur. Stand., **37**, U.S. Government Printing Office: Washington, D.C., 1971.

[5] C. H. Bamford and M. J. S. Dewar, J. Chem. Soc., 2877 (1949).

[6] P. G. Blake and G. E. Jackson, J. Chem. Soc.(B), 1153 (1968); P. G. Blake and G. E. Jackson, J. Chem. Soc.(B), 94 (1969).

[7] J. C. Mackie and K. R. Doolan, Int. J. Chem. Kin. **16**, 525 (1984).

[8] K. Saito, T. Sasaki, I. Yoshinobu, and A. Imamura, Chem. Phys. Lett. **170**, 385 (1990).

[9] A. J. Grimley and J. C. Stephenson, J. Chem. Phys. **74**, 447 (1981).

[10] D. Feldman, J. Laukemper, and K. H. Welge, J. Chem. Phys. **79**, 278 (1983).

[11] E. J. Hintsa, A. M. Wodtke, and Y. T. Lee, J. Phys. Chem. **92**, 5379 (1988).

[12] A. M. Wodtke and Y. T. Lee, In *Advances in Gas Phase Photochemistry and Kinetics*, M. N. R. Ashfold and J. E. Baggott, Eds.; Royal Society of Chemistry: London, 1987.

[13] P. Ruelle, Chem. Phys. **110**, 263 (1986).

[14] M. T. Nguyen and P. Ruelle, Chem. Phys. Lett. **138**, 486 (1987).

[15] J. F. Xie, J. G. Yu, W. L. Feng, R. Z. Liu, J. Mol. Struc. **201**, 249 (1989).

[16] X. Duan and M. Page, J. Am. Chem. Soc. **117**, 5114 (1995).

[17] K. R Doolan, J. C. Mackie, and C. R. Reid, *Int. J. Chem. Kin.* **18**, 575 (1986).

[18] A small barrier to this reaction has been suggested which would increase the activation energy necessary for decomposition. S. S. Hunnicutt, L. D. Waits, and J. A. Guest, J. Phys. Chem. **93**, 5188 (1989); J. Phys. Chem. **95**, 562 (1991).

[19] D. Proch and T. Trickl, Rev. Sci. Instrum. **60**, 713 (1989).

[20] J. Chao and B. J. Zwolinski, J. Phys. Chem. Ref. Data, **7**, 363 (1978).

[21] See, for example, B. A. Balko, Ph.D. Thesis, University of California, Berkeley (1991).

[22] A M. Wodtke, Ph.D. Thesis, University of California, Berkeley (1986); X. Zhao, Ph.D. Thesis, University of California, Berkeley (1988).

[23] Due to some modifications made to the CMLAB2 program it is relatively straightforward to obtain branching ratios. See J. D. Myers, Ph.D. Thesis, University of California, Berkeley (1993).

[24] A.-M. Schmoltner, Ph.D. Thesis, University of California, Berkeley (1989).

[25] W. L. Fitch and A. D. Sauter, Anal. Chem. **55**, 832 (1983).

[26] S. W. Benson, *Thermochemical Kinetics*, 2nd ed.; Wiley: New York, 1976; p. 169.

[27] A. M. Wodtke, E. J. Hintsa, and Y. T. Lee, J. Phys. Chem. **90**, 3459 (1986).

[28] Aa. S. Sudbo, P. A. Schulz, Y. R. Shen, and Y. T. Lee, J. Chem. Phys. **69**, 2312 (1978).

[29] P. Ho, D. J. Bamford, R. J. Buss, Y. T. Lee, and C. B. Moore, J. Chem. Phys. **76**, 3630 (1982).

[30] M. Page, North Dakota State University, Personal Communication.

[31] E. J. Hintsa, Atmospheric Research Project, Harvard University, Personal Communication.

[32] D. Krajnovich, F. Huisken, Z. Zhang, Y. R. Shen, and Y.T. Lee, J. Chem. Phys. **77**, 5977 (1982).

[33] M. T. Nguyen, D. Sengupta, G. Raspoet, L. G. Vanquickenborne, J. Phys. Chem. **99**, 11883 (1995).

[34] N. I. Butkovskaya, G. Manke, and D. W. Setser, J. Phys. Chem. **99**, 11115 (1995).

Table 2-1: Mass Spectrum of IRMPD Fragments of CH_3COOH

detected ion mass	identity of ion	neutral fragment	signal intensity[a]
44	CO_2^+	CO_2	0.091
42	CH_2CO^+	CH_2CO	0.148
41	$CHCO^+$	CH_2CO	0.097
40	CCO^+	CH_2CO	0.047
29	HCO^+	CH_2CO	0.037
28	CO^+	CO_2, CH_2CO	0.096
18	H_2O^+	H_2O	0.013
17	HO^+	H_2O	0.018
16	O^+, CH_4^+	H_2O, CH_4	0.009
	O^+	CO_2	0.005
15	CH_3^+	CH_4	0.012
14	CH_2^+	CH_4	0.009
		CH_2CO	0.064
13	CH^+	CH_2CO	0.110

[a] Ion counts / laser pulse at 20°.

Table 2-2: Ratio of Dimer/Monomer Dissociation Signal at Varying Temperatures

Source Temperature in °C	[Dimer]/[Monomer]
170	4.2
264	3.5
340	2.9

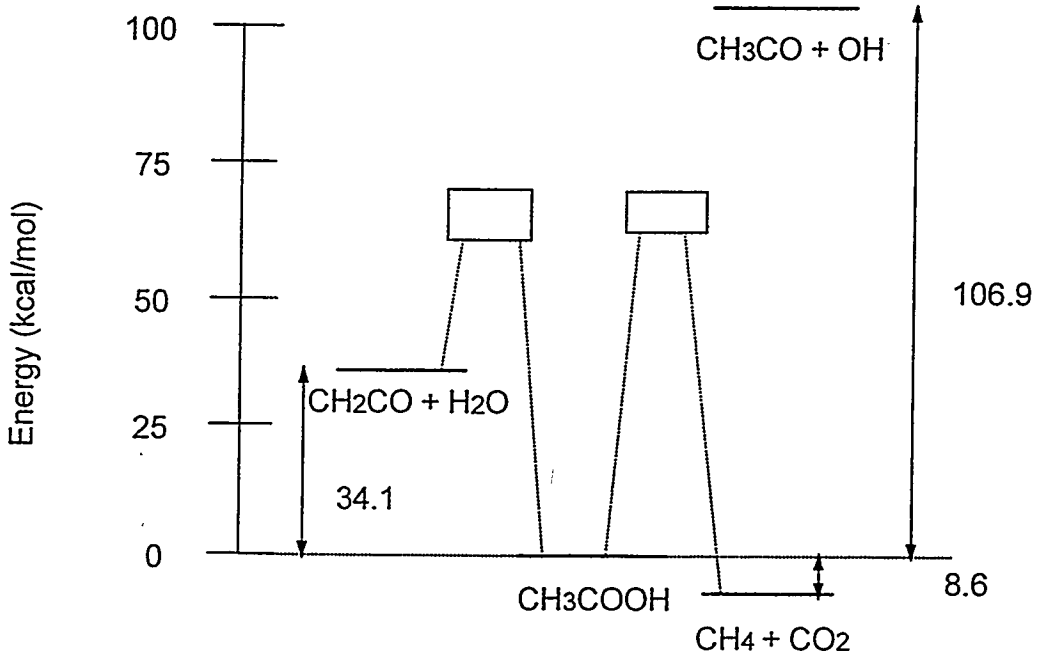

Figure 2-1. Energy level diagram showing possible dissociation channels for acetic acid. Both primary channels that we observed are shown with a dashed line. The boxes indicate the range of activation energies determined by previous experiments.[5-8]

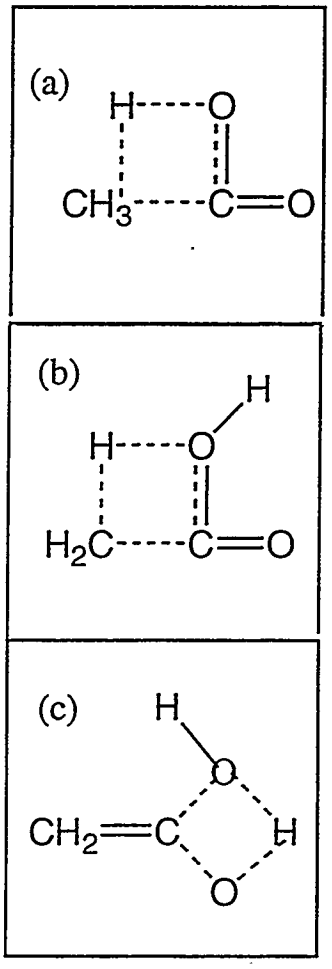

Figure 2-2. Three transition states relevant to the decomposition of acetic acid. (a) Transition state which produces the products methane and carbon dioxide. (b) The commonly accepted transition state resulting in the products ketene and water. (c) An alternate transition state also leading to dehydration, in this case a rearrangement must take place first.

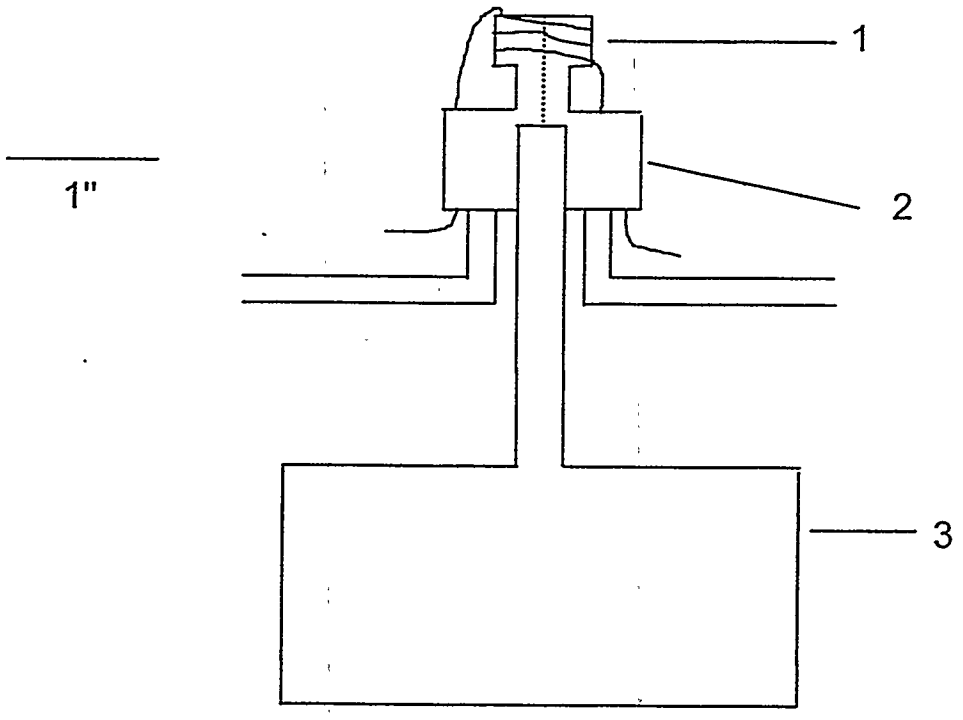

Figure 2-3. Heated pulsed valve source. A 0.040" channel extends through the heated area. A thermocouple attached by a screw measures the temperature of the copper extension. The Trickl pulsed valve is quite sensitive to heat owing to the viton/buna o-ring used to seat the pluger so water cooling is essential. (1) Copper extension wrapped with coaxial wire. (2) Stainless steel water cooled extension. (3) Pulsed valve body.

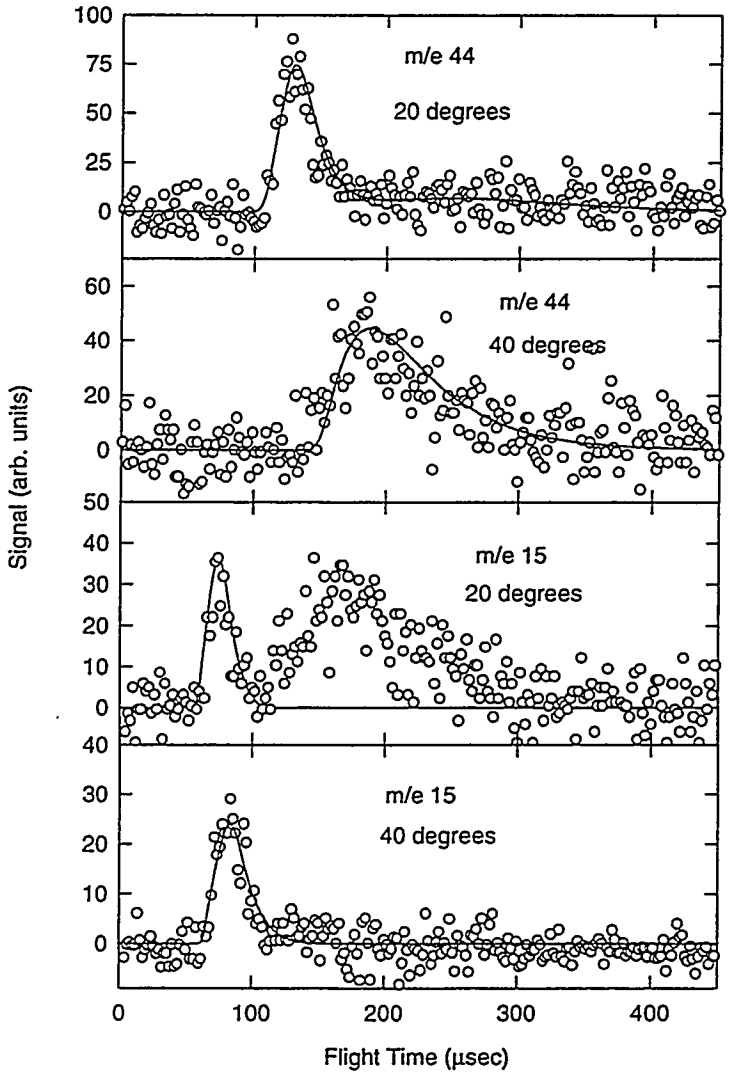

Figure 2-4. Time-of-flight spectra of products from reaction (1) at 20° and 40°. The open circles represent data points and the solid lines are the fit to the data using the forward convolution method. The derived translational energy distribution is shown in Figure 2-5a.

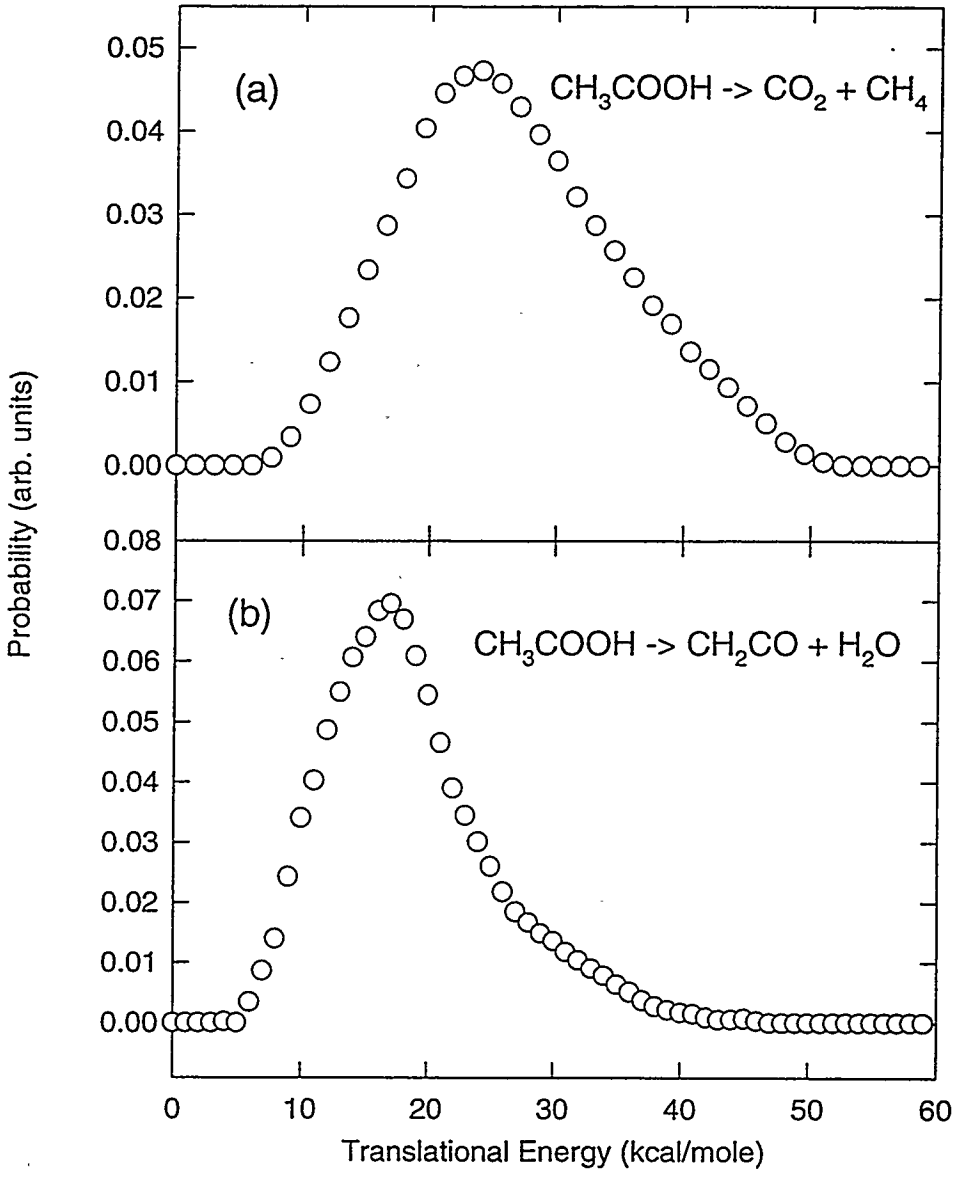

Figure 2-5. Translational energy distributions derived from the data in Figures 2-4 and 2-6. (a) Translational energy distribution for reaction 2-1. (b) Translational energy distribution for reaction 2-2.

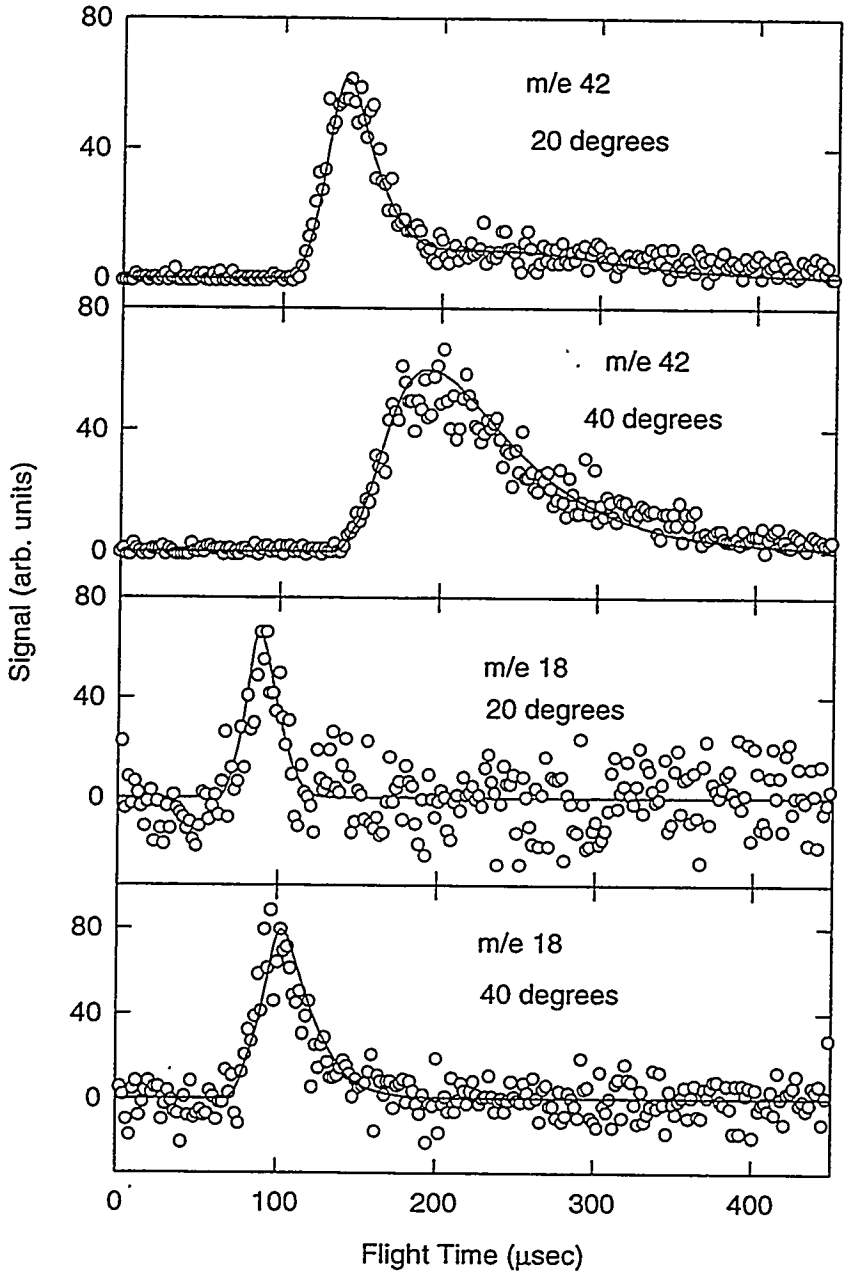

Figure 2-6. Time-of-flight spectra of products from reaction 2-2 at 20° and 40° analogous to Figure 2-4. The center-of-mass translational energy distribution is shown in Figure 2-5b.

Chapter 3

Competing Pathways in the Infrared Multiphoton Dissociation of Hexafluoropropene

3.1. Introduction

The decomposition of hexafluoropropene has been previously investigated using both thermal and infrared multiphoton dissociation (IRMPD) techniques. A single primary reaction (3-1) was proposed based on a thermal decomposition experiment, although neither of the products, tetrafluoroethylene or difluorocarbene, were directly observed.[1]

$$C_3F_6 \rightarrow C_2F_4 + CF_2, \qquad (3\text{-}1)$$

An activation energy of 75 kcal/mol was estimated for reaction 1, however, because of the circuitous method used to obtain this value, it is listed as highly questionable in a compilation of gas kinetic data.[2] In a later investigation, perfluoroisobutene as well as perfluoro-1-butene and perfluoro-2-butene were identified as pyrolysis products of hexafluoropropene, highlighting the extensive role of recombination in this reaction.[3]

In a more recent study, a free-piston adiabatic compression setup was used to decompose hexafluoropropene.[4] In the initial compression stages the only product identified was tetrafluoroethylene, and an activation energy of 82.7 ± 1 kcal/mol was obtained for reaction 1. From their experiment Buravtsev et al. predict that the precursor to tetrafluoroethylene (C_2F_4) is trifluoromethylfluorocarbene (CF_3CF) which initially forms in the dissociation of hexafluoropropene (3-2).

$$C_3F_6 \rightarrow CF_3CF + CF_2 \qquad (3\text{-}2)$$

A subsequent 1,2-fluorine atom shift (reaction 3-3) was suggested to take place without a barrier, with the carbene species 17 ± 1.5 kcal/mol higher in energy than tetrafluoroethylene.

$$CF_3CF \rightarrow C_2F_4 \qquad (3\text{-}3)$$

Reaction 3-3 has also been suggested in mercury-sensitized photolysis[5] and flash photolysis[6] studies of hexafluoropropene. Nevertheless, the prediction of a barrierless reaction from the adiabatic compression studies is somewhat surprising as experimental[7] and theoretical[8] studies on fluorine atom shifts in CF_3CH have found barriers of ~25 kcal/mol.

With the widespread availability of high power CO_2 lasers, IRMPD studies have become a practical alternative to thermal studies. The possibility of exciting the C-F stretch on the central carbon of hexafluoropropene at 1037 cm^{-1} makes this compound a viable candidate for such infrared multiphoton pumping.[9,10] In a previous IRMPD experiment, the products C_2F_4 and C_2F_6 were identified.[10] The production of C_2F_4 is postulated to result from reaction 1 as well as from the recombination of CF_2 radicals. One possible mechanism used to explain the presence of C_2F_6 is a fluorine abstraction, reaction 3-4, followed by recombination (3-5).

$$CF_2 + CF_2 \rightarrow CF_3 + CF \qquad (3\text{-}4)$$

$$CF_3 + CF_3 \rightarrow C_2F_6 \qquad (3\text{-}5)$$

In another IRMPD study, the major products, C_2F_4 and C_2F_6, were identified by their infrared absorption spectra.[11] The fluence dependence of the yield of the products was further probed as discussed in a subsequent paper.[12] Higher fluence favors formation of

C_2F_6, but with prolonged irradiation C_2F_6 and C_2F_4 production decreases. The authors suggested that reactions 3-1, 3-4, and 3-5 cannot completely describe the hexafluoropropene dissociation mechanism. Upon further examination of the infrared spectra, absorption lines attributable to polytetrafluoroethylene were identified. It is hypothesized that the incorporation of CF into polytetrafluoroethylene ($-CF_2-CF_2-$) does not change the absorption spectra significantly and can explain the eventual fate of the CF radicals from reaction 3-4.

As indicated by the experiments carried out so far, the results of the decomposition experiments of hexafluoropropene are difficult to interpret. This is because of the multiple collisions that take place after the initial unimolecular decomposition obscuring the primary decomposition pathways. Besides the primary reactions already discussed (3-1, 3-2), rupture of the carbon-carbon single bond may be possible (3-6).

$$C_3F_6 \rightarrow CF_3 + C_2F_3 \qquad (3\text{-}6)$$

Because molecular beam techniques allow for the direct detection of the primary products in a unimolecular reaction, the present study using photofragment translational spectroscopy[13] coupled with IRMPD was undertaken.

In addition to the identification of the primary products, photofragment translational spectroscopy yields insight into the dissociation dynamics of a reaction through measurement of the translational energy release of the products. The observed translational energy distributions in hexafluoropropene decomposition may facilitate understanding of the CF_2 loss reaction. Although cleavage of a carbon-carbon double bond seems unusual, it is not unprecedented. In the 193 nm dissociation of

tetrafluoroethylene, formation of two CF_2 fragments occurred via double bond cleavage. (3-7).[14]

$$C_2F_4 \rightarrow 2\ CF_2 \qquad (3\text{-}7)$$

In that case, a large translational energy release, peaked well away from zero, was observed as well as a polarization dependence, indicating dissociation from an excited state. It will be informative to compare the translational energy distributions and therefore the dynamics of these two systems, as the IRMPD of hexafluoropropene results in rupture of the double bond from the ground electronic state.

3.2. Experimental Section

These experiments were carried out at the Institute of Atomic and Molecular Sciences in Taiwan.[15] This machine is virtually identical to the Berkeley rotating source machine. Briefly, a mixture of 5% C_3F_6 in helium was passed through a solenoid-type pulsed valve (General Valve, Series 9) with a 0.020" nozzle, operating at room temperature with a typical stagnation pressure of 1 atm. Shown in Figure 3-1 is the pulsed valve mount built in Berkeley and used on the Taiwan rotating source machine. The two advantages of this mount are the adjustable nozzle-skimmer distance and the automatic alignment. Without this alignment based on the source flange key, it would have been necessary to vent the detector to align the source. The supersonic expansion of hexafluoropropene was characterized by standard time-of-flight techniques with a spinning slotted wheel, and a mean velocity of 900 m/s with a spread of ~ 12 % was found.

The molecular beam was collimated with two skimmers resulting in an angular divergence of slightly less than 3 degrees. A Lambda Physik EMG 202 pulsed CO_2 laser was tuned to the P(26) line of the 9.6 μm branch (1041 cm^{-1}) and crossed the molecular beam at right angles in the interaction region. The laser beam was focused to a 1.5 x 2 mm^2 spot using a 1" ZnSe lens with a 25 cm focal length, resulting in a fluence of ~ 10 J/cm^2.[16] The fragments created by IRMPD traveled 36.7 cm to a universal detector that has been described in Chapter One. The detector was backed by an Uninterruptible Power Supply which essentially eliminated down time from power outages. A multichannel scaler triggered by the laser collected the ion counts as a function of the flight time from the interaction region to the detector.

3.3. Results and Analysis

Measurements were taken at source to detector angles of 15°, 20°, 30°, and 40°, and laser-correlated dissociation signal was observed at *m/e* ratios 100 ($C_2F_4^+$ or $CFCF_3^+$), 81 ($C_2F_3^+$), 69 (CF_3^+), 62 ($C_2F_2^+$), 50 (CF_2^+) and 31 (CF^+). The resulting data was analyzed using standard forward convolution techniques as discussed in Chapter Two and in more detail elsewhere.[17] The signal at *m/e* = 100 is unambiguous evidence for the CF_2 loss channel. For the time being, this reaction will be referred to as reaction 3-1. As will be shown later, the laser-correlated signal at *m/e* = 81 is notably broader than that at *m/e* = 100, indicating the presence of a second primary channel, (3-6). In addition, *m/e* = 50 shows evidence of secondary dissociation channel.

3.3.1. Primary and Secondary Reactions

3.3.1.1. $C_3F_6 \rightarrow C_2F_4 + CF_2$. The time-of-flight spectrum for *m/e* = 100 is shown in Figure 3-2a. This confirms the unimolecular dissociation of hexafluoropropene by either reaction 3-1 or reaction 3-2 under collisionless conditions. The corresponding momentum matched partner, *m/e* = 50, will be discussed later. The translational energy distribution is derived from *m/e* = 100 time-of-flight spectra at 20°, 30°, and 40°. This distribution, which is peaked away from zero, is shown in Figure 3-2b. The average translational energy release is 13.3 kcal/mol.

3.3.1.2. $C_3F_6 \rightarrow CF_3 + C_2F_3$. As mentioned above, the signal observed at *m/e* = 81 ($C_2F_3^+$) could not be explained by assuming the only contribution was fragmentation of *m/e* = 100 in the electron impact ionizer. The discrepancy in the fit occurs at longer times, indicating the contribution of another channel with little translational energy. The differences between the *m/e* = 81 and the *m/e* = 100 spectra can be explained by assuming a second primary channel involving CF_3 loss. The time-of-flight spectrum for *m/e* = 81 at 20° is shown in Figure 3-3a along with the corresponding translational energy distribution, Figure 3-3b. As expected, the translational energy distribution for the simple bond rupture reaction peaks near zero with a low average translational energy release. Further evidence of this slow channel is apparent in the time-of-flight spectra at *m/e* = 69, CF_3^+, and *m/e* = 62, $CFCF^+$ (Figure 3-4). The signal observed at these masses cannot be explained without considering reaction 3-6.

3.3.1.3. $C_2F_4/CF_3CF \rightarrow 2CF_2$. As fluorocarbons readily fragment in the electron impact ionizer, contributions from many higher molecular weight products are found in the lower *m/e* spectra. However, there is a portion of the *m/e* = 50 and *m/e* = 31 time-of-flight spectra that cannot be explained by the two primary reactions discussed above. Since the time-of-flight spectrum at *m/e* = 31 results solely from fragmentation of *m/e* = 50 giving no new information, we will focus on the *m/e* = 50 spectrum. In Figure 3-5a it is evident that the contributions from fragmentation of *m/e* = 100, *m/e* = 81, and *m/e* = 69 are not fast enough to fully explain the time-of-flight spectrum observed. CF_2 is also a primary product from reaction 3-1 and its contribution is illustrated in Figure 3-5a. It is constrained to be momentum matched to *m/e* = 100, and it is too fast to explain the additional signal observed. The secondary dissociation of the *m/e* = 100 species to form two CF_2 fragments seems to be the only viable explanation.

Determining the extent of secondary dissociation in hexafluoropropene is complicated by the overlapping signal of the primary and secondary reactions at *m/e* = 50. Figure 3-5b illustrates one limiting case in which the secondary dissociation products have the minimum possible translational energy, while Figure 3-5c is a fit with faster secondary dissociation products. Figure 3-6 illustrates the range of these two secondary translational energy distributions. The distributions are both peaked away from zero, near 5 kcal/mol, while the average translational energy release ranges from 5.6 to 7.2 kcal/mol, respectively.

As a consequence of the secondary dissociation of the C_2F_4/CF_3CF species, the primary translational energy distribution for reaction 3-1 cannot be obtained from the *m/e* = 100 time-of-flight spectrum. The translational energy distribution derived from *m/e* = 100,

shown in Figure 3-2b, is biased towards faster molecules with less internal energy since they do not undergo as much secondary decomposition. In other molecules, the primary translational energy distribution could be obtained by observing the corresponding momentum matched fragment. However, in hexafluoropropene the signal from CF_2 produced in the primary process cannot be separated from the secondary decomposition signal, which also results in CF_2. A comparison of the translational energy distributions obtained from the *m/e* = 100 time-of-flight spectrum (Figure 3-2a) and those obtained from the *m/e* = 50 primary dissociation signal (Figures 3-5b and 3-5c) is shown in Figure 3-2b. The difference between the *m/e* = 100 and the *m/e* = 50 distributions was used as the primary translational energy distribution for the secondary dissociation products in both cases as previously discussed.[13a]

The method for calculating the experimental branching ratio between the two primary reactions has been discussed in detail earlier.[18] The branching ratio between reactions 3-1 and 3-6 was only determined at the maximum attainable fluence, ~10 J/cm^2, owing to limitations in detector sensitivity at lower fluences. The relative contribution from each primary fragment, C_2F_4, C_2F_3, CF_3 and CF_2, at each *m/e* ratio was determined. In the case of secondary dissociation, the contribution at *m/e* = 50 and *m/e* = 31 was included in the C_2F_4 yield, taking into account that each *m/e* = 100 fragment produces two CF_2 fragments. The contributions of fragmentation at lower masses could not be quantified which adds to the overall uncertainty. The branching ratio between reactions 3-1 and 3-6, $[CF_2]/[CF_3]$, was found to be 4.0 ± 1.0.

3.3.2. Using RRKM Theory to Obtain a Simple Bond Rupture Activation Energy

RRKM theory is often used to calculate dissociation rate constants for unimolecular reactions.[19] In the case of a simple bond rupture reaction without an exit barrier, one can predict the translational energy distribution based on the total available energy.[20] The resulting translational energy distribution is typically peaked at zero and decays exponentially. An extension of RRKM theory has been used in our group to calculate dissociation barriers in situations where a simple bond rupture and a concerted reaction compete.[13] In order to determine a dissociation barrier for reaction "A" it is necessary to know the activation energy for reaction "B", the experimental branching ratio and the simple bond rupture translational energy distribution. A program that models the competition between absorption, stimulated emission and dissociation is used to obtain the population created by the laser and the yield of each channel.[21] RRKM translational energy distributions at each energy level above dissociation are weighted by the population distribution of the excited parent and summed to create the overall translational energy distribution, which is compared to the experiment.[22] This iterative process entails modifying the quasi-continuum cross-sections using different barrier heights until the experimental branching ratio and translational energy distribution are reproduced.[23]

The dissociation rate constants and translational energy distributions for hexafluoropropene were determined using a readily available RRKM program.[24] The ground state vibrational frequencies necessary for the RRKM calculations were obtained from the literature.[9b] The transition state frequencies were assumed to be similar to the

ground state and then varied to reproduce the pre-exponential A-factor. For reaction 3-1 an A-factor of 13.0 was utilized,[1,2] while for reaction 3-6 a typical A-factor for fluorocarbons undergoing simple bond rupture of 16.1 was assumed.[25] Table 3-1 lists the relevant RRKM parameters. To predict the population created by infrared multiphoton excitation, a laser pulse consisting of a 100 nsec spike followed by a 1 μsec tail was used.[26] We assumed the spike contained 70% of the total available energy as has been reported for CO_2 laser pulses.[27]

Two values have been measured for the activation energy of reaction 3-1 (75[1,2] and 82.7[4] kcal/mol). In Figure 3-3b, the dotted line represents the best fit using an activation energy of 75 kcal/mol for reaction 1; a barrier height of 100 kcal/mol was obtained for reaction 3-6. The solid line represents a second calculation using 82.7 kcal/mol as the activation energy for CF_2 elimination. In this instance, a barrier height of at least 105 kcal/mol is necessary to reproduce the experimental translational energy distribution. There is a large uncertainty in assigning an activation barrier to reaction 3-6 owing to the uncertainty in the value of the activation energy for reaction 3-1. In addition, the range of translational energy distributions that can be used to fit reaction 3-6 is large, as seen by the cross-hatched area in Figure 3-3b. At best, we can estimate that the barrier height for simple bond rupture of hexafluoropropene is 100-105 kcal/mol.

3.4. Discussion

There is clear experimental evidence for reactions 3-1, 3-6, and a secondary dissociation reaction in the IRMPD of hexafluoropropene. The formation of CF_3 from

reaction 3-6 can explain the presence of C_2F_6 in earlier IRMPD studies[10-12] as recombination of the trifluoromethyl radicals is possible. The secondary dissociation reaction highlights the reactivity of C_3F_6, which may explain the extensive polymerization seen in previous experiments.[1,3,4,10-12] In the following paragraphs, we discuss possible reaction mechanisms for reaction 3-1 and the identity of the heavier species which undergoes secondary decomposition.

3.4.1. Difluorocarbene Loss. The mechanism by which CF_2 is formed in the dissociation of hexafluoropropene is not well understood. Although tetrafluoroethylene has been detected in a number of IRMPD and thermal experiments there is still uncertainty as to whether it is formed in the primary decomposition step of hexafluoropropene. The adiabatic compression studies suggest that $CFCF_3$ is formed initially and then isomerizes to tetrafluoroethylene.[4] The consensus of the IRMPD studies is that tetrafluoroethylene is generated directly from hexafluoropropene, however, no mechanism is given.[10-12] Benson suggests that an intermediate, cyclohexafluoropropane, proceeds tetrafluoroethylene formation.[2] Another intermediate that could be involved is the diradical $CF_2CF_2CF_2$; the presence of its hydrocarbon analog, trimethylene, has been predicted in the isomerization from cyclopropane to propene.[28]

By examining the possible dissociation pathways and the expected reaction mechanism dynamics it may be possible to eliminate some mechanisms based on the observed translational energy distribution. The formation of the cyclic isomer, cyclohexafluoropropane, is energetically possible as it lies only 35.1 kcal/mol above the ground state of hexafluoropropene.[29] Direct dissociation of cyclohexafluoropropane should

result in the expulsion of CF_2 as two single bonds are broken while a double bond closed shell species (tetrafluoroethylene) is formed (Figure 3-8a). This repulsion would result in a translational energy distribution peaked away from zero. If dissociation occurred from the diradical species, $CF_2CF_2CF_2$, the transition state might be expected to look like that of a simple bond rupture with one of the carbon-carbon single bonds stretching until two distinct species are formed (Figure 3-8b). Although some electronic rearrangement would be necessary to form tetrafluoroethylene, the translational energy distribution should peak at or near zero. An important caveat is that the $CF_2CF_2CF_2$ diradical may not be a distinct transition state; a concerted mechanism whereby a fluorine migrates as tetrafluoroethylene forms is plausible (Figure 3-8c). This concerted reaction might be expected to have an exit barrier which would result in a translational energy distribution peaked away from zero.

On the other hand, if the products CF_2 and $CFCF_3$, are formed, they could result from direct cleavage of the carbon-carbon double bond (Figure 3-8d). One might initially think that the stretching of this bond to form two carbenes would result in a translational energy distribution similar to that for a simple bond rupture reaction. However, if we assume that C_3F_6 behaves in a similar manner to C_2F_4, the application of the Woodward-Hoffman rules predict a barrier to the formation of the parent from two singlet species.[30] The unusual stability of singlet CF_2, owing to the large electronegativity and lone pairs on the fluorine atom,[30] results in a singlet-triplet splitting of 56.6 kcal/mol.[31] On the other hand, the singlet-triplet splitting for $CFCF_3$ has been calculated to be only 9.2 kcal/mol.[32] These ground state singlet species, CF_2 and $CFCF_3$, have no open shell electrons and therefore require energy for the excitation of each species in order to form covalent bonds.[33] The

energy released from electron pairing to form the two singlet species in the reverse reaction of C_3F_6 dissociation would result in a translational energy distribution peaked away from zero.

The range of the primary translational energy distribution for the formation of CF_2 and its momentum matched partner is represented in Figure 3-2b. The uncertainty in this distribution, as discussed earlier, lies in our inability to separate CF_2 formed in the primary step from that produced in the secondary dissociation reaction. This distribution does peak away from zero to a maximum of 10 kcal/mol and extends to 30 kcal/mol which eliminates the involvement of the diradical (Figure 3-8b) as an intermediate. The isomerization of hexafluoropropene to perfluorocyclopropane, the concerted fluorine migration, or cleavage of the double bond could all result in the observed primary translational energy distribution. Although the barrier from hexafluoropropene to perfluorocyclopropane is estimated to be greater than 90 kcal/mol,[34] the IRMPD/RRKM calculations suggest that the excited fluorocarbon contains at least 100-105 kcal/mol which may be enough for this isomerization to take place.

The possibility of isomerizations (Figure 3-8a) or fluorine migrations (Figure 3-8c) cannot be definitively ruled out in the IRMPD of hexafluoropropene. In both the IRMPD of hexafluoropropene and the UV photolysis of tetrafluoroethylene[14] the translational energy distributions peak away from zero in the reaction which destroys the double bond, but the dynamics are not similar. In the case of tetrafluoroethylene photodissociation at 193 nm, the cleavage of the carbon-carbon double bond occurs on a short (picosecond) time scale as indicated by the slight polarization dependence (β = -0.2). In the IRMPD of

hexafluoropropene, where the dissociation occurs on the nanosecond or longer time scale, it is unclear whether direct cleavage of the double bond is the mechanism that takes place.

3.4.2. Secondary Dissociation. The primary product, $CFCF_3$ or C_2F_4, undergoes further dissociation to produce two difluorocarbene species. The translational energy distribution from the secondary dissociation of hexafluoropropene, Figure 3-6, peaks near 5 kcal/mol and extends to ~ 16 kcal/mol. A similar translational energy distribution is observed in the IRMPD of 2-chloro-1,1,1,2-tetrafluoroethane. [35] The complementary fragment in the elimination of HCl is CF_3CF and the secondary dissociation of this fragment results in a translational energy distribution peaked at 3 kcal/mole and extending to ~ 20 kcal/mol. These two very similar distributions indicate that the same dissociation mechanisms occur in both hexafluoropropene and 2-chloro-1,1,1,2-tetrafluoroethane. One pathway, suggested by Yokoyama and co-workers, is that trifluoromethylfluorocarbene directly undergoes a three-centered concerted dissociation reaction to form two CF_2 carbenes. This is the reverse reaction of CF_2 insertion into the CF bond of CF_2, and typically insertion reactions of carbenes with singlet ground states such as CF_2 will have barriers.[36] This entrance barrier translates into an exit barrier for $CFCF_3$ dissociation and will lead to a translational energy distribution peaked away from zero as observed.

A 1,2-fluorine atom shift to tetrafluoroethylene followed by dissociation could also produce the CF_2 observed in the secondary dissociation of hexafluoropropene and 2-chloro-1,1,1,2-tetrafluoroethane. In the analogous hydrocarbon system, $^1CH_3CH$ is predicted to have only a 0.6 kcal/mol barrier to the formation of ethylene via a 1,2 H shift.[37] In general, the activation energy for a 1,2 shifts increases in the following manner: Cl < H < alkyl < F.[7]

Although calculations[8] and experiments[7] on $^1CF_3CH$ indicate a barrier greater than 20 kcal/mol for fluorine migration, it could occur as suggested by Buravtsev et al.[4] As discussed earlier, the formation of two singlet species in the cleavage of a double bond is likely to result in a translational energy distribution peaked away from zero. Preliminary results from the IRMPD of octafluorocyclobutane show that the C_2F_4 produced in the primary reaction dissociates further to CF_2.[38] The translational energy distribution for CF2 is peaked away from zero at ~ 4.5 kcal/mol and extends to 20 kcal/mol which is similar to both our experiments and Yokoyama and co-workers. Although the same species appears to be undergoing secondary dissociation in all three experiments it remains unknown whether dissociation occurs from C_2F_4, $CFCF_3$, or an intermediate species. It is not possible in this situation to determine the identity of the dissociation product based solely on the observed translational energy distribution.

3.5 Conclusions

Two primary pathways, CF_3 loss and CF_2 loss, have been observed in the IRMPD of hexafluoropropene. The loss of CF_3 has not been previously observed in the unimolecular decomposition of this molecule and may explain the observation of C_2F_6 in bulk experiments. Modeling the dissociation with a well-known RRKM/IRMPD model gives an activation energy of 100-105 kcal/mol for this simple bond rupture reaction. CF_2 loss was seen to be the predominant channel accounting for 80% of the products, with significant secondary dissociation of the heavier fragment producing additional CF_2.

References and Notes

[1] B. Atkinson and A. B. Trenwith, J. Chem. Soc. 2082 (1957).

[2] S. W. Benson and H. E. O'Neal, *Kinetic Data on Gas Phase Unimolecular Reactions*; Nat. Bureau of Standards. U. S. Government Printing Office: Washington, D. C., 1970; p. 493.

[3] R. A Matula, J. Phys. Chem. **72**, 3054 (1968).

[4] N. N. Buravtsev, A. S. Grigor'ev, and Y. A. Kolbanovskii, Kinetics and Catalysis **30**, 13 (1989).

[5] J. Heicklen and V. Knight, J. Phys. Chem. **69**, 3600 (1965).

[6] F. W. Dalby, J. Chem. Phys. **41**, 2297 (1964).

[7] B. E. Holmes and D. J. Rakestraw, J. Phys. Chem. **96**, 2210 (1992).

[8] S. P. So, J. Phys. Chem. **97**, 11908 (1993).

[9] (a) W. F. Edgell, J. Am. Chem. Soc. **70**, 2816 (1948); (b) J. R. Nielsen, H. H Classen, and D. C. Smith, J. Chem. Phys. **20**, 1916 (1952).

[10] W. S. Nip, M. Drouin, P. A. Hackett, and C. Willis, J. Phys. Chem. **84**, 932 (1980).

[11] M. Santos, C. Siguenza, J. A. Torresano, and P. F. Gonzalez-Diaz, Spectra. Acta., **64A**, 455 (1990); C. Siguenza, M. Santos, J. A. Torresano, A. Pino, P. F. Gonzalez-Diaz, Spectra. Acta., **46A**, 1499 (1990).

[12] J. A. Torresano, M. Santos, and P. F. Gonzalez-Diaz, Laser Chem. **14**, 217 (1994).

[13] (a) E. J. Hintsa, A. M. Wodtke, and Y. T. Lee, J. Phys. Chem., **92**, 5379 (1988); (b) A. M. Wodtke, E. J. Hintsa, and Y. T. Lee, J. Phys. Chem., **90**, 3549 (1986);. (c) A. M. Wodtke, and Y. T. Lee, In *Advances in Gas Phase Photochemistry and Kinetics*, M. N. R. Ashfold and J. E. Baggot, Eds.; Royal Society of Chemistry: London; 1987.

[14] T. K. Minton, P. Felder, R. C. Scales, and J. R. Huber, Chem. Phys. Lett., **164**, 113 (1989).

[15] Y. R. Lee, F. T. Chen, C. C. Hsueh, H. M. Chou, H. C. Chen, Y. J. Yang, and S. M. Lin, Proc. Natl. Sci. Counc. ROC(A) **18**, 55 (1994).

[16] This CO_2 laser was a prototype for Lambda Physik and only sold for one year. To ensure a constant fluence and laser spot position during the experiments a repetition rate of 5 Hz was used and the spot power and position monitored every 5-10,000 laser shots.

[17] A. M. Wodtke, Ph. D. Thesis, University of California, Berkeley (1986); X. Zhao, Ph. D. Thesis, University of California, Berkeley (1988).

[18] J. D. Myers, Ph. D. Thesis, University of California, Berkeley (1993).

[19] P. J. Robinson and K. A. Holbrook, *Unimolecular Reactions*; Wiley: London, 1972. W. Forst, *Theory of Unimolecular Reactions*; Academic Press: New York, 1973.

[20] S. A. Safron, N. D. Weinstein, D. R. Herschbach, and J. C. Tully, Chem. Phys. Lett. **12**, 564 (1972).

21 This program was first reported by P.A. Schulz, As. S. Sudbo, E. R. Grant, Y. R. Shen, and Y. T. Lee, J. Chem. Phys. **72**, 4495 (1980).

[22] L. J. Butler, R. J. Buss, R. J.; Brudzynski, and Y. T. Lee, J. Phys. Chem. **87**, 5106 (1983).

[23] A program written by Dr. T. T. Miau alleviated the tediousness of this process. Called IRMPD this program takes translational energy distributions generated by the RRKM program for each photon energy, multiples each by the population probability and sums them to obtain one translational energy distribution.

[24] W. L. Hase and D. L. Bunker, Quantum Chemistry Program Exchange, Indiana University, Prog. No. QCPE 234.

[25] E. Tschuikow-Roux, J. Chem. Phys. **43**, 2251 (1965); S. Kato, Y. Makide, T. Tominaga, and K. Takeuchi, J. Phys. Chem. **91**, 4278 (1987).

[26] P. K. Chowdhury, D. V. S. Rama Rao, and J. P. Mittal, J. Phys. Chem., **92**, 102 (1988).

[27] A. J. Grimley and J. C. Stephenson, J. Chem. Phys. **74**, 447 (1981); J. C. Stephenson and D. S. King, J. Chem. Phys. **69**, 1485 (1978); J. A. Beaulieu, Proc. of the IEEE **59**, 667 (1971).

[28] R. J. Bergmen, In *Free Radicals*; Kochi, J. K., Ed.; Wiley: New York; 1973; Vol. 1, Chapter 5.

[29] D. S. Bomse, D. W. Berman, and J. L. Beauchamp, J. Am. Chem. Soc. **103**, 396. (1981).

[30] The orbital and state correlation diagrams for the formation of C_2F_4 from two singlet species can be drawn and indicate a barrier exists between reactants and products. R. B. Woodward and R. Hoffmann, *The Conservation of Orbital Symmetry*; Verlag Chemie and Academic Press; 1970. P. W. Atkins, *Molecular Quantum Mechanics*, 2nd Ed; Oxford University Press: New York; 1983; pp 336-345.

[31] S. Koda, Chem. Phys. Lett. **55**, 353 (1978); Chem. Phys., **66**, 383 (1982).

[32] D. A. Dixon, J. Phys. Chem. **90**, 54 (1986).

[33] E. A. Carter and W. A. Goddard, J. Phys. Chem. **90**, 998 (1986).

[34] D. W. Berman, D. S. Bomse, and J. L. Beauchamp, Int. J. Mass. Spectrom. Ion Phys., **39**, 263 (1981).

[35] A. Yokoyama, K. Yokoyama, and G. Fujisawa, J. Chem. Phys. **100**, 6487 (1994).

[36] R. D. Bach, M.-D. Su, E. Aldabbagh, J. L. Andres, and H. B. Schlege, J. Am. Chem. Soc., **115**, 10237 (1993); R. N. Haszeldine, C. Parkinson, P. J. Robinson, and W. J. Williams, J. Chem. Soc. Perkin II 954 (1979)

[37] K. D. Evanseck and K. N. Houk, J. Phys. Chem. **94**, 5518 (1990).

[38] Y. R. Lee and S. M. Lin, To be published.

Table 3-1. Parameters used in the RRKM Calculations

Parameter	(cm^{-1})	Description	Molecule	CF_3 Loss Critical Configuration[a]	CF_2 Loss Critical Configuration[a]
Vibrational Frequencies	1797	C=C stretch	1797	1797	**rxn coor**
	1399	C-F	1399	1399	1399
	1333	stretch,CF_3	1333	1333	1333
	1211	Ass CF_2	1211	1211	1211
	1179	C-F	1179	1179	1179
	1122	stretch,CF_3	1122	1122	1122
	1037	C-F	1037	1037	1037
	767	stretch,CF_3	767	**rxn coor**	767
	655	C-F stretch	655	655	655
	609	C-F stretch	609	**100**	609
	559x2	C-C stretch	559x2	**100x2**	559x2
	513	CF_2 def	513	513	513
	462	sym CF_3 def	462	462	462
	370	asy CF_3 def	370	370	370
	364	CF_2 rock	364	**100**	364
	250x2	CF_2 wag	250x2	250x2	250x2
	171	CF wag	171	171	**700**
	134	C-C-C def	not used	not used	not used
	94	C-F rock- CF_2 twist CF_3 twist CF_3 rock	94	94	94
Reduced Moment of Inertia for Internal Rotations (amu-A^2)[b]			79	79	79
External Moments of Inertia (amu-A^2)[c]			198, 403, 512		
Energy Threshold (kcal/mole)			---	varied	75, 82.7
Calculated Value $\log_{10}A$			---	16.1	13.0

[a]The transition state frequencies in bold were modified to reproduce the pre-exponential A-factor. [b]The CF_3 twist was treated as an internal rotation, see, for example, W. Gordy and R. L. Cook, In *Microwave Molecular Spectra,* 3rd Ed.; Wiley: New York, 1984; p 574. [c]The external rotations were obtained from the rotational constants in E. J. Jacob and D. R. Lide, J. Chem. Phys. **59**, 5877 (1973).

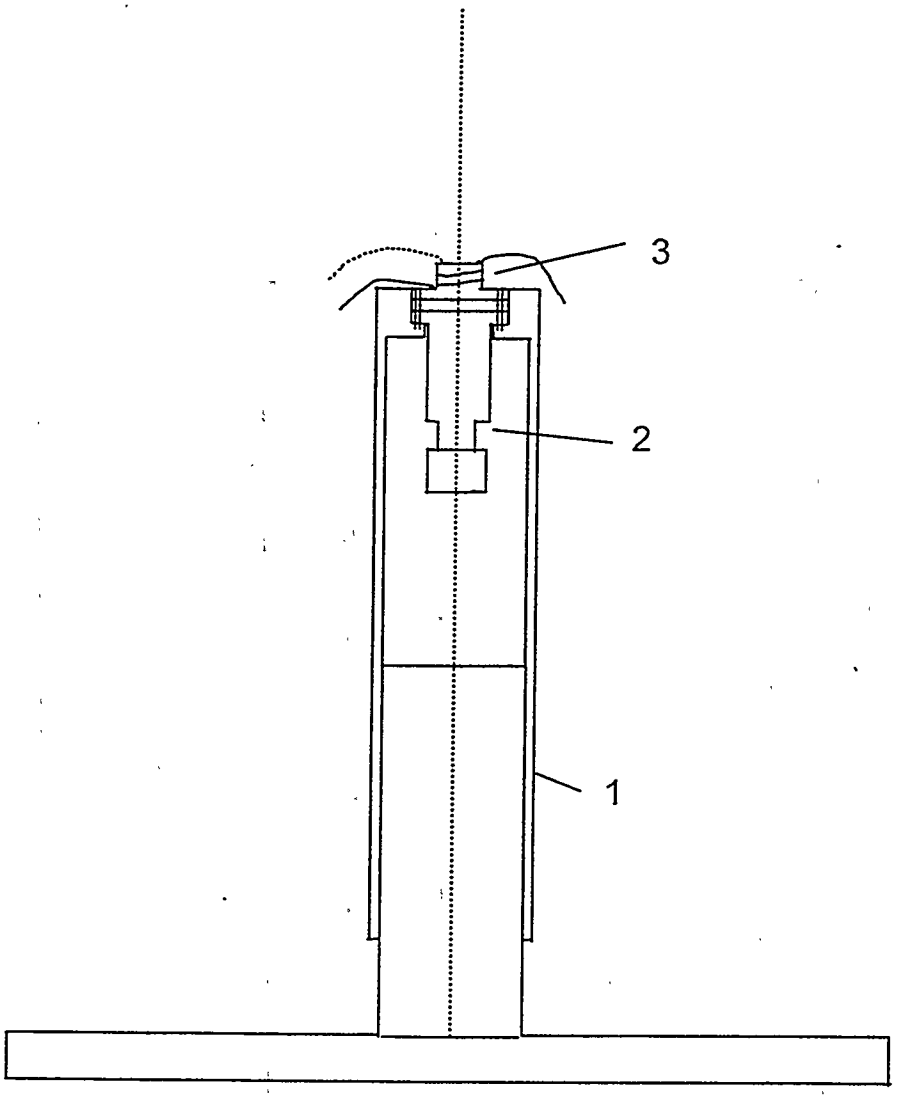

Figure 3-1. Source Mount for General Valve pulsed valve. (1) A stainless steel support with a stainless steel sleeve allows for an adjustable nozzle-skimmer distance. (2) The General Valve keys into this sleave for automatic alignment. (3) A ceramic spacer and copper extension wrapped with coaxial wire allow heating of the nozzle if necessary.. The solid lines represent the coaxial wire and the dashed line is a thermocouple.

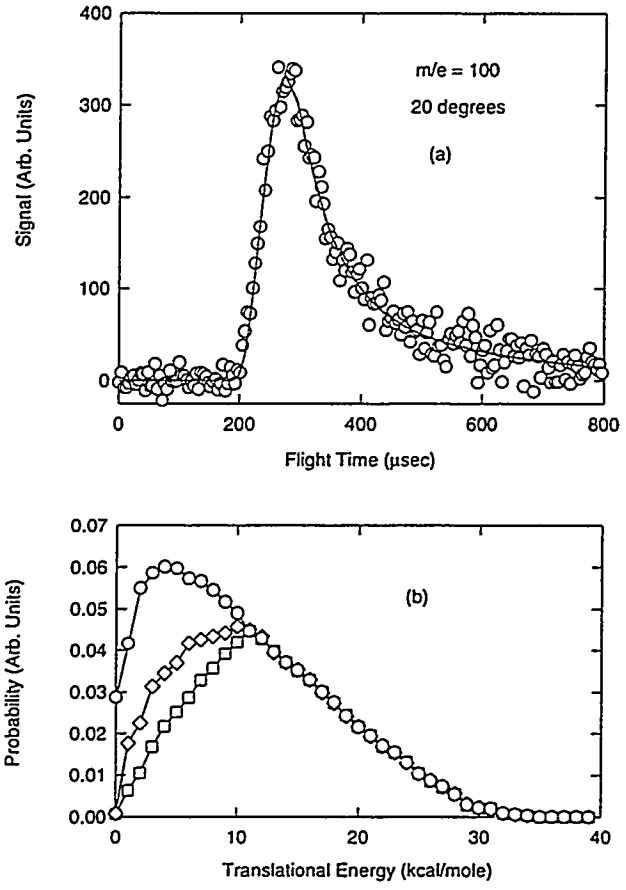

Figure 3-2. Experimental evidence for reaction 3-1. (a) Time-of-flight spectrum for *m/e* = 100 at 20°. The open circles represent data points and the solid line is the fit to the data using the forward convolution method. (b) The center-of-mass translational energy distribution derived from *m/e* = 100 is represented by the open squares. Due to the secondary dissociation of *m/e* = 100 this distribution is biased towards molecules with greater translational energy. The open diamonds represent the translational energy distribution derived from *m/e* = 50 in Figure 4b while the open circles are derived from Figure 3-4c. See text for details.

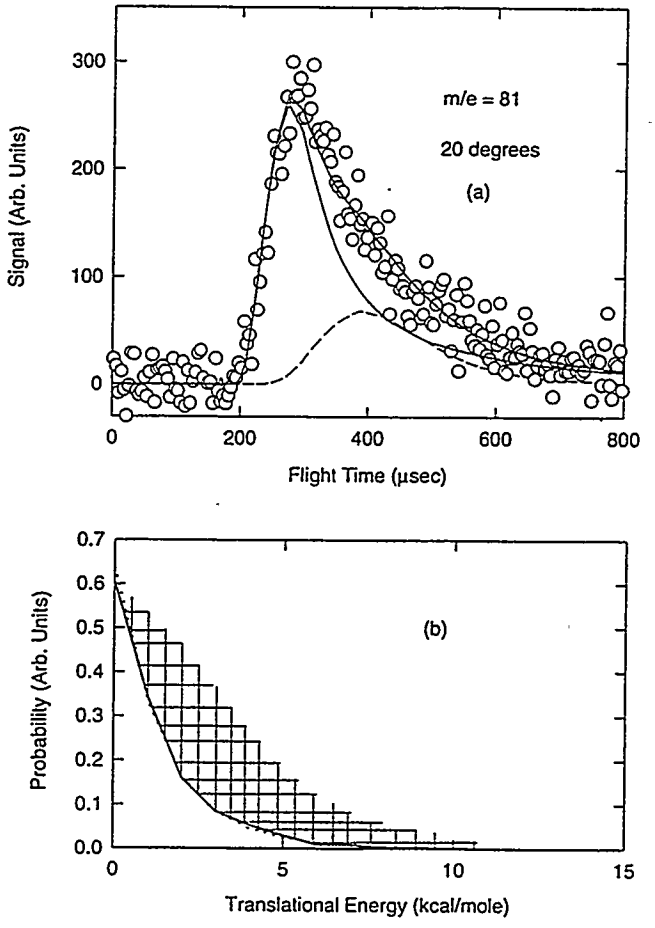

Figure 3-3. Evidence for the simple bond rupture reaction. (a) Time-of-flight spectrum for *m/e* = 81 at 20°. The solid line represents the *m/e* = 100 species that fragments in the ionizer to $C_2F_3^+$ while the dashed line represents the contribution of reaction 3-6 at *m/e* = 81. (b) The translational energy distribution of the products of reaction 3-6. The cross-hatched area represents the uncertainty associated with this measurement. The solid and dotted lines are the result of the IRMPD modeling calculations and are further explained in Section 3.3.2.

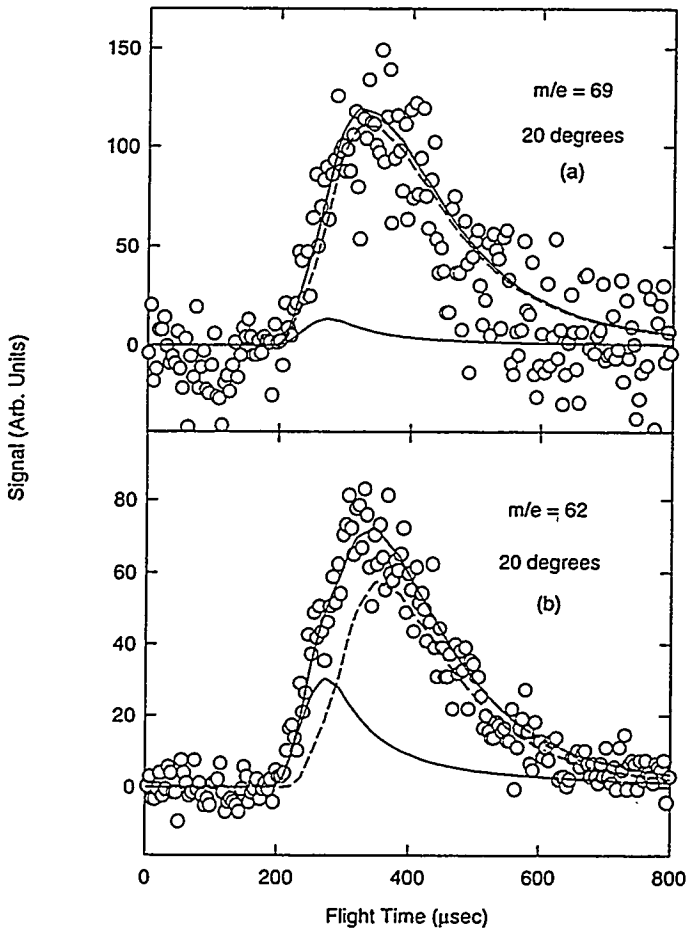

Figure 3-4. Time-of-flight spectra for *m/e* = 69 and *m/e* = 62 at 20°. (a) The trifluoromethyl fragment shows a large contribution from reaction 3-6 as indicated by the dashed line. It is the momentum matched partner of *m/e* = 81 shown in Figure 3-3a. A fast contribution, shown with the solid line, from the fragmentation of *m/e* = 100 in the electron impact ionizer is possible but not significant. (b) At *m/e* = 62 the dashed line indicates fragmentation from *m/e* = 81 while the solid line is fragmentation from *m/e* = 100. CFCF is not formed in any primary processes.

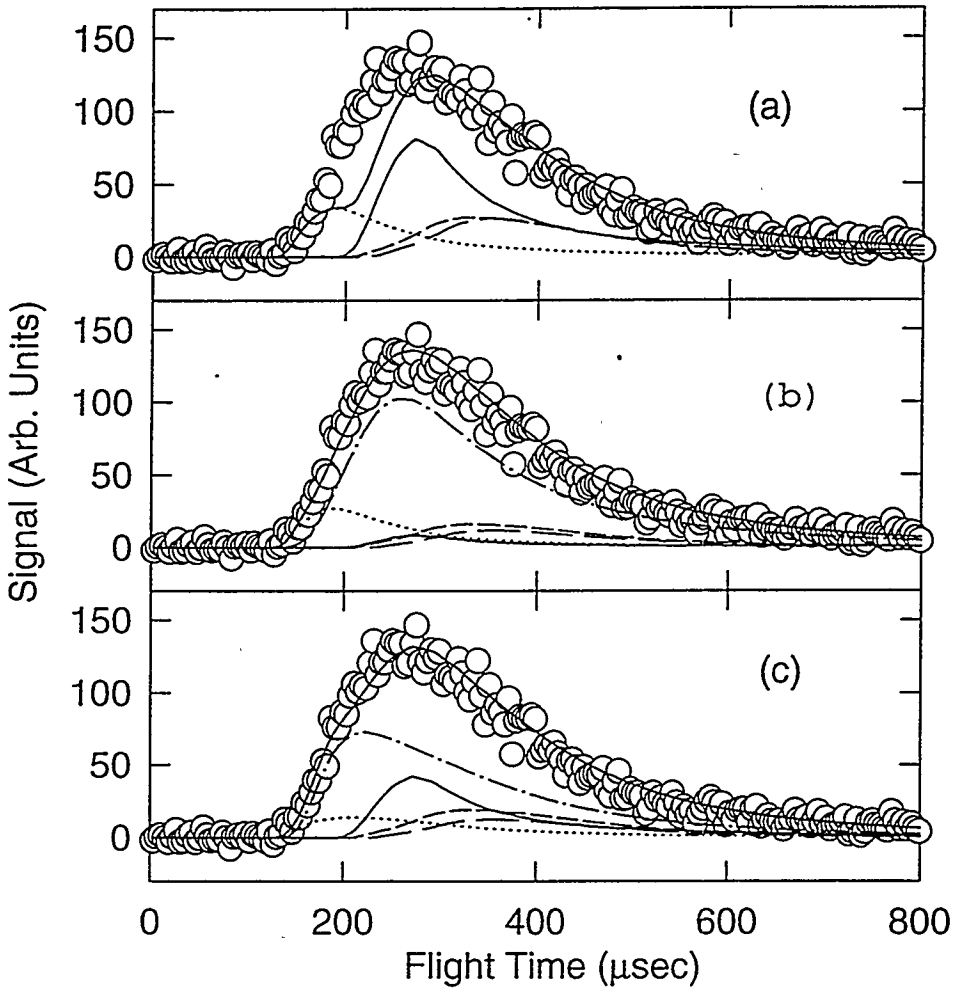

Figure 3-5. Time-of-flight spectra for *m/e* = 50 at 20°. (a) Contributions from *m/e* = 100 (solid line), *m/e* = 81 (long dashed line), *m/e* = 69 (short dashed line) and *m/e* = 50 (dotted line) cannot completely explain the signal observed at this mass. (b) The dash-dot-dash line represents the slowest possible contribution from secondary decomposition. The corresponding secondary translational energy distribution is shown in Figure 3-6. (c) In this representation the secondary dissociation (dash-dot-dash line) is as fast as possible while retaining a significant contribution of primary *m/e* = 50. The translational energy distribution in this case is also shown in Figure 3-6.

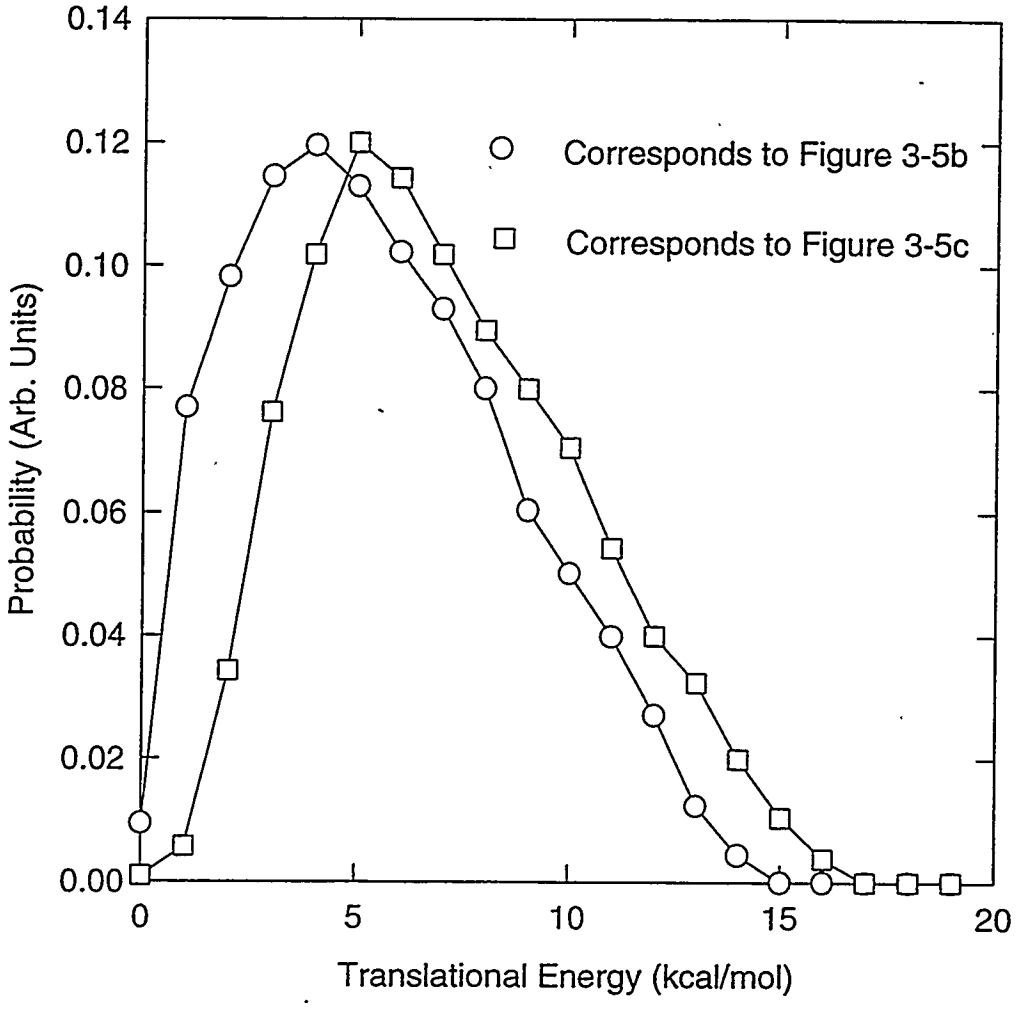

Figure 3-6. The limiting translational energy distributions for the secondary dissociation of *m/e* = 100. These distributions are derived from the dash-dot-dash lines in Figures 3-5b and 3-5c.

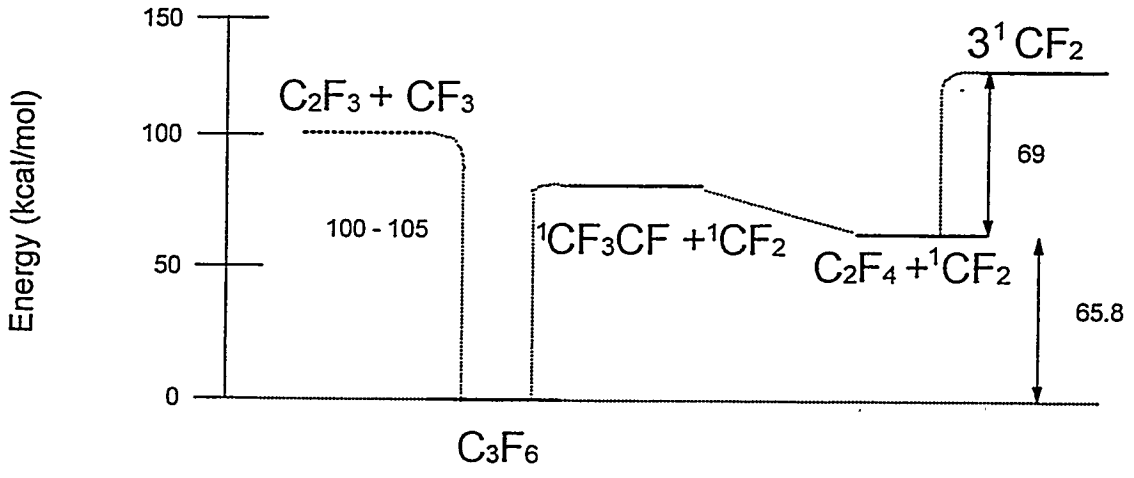

Figure 3-7. Energy level diagram for hexafluoropropene illustrating the observed dissociation pathways. The heats of formation at 298 K were obtained from the following sources: C_3F_6, -268.9 ± 2 kcal/mole, reference 29; C_2F_4, -157.4 ± .7 kcal/mole, J. Phys. Chem. Ref. Data **14**, Supplement 1, p. 655 (1985); $CFCF_3$, -140.4 ± 2 kcal/mole, reference 4; $^1CF_2$, -44.2 ± 1 kcal/mole, reference 29. The dashed line illustrates the three competing pathways. The channel producing $^1CF_2$ and C_2F_4 may necessitate rearrangement from CF_3CF with a significant activation energy. The activation energy for reaction 3-6, $CF_3 + C_2F_3$, is an estimate from IRMPD modeling.

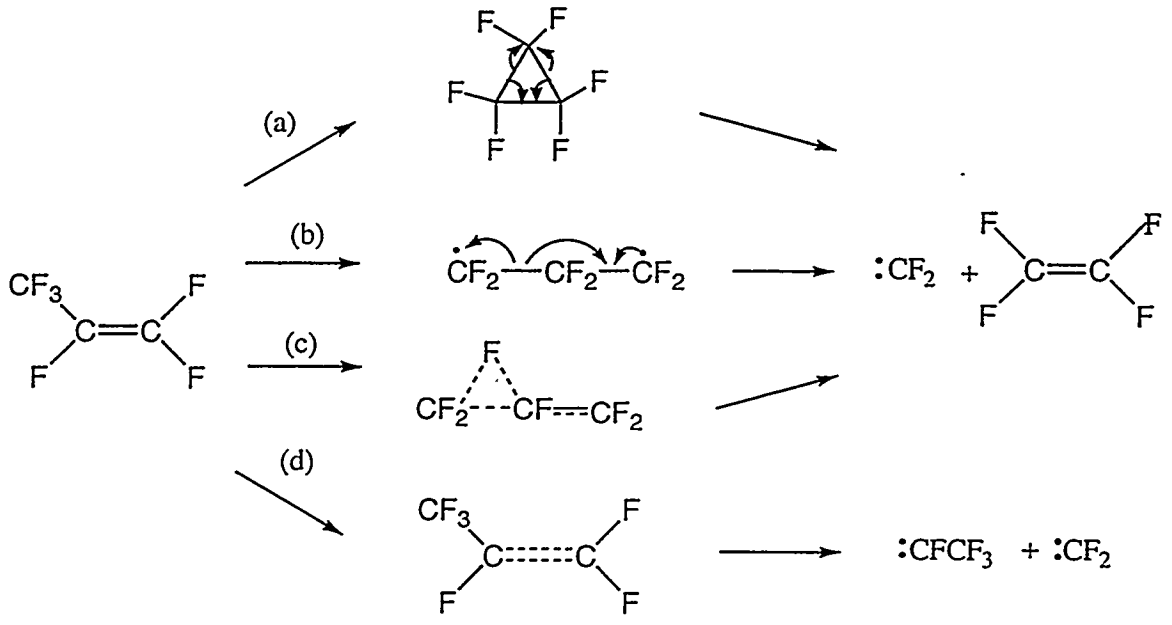

Figure 3-8. Four dissociation mechanisms for the elimination of CF_2 are illustrated. (a) Isomerization to hexafluorocyclopropane occurs prior to dissociation. (b) A diradical, $CF_2CF_2CF_2$, is formed by fluorine migration. (c) A concerted mechanism in which fluorine migration and tetrafluoroethylene formation occur simultaneously. (d) Direct cleavage of the double bond occurs as the carbon-carbon double bond elongates.

Chapter 4

The Photodissociation Dynamics of Hexafluoropropene Examined at 193 nm

4.1. Introduction

In a flash photolysis experiment on hexafluoropropene using UV light the major product, C_2F_4, was attributed to the recombination of CF_2 radicals produced in reaction 4-1.[1]

$$C_3F_6 \rightarrow CFCF_3 + CF_2 \qquad (4\text{-}1)$$

In a mercury-sensitized photolysis experiment, $h\nu > 220$ nm, the only products detected were C_2F_4 and 2-octafluorobutene.[2] A stepwise reaction mechanism whereby reaction 4-1 is followed by isomerization (4-2) was suggested.

$$CFCF_3 \rightarrow C_2F_4 \qquad (4\text{-}2)$$

Detection of octafluoro-2-butene indicates reaction products of hexafluoropropene undergo extensive recombination, as observed in many thermal bulk experiments.[3,4]

The UV absorption spectrum of hexafluoropropene has not been measured except for the narrow wavelength range from 185 - 210 nm.[5] Over this wavelength range, the product CF_2 was monitored by UV absorption spectroscopy and its quantum yield was found to be 1.0. In addition, from the structureless absorption spectra of C_3F_6, excitation to a repulsive electronic state and dissociation within 100 femtoseconds was predicted for reaction 4-1. Recently the formation of F atoms, via reaction 4-3, in the 193 nm

photolysis of hexafluoropropene in a mixture containing hexafluoropropene was suggested.[6]

$$C_3F_6 \rightarrow F + C_3F_5 \qquad (4\text{-}3)$$

The quantum yield for this reaction was not measured.

The infrared multiphoton dissociation (IRMPD) of hexafluoropropene has been previously studied using photofragment translational spectroscopy and is fully discussed in Chapter Three. Simple bond rupture of the carbon-carbon single bond (4-4) was observed with an activation energy estimated at 100-105 kcal/mol.

$$C_3F_6 \rightarrow CF_3 + C_2F_3 \qquad (4\text{-}4)$$

In addition, CF_2 was a primary dissociation product, however, the identity of its momentum matched partner was unclear. The formation of either trifluoromethylfluorocarbene (4-1) or tetrafluoroethylene (4-5) with CF_2 was thermodynamically feasible.

$$C_3F_6 \rightarrow C_2F_4 + CF_2 \qquad (4\text{-}5)$$

Reaction 4-1 results from direct cleavage of a carbon-carbon double bond while reaction 4-5 requires a fluorine migration or isomerization before the final products are formed. Breaking a carbon-carbon double bond has been previously observed in the photolysis of tetrafluoroethylene.[7] In that experiment $^1CF_2$ and $^3CF_2$ were the only products observed by photofragment translational spectroscopy. The results of the photodissociation of hexafluoropropene at 193 nm should allow us to determine the relative importance of C-F bond rupture in comparison with cleavage of the carbon-carbon double or single bond. A recent kinetics experiment has identified C_2F_3 as a photolysis product of C_3F_6 indicating

that simple bond rupture does take place.[8] Furthermore, comparing the UV and IRMPD dissociation pathways will give information about direct versus thermal-type dissociation, where direct dissociation involves an excited electronic state and thermal-type dissociation occurs on the ground potential energy surface. If the dynamics from both the UV and IRMPD studies are similar, it implies that UV dissociation proceeds via internal conversion to the ground state.

4.2. Experimental Section

These experiments were performed on the Taiwan rotating source molecular beam machine that has been previously described in Chapters 1 and 3. Conditions similar to those in the IRMPD experiment (see Chapter 3) were used, except that a Lambda Physik EMG 101 Excimer laser operating on the ArF transition (193 nm) crossed the molecular beam at the interaction region instead of a CO_2 laser. The laser was unpolarized in the time-of-flight spectra measurements used to obtain the translational energy. A linear power dependence was measured up to 25 mJ/pulse, indicating the observed signal results from single-photon dissociation. To obtain the anisotropy parameter (β), the unpolarized light from the Excimer laser was passed through a stacked pile of 8 fused-silica plates at Brewster's angle, resulting in 85% polarized light.[9] The polarization angle was determined using a half-wave retarder. Typical polarization measurements were obtained at two polarization angles that were parallel and perpendicular to the center-of-mass velocity of the product.[10] This resulted in the greatest difference in product intensity,

allowing a minimum number of measurements at the necessarily low laser power (10 mJ/pulse) used to avoid saturation effects.

4.3. Results and Analysis

4.3.1. $C_3F_6 \rightarrow C_3F_5 + F$. Unambiguous evidence for the fluorine atom elimination channel is found in the time-of-flight spectrum for $C_3F_5^+$ (*m/e* = 131) shown in Figure 4-1a. The time-of-flight spectrum in Figure 4-1b from $C_3F_4^+$ (*m/e* = 112) results entirely from fragmentation of C_3F_5 in the electron impact ionizer. The difference in the slow edge of these two features results from the high molecular beam background at C_3F_5, which makes subtraction of the background problematic. At the low laser powers (~25 mJ/pulse) used, no useful signal was observed from the fluorine atom (*m/e* = 19). This is attributed to the low ionization cross-section of the fluorine atom as well as the high background at *m/e* = 19, mainly from the leakage of *m/e* = 18 (H_2O^+) in the quadrupole mass spectrometer. The translational energy distribution shown in Figure 4-2 is peaked well away from zero, and the average energy is 17.7 kcal/mol.

The polarization dependence for *m/e* = 131, measured at two angles, is shown in Figure 4-3a. The value of the anisotropy parameter, β, in the well-known electric dipole expression (4-6) can range from -1 to 2 for totally perpendicular or parallel transitions, respectively.[11]

$$I(\theta) = (1/4\pi)[1 + \beta P_2(\cos\theta)] \qquad (4\text{-}6)$$

In equation 4-6, θ is the angle between the electric vector of the laser and the center-of-mass velocity vector of the products, and $P_2(\cos\theta)$ is the second degree Legendre polynomial. An overall anisotropy parameter of -0.32 was determined. Taking into account the use of only 85% polarized light gives a β parameter of -0.44.[12]

4.3.2. $C_3F_6 \rightarrow CFCF_3/C_2F_4 + CF_2$ The time-of-flight spectrum of *m/e* = 100 ($CFCF_3^+/C_2F_4^+$) in Figure 4-1c reveals a fast component that cannot be attributed to the fragmentation of slower C_3F_5. The translational energy distribution for this channel (Figure 4-2) is peaked near 7 kcal/mol, with an average of 9.6 kcal/mol. The contribution of C_3F_5 at this mass is found to be negligible. If any portion of this spectrum is attributed to *m/e* = 131, the signal observed at the momentum matched partner CF_2 (Figure 4-4c) cannot be completely explained. A slight polarization dependence for this reaction is also observed with an anisotropy parameter, β, of 0.15 (Figure 4-3b). This value is corrected to 0.22 as above.

4.3.3. $C_3F_6 \rightarrow CF_3 + C_2F_3$. The time-of-flight spectra for *m/e* = 81 ($C_2F_3^+$), *m/e* = 69 (CF_3^+), and *m/e* = 50 (CF_2^+) are shown in Figure 4-4. The $C_2F_3^+$ (Figure 4-4a) signal consists of fragmentation from *m/e* = 100 and *m/e* = 131 as well as a contribution from a third primary channel. The decision to include a third primary channel was based on the time-of-flight spectrum of *m/e* = 69 (CF_3^+) that is shown in Figure 4-4b. The slow products observed in the time-of-flight distribution could not be completely explained by contributions from fragmentation of $C_3F_5^+$ and $CF_3CF^+/C_2F_4^+$, but including the third channel gives a good total fit. The translational energy distribution resulting from this

third channel, a simple C-C bond rupture, is peaked near zero with an average of 2.2 kcal/mol. As illustrated in Figure 4-4c, the signal at m/e = 50 can be completely explained using these three primary channels.

4.4. Discussion

A summary of possible channels in hexafluoropropene dissociation at 193 nm is shown in Figure 4-5.[13] The branching ratio[14], CF_2:F:CF_3, is 1.0:0.75:0.35 at 25 mJ/pulse. The uncertainty in this ratio is approximately ± 0.2 for each channel. This uncertainty results from the poor signal-to-noise ratio at this laser power, the difficulty in assignment of parent ion fragmentation, and the previously mentioned limitations on fluorine atom detection. The identity of the products of reactions 4-3 and 4-4 are straightforward. In reaction 4-3, the elimination of a fluorine atom allows for determination of the bond dissociation energy. For the CF_2 loss channel, the chemical composition of the momentum matched partner to CF_2 is C_2F_4. There are two possible isomers, tetrafluoroethylene (C_2F_4) or trifluoromethylfluorocarbene ($CFCF_3$). In addition, formation of both $^1CF_2$ and $^3CF_2$ with either of these isomers is energetically possible at 193 nm. A discussion of which of the possible dissociation pathways best agrees with the data obtained follows.

4.4.1. Bond Dissociation Energies. From the conservation of energy an estimate of the bond dissociation energy for a reaction channel can be obtained from these photofragment translational spectroscopy experiments by using Equation 4-7.

$$E_{int}(\text{reactant}) + E_{h_\nu} = D^o + E_T + E_{int}(\text{products}) \qquad (4\text{-}7)$$

If the internal energy of the reactant is assumed to be minimal and the maximum translational energy corresponds to products with no internal energy, a simple calculation (4-8) gives the bond dissociation energy.

$$D^{o} = E_{h\nu} - E_{T}(max) \qquad (4\text{-}8)$$

For reaction 4-3, Equation 4-8 gives a C-F bond dissociation energy of 121 kcal/mol for hexafluoropropene. The uncertainty in this value is at least ± 2 kcal/mol, however it compares favorably with an estimate for D^{o}(C-F) in tetrafluoroethylene of 125 kcal/mol.[15] In addition, the existence of this F-atom elimination channel, not observed in any IRMPD or thermal experiments, indicates that this dissociation process takes place on an excited potential energy surface. For the other channels, CF_2 and CF_3 loss, that form two polyatomic species, the use of Equation 4-8 to find the bond dissociation energy is not as reliable, since both fragments can contain significant amounts of internal energy.

4.4.2. Anisotropy Parameters. The anisotropy parameters observed for CF_2 loss (0.22) and fluorine atom loss (-0.44) are less than that expected for a predominantly perpendicular (-1.0) or parallel (2.0) transition. Many factors can reduce the polarization effect in a large polyatomic molecule such as hexafluoropropene, including laser saturation, rotation before dissociation, the product recoil direction, and simultaneous excitation of two electronic transitions to give one product channel.[16] Saturation of the transition should not occur at the minimal laser power used (10 mJ/pulse) for the anisotropy measurements. In the event of predissociation (as opposed to direct dissociation) from an excited state of hexafluoropropene, rotational averaging effects could be significant. The simultaneous excitation of two electronic transitions leading to

two different product channels is a very probable explanation of the difference in the sign of the β parameter. However, as the electronic surface(s) involved at 193 nm are unknown, further speculation on the likelihood of multiple electronic excitations decreasing the anisotropy are meaningless. A long (on the order of a rotational period) excited state lifetime before dissociation is the most reasonable explanation for the weak anisotropy observed.

4.4.3. Comparison with the IRMPD experiment. In both the IRMPD (Chapter Three) and these UV experiments, CF_2 loss and CF_3 loss were observed. In Figure 4-6 is a comparison of the translational energy distribution obtained for the simple bond rupture reaction (4-4). The translational energy distribution for CF_3 loss from the UV dissociation of hexafluoropropene lies between the two extremes of the range of translational energy distributions determined from CF_3 loss in the IRMPD of hexafluoropropene. This confirms that internal conversion to the ground state occurs before the C-C single bond breaks.

The translational energy distributions for the loss of CF_2 are compared in Figure 4-7. As discussed in Chapter Three because the m/e = 100 fragment undergoes further dissociation in the IRMPD experiment it is biased towards the faster fragments. A range of distributions were determined using m/e = 50. The translation energy derived from the UV experiments lies in this range. This also indicates that CF_2 loss occurs after internal conversion to the ground state. Competition between CF_3 loss and CF_2 loss is expected on the ground potential energy surface as shown by the IRMPD experiments. A branching ratio, $[CF_2]/[CF_3]$ of 4.0 for the IRMPD experiments contrasts to one of 2.9 for

the UV experiment. Internal conversion likely occurs to a higher level on the ground potential energy surface where the larger A factor for CF_3 loss begins to affect the branching ratio.

At first glance, internal conversion and observation of a non-zero anisotropy parameter seem incompatible. However, if the rate of internal conversion is fast the anisotropy resulting from the initial laser excitation could extend to the products. Internal conversion rates can vary from at least 1 ps to 10 μsec.[17] In the UV dissociation of cyclohexene a slight polarization dependence (β = -0.21) was measured. The products, butadiene and ethylene, were assigned to a ground state dissociation following rapid internal conversion.[18] In our overall picture of the dissociation process, hexafluoropropene is initially excited to two different electronic states. Dissociation from one electronic state results in F atom and C_3F_5 formation, while the other electronic state undergoes rapid internal conversion to produce the ground state products CF_3, C_2F_3, CF_2, and C_2F_4.

4.4.4. Reaction Mechanisms. Although Zewail and co-workers have observed hydrogen migrations taking as little as 60 femtoseconds,[19] migration of the much heavier fluorine atom would not be expected to occur on such a short time scale. However, it may be possible for a fluorine migration to take place on the same time scale as internal conversion. Predissociation of hexafluoropropene to the products trifluoromethylfluorocarbene or tetrafluoroethylene and $^1CF_2$ are both consistent with our experimental observations. The translational energy distribution is peaked at 7 kcal/mol which suggests an exit barrier in the reaction channel. As discussed in Chapter Three

Section 3.4.1, this exit barrier could result from the electron pairing energy gained to form two singlet species (CF_2 and $CFCF_3$) or from the formation of the closed shell species tetrafluoroethylene.

There are still three other reactions that are energetically accessible at 193 nm (see Figure 4-5). The formation of $^3CF_2$ with trifluoromethylfluorocarbene or tetrafluoroethylene is possible. There is no distinct evidence for either of these channels and a third electronic excited state would have to be involved. However, to confirm the minor roles of these channels, phosphorescence from the photolysis products of hexafluoropropene should be measured. Similar experiments have been performed on tetrafluoroethylene.[8] Production of three $^1CF_2$ fragments is another possible channel, but the time-of-flight spectrum for CF_2 can be explained without any contributions from this channel. Moreover, this process, which involves a fluorine migration, is likely to have a barrier on the order of 20 kcal/mol and be inaccessible at 193 nm.[20]

4.5. Conclusions

Three primary channels have been observed in the UV photolysis of hexafluoropropene. F atom elimination (4-3) is unique to photolysis and thus indicates an as yet uncharacterized excited state is involved in the dissociation processes. Comparison of the UV and IRMPD experiments suggest involvement of a second uncharacterized electronic state from which rapid internal conversion takes place. Competition between the simple bond rupture channel (4-4) and CF_2 loss takes place on the ground potential energy surface.

References and Notes

[1] F. W. Dalby, J. Chem. Phys. **41**, 2297 (1964).

[2] J. Heicklen and V. Knight, J. Phys. Chem. **69**, 3600 (1965).

[3] B. Atkinson and A. B. Trenwith, J. Chem. Soc. 2082 (1957).

[4] N. N. Buravtsev, A. S. Grigor'ev, and Y. A. Kolbanovskii, Kinetics and Catalysis **30**, 13 (1989).

[5] S. Sharpie, B. Hartnett, H. S. Sethi, and D. S. Sethi, J. Photochem. **38**, 1 (1987).

[6] A. McIlroy and F. P. Tully, J. Phys. Chem. **97**, 610 (1993).

[7] T. K. Minton, P. Felder, R. C. Scales, and J. R. Huber, Chem. Phys. Lett. **164**, 113 (1989).

[8] F. Battin-Leclerc, T. P. Murrells, A. P. Smith, and G. D. Hayman, Accepted Faraday Transactions, May 1996.

[9] Y. R. Lee, C. L. Chiu, and S. M. Lin, J. Chem. Phys. **100**, 7376 (1994).

[10] P. Felder, Chem. Phys. **155**, 435 (1991).

[11] R. N. Zare, Mol. Photochem. **4**, 1 (1972).

[12] M. Dzvonik, S. Yang, and R. Bersohn, J. Chem. Phys. **61**, 4408 (1974).

[13] The heats of formation at 298 K were obtained from the following sources: C_3F_6, -268.9 ± 2 kcal/mol and $^1CF_2$, -44.2 ± 1 kcal/mol, D. S Bomse, D. W. Berman, and J. L. Beauchamp, J. Am. Chem. Soc. **103**, 3967 (1981); C_2F_4, -157.4 ± .7 kcal/mol, J. Phys. Chem. Ref. Data, **14**, Supplement 1, 655 (1985); $CFCF_3$, -140.4 ± 2 kcal/mol, reference

4; $^3CF_2$, 12.4 kcal/mol, S. Koda,. Chem. Phys. Lett. **55**, 353 (1978); Chem. Phys. **66**, 383 (1982); F, 18.86 kcal/mol, D. R. Stull and H. Prophet, JANAF Thermochemical Tables, Natl. Stand. Ref. Data Ser., U.S. Natl. Bur. Stand. No. 37, U.S. Gov. Printing Office: Washington, DC,1971. A value for C_3F_5 of -167 ± 4 kcal/mol can be estimated from our C-F bond dissociation energy of 121 kcal/mol.

[14] For a complete description of obtaining branching ratios from photofragmentation translational spectroscopy experiments see J. D. Myers, Ph. D. Thesis, University of California, Berkeley (1993).

[15] W. M. D. Bryant, J. Polymer Sci. **56**, 277 (1962).

[16] T. K. Minton, G. M. Nathanson, and Y. T. Lee, J. Chem. Phys. **86**, 1991 (1987).

[17] N. J. Turro, *Modern Molecular Photochemistry*; Benjamin/Cummings Pub. Co., Inc.: Menlo Park, Ca; 1978; pp 180 - 185.

[18] X. Zhao, R. E. Continetti, A. Yokoyama, E. J. Hintsa, and Y. T. Lee, J. Chem. Phys. **91**, 4118 (1989).

[19] J. L. Herek, S. Pedersen, L. Banares, and A. H. Zewail, J. Chem. Phys. **97**, 9046 (1992).

[20] B. E. Holmes, D. J. Rakestraw, J. Phys. Chem. **96**, 2210 (1992).

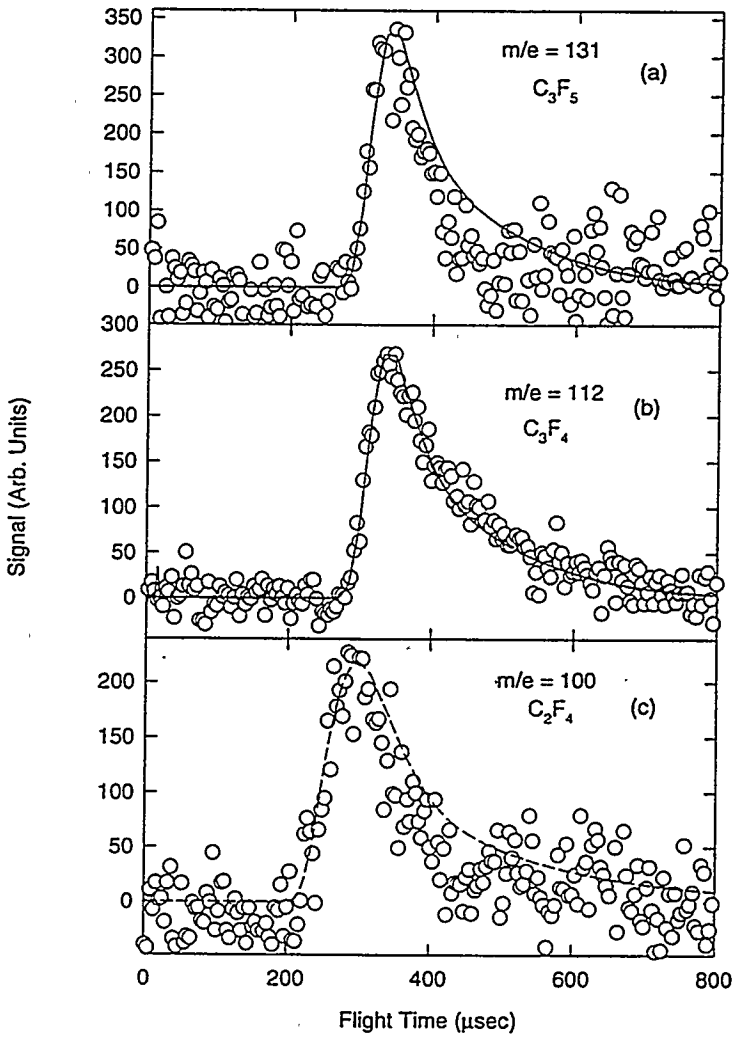

Figure 4-1. Time-of-flight spectra for the heavy *m/e* fragments from the UV photolysis of hexafluoropropene. (a) The circles are the data points and the line is the fit to *m/e* = 131 ($C_3F_5^+$) at 20°. The derived translational energy distribution is shown in Figure 4-2. (b) Time-of-flight spectrum for *m/e* = 112 ($C_3F_4^+$) at 20° resulting from fragmentation of *m/e* = 131. (c) Time-of-flight spectrum for *m/e* = 100 ($CFCF_3^+/C_2F_4^+$) at 20°. A second primary channel is represented by the dashed line.

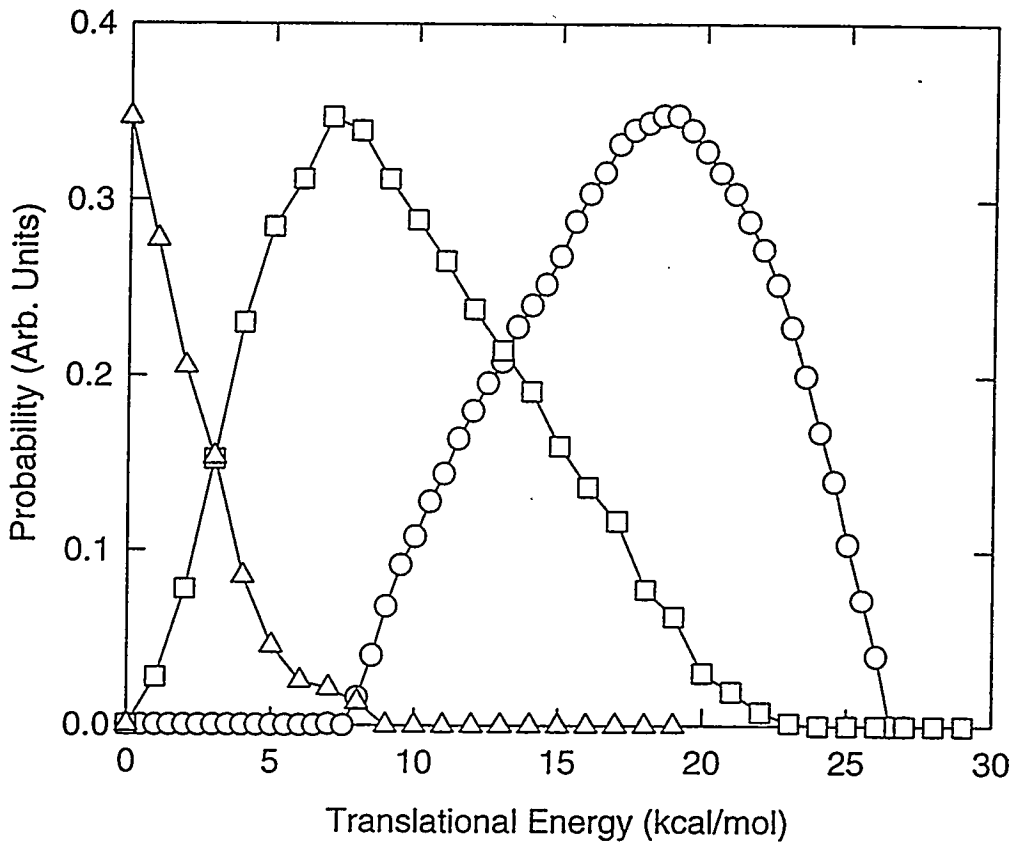

Figure 4-2. Center-of-mass translational energy distributions derived from the time-of-flight data in Figures 4-1 and 4-3. The open squares represent the CF_2 loss channel while the open circles indicate the range of translational energy resulting from the fluorine atom elimination channel. The simple bond rupture channel results in the distribution shown by the open triangles.

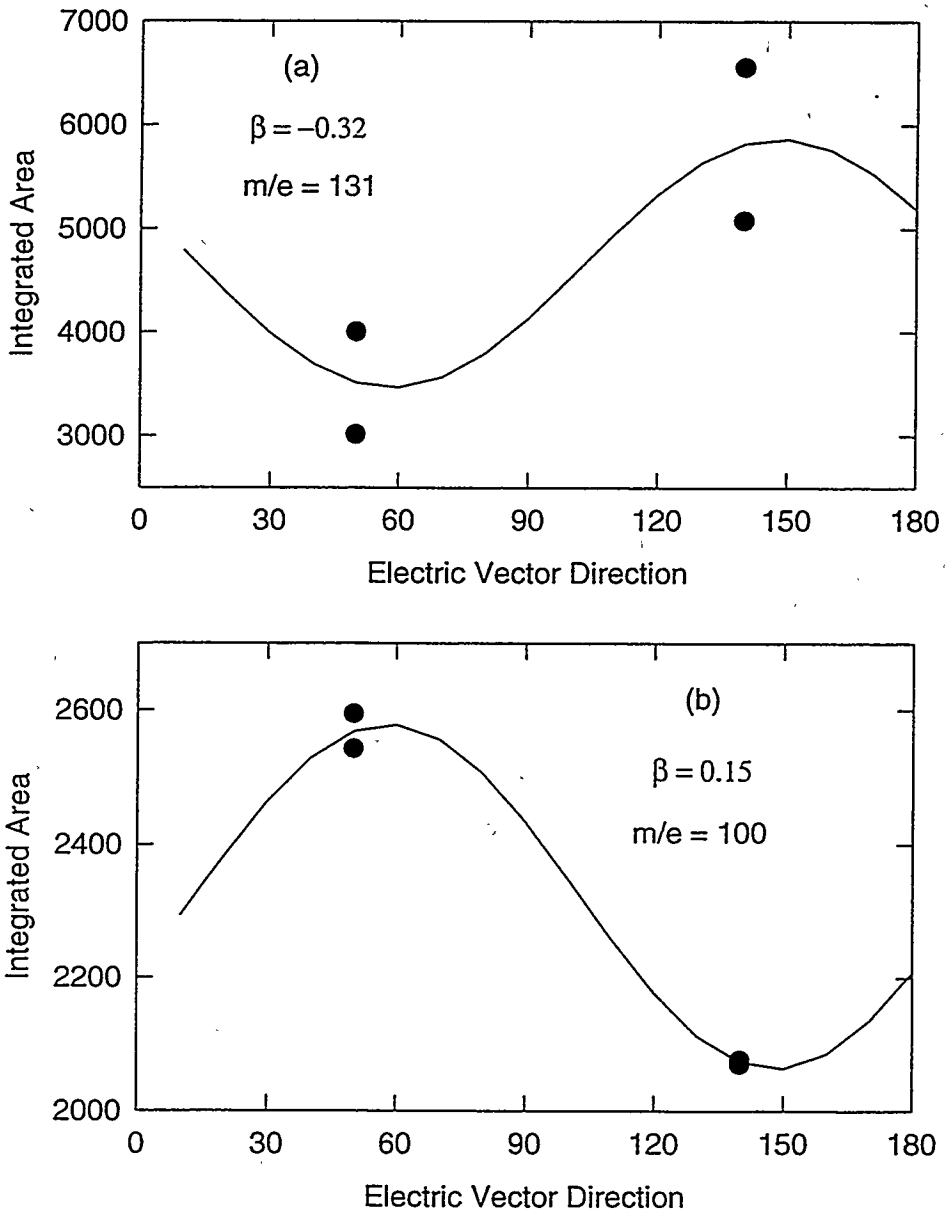

Figure 4-3. Polarization dependence measurements. (a) The fluorine atom channel shows a perpendicular polarization dependence with an uncorrected β value of -0.32. (b) The polarization dependence for *m/e* = 100 indicates a parallel transition with β = 0.15.

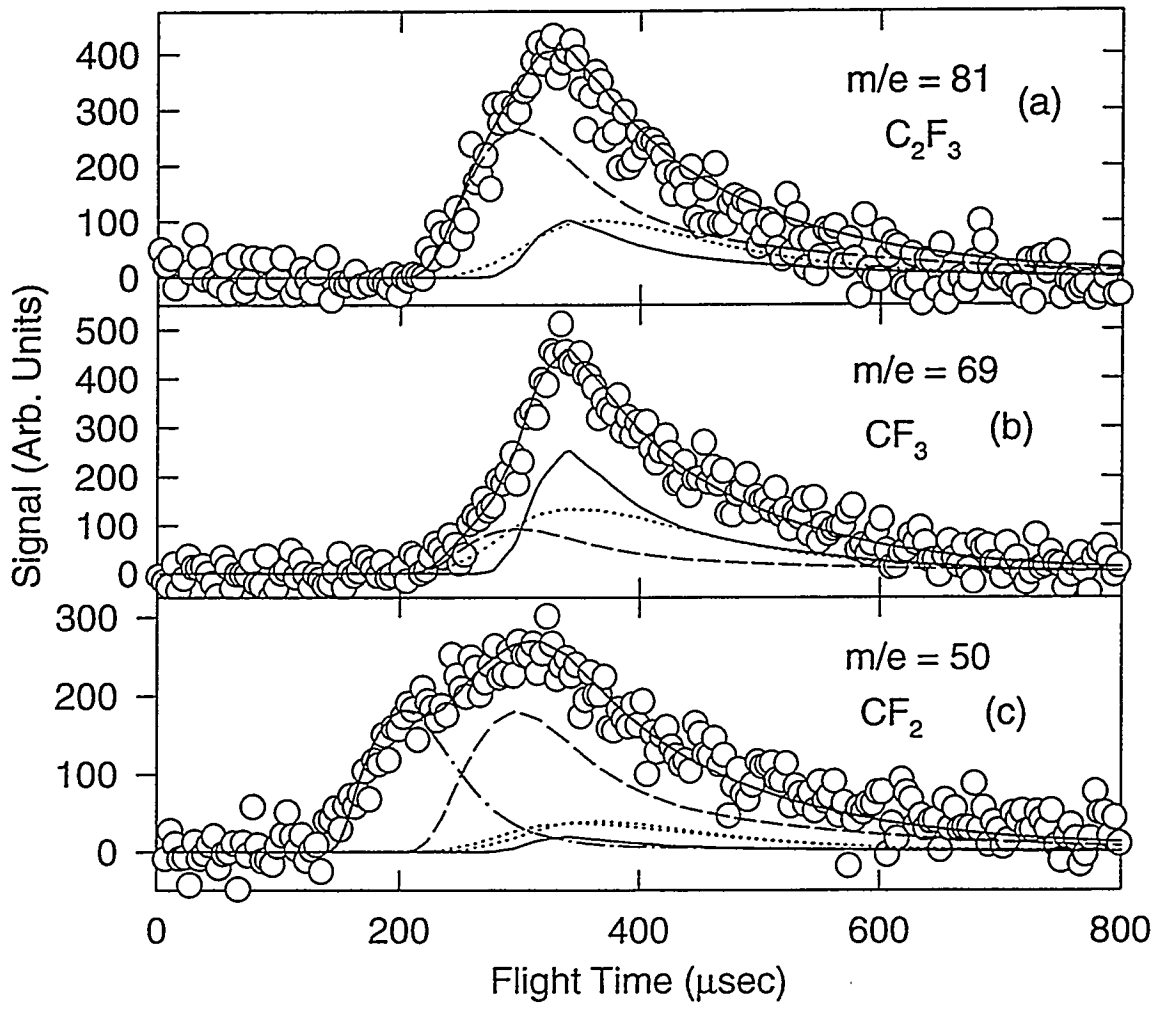

Figure 4-4. Time-of-flight spectra for lower molecular weight products at 20°. (a) The time-of-flight spectrum for *m/e* = 81 ($C_2F_3^+$) has a contribution from *m/e* = 131 (solid line), *m/e* = 100 (dashed line), and a third contribution (dotted line) from reaction 4-4, which produces C_2F_3 directly. (b) The contributions at *m/e* = 69 (CF_3^+) include fragmentation of *m/e* = 131 (solid line), *m/e* = 100 (dashed line) and the momentum matched partner to C_2F_3 (dotted line) from reaction 4-4. (c) The predominant contributions at *m/e* = 50 (CF_2^+) are from the fragmentation of *m/e* = 100 (dashed line) and its momentum matched partner, CF_2, which is represented by the dash-dot-dash line. Possible contributions from both products of reaction 4-4 are shown by the dotted lines.

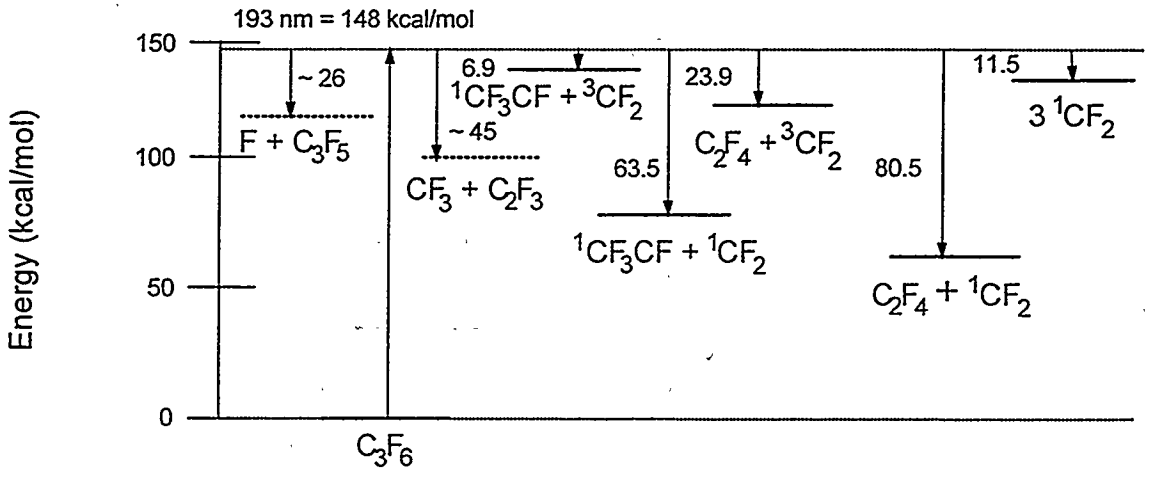

Figure 4-5. Energy level diagram for hexafluoropropene. Possible dissociation pathways and the maximum amount of energy available for translation are shown. The amount of energy available for reaction 4-3 is found in this experiment (see text) while the estimate for reaction 4-4 is from previous studies using IRMPD.[7]

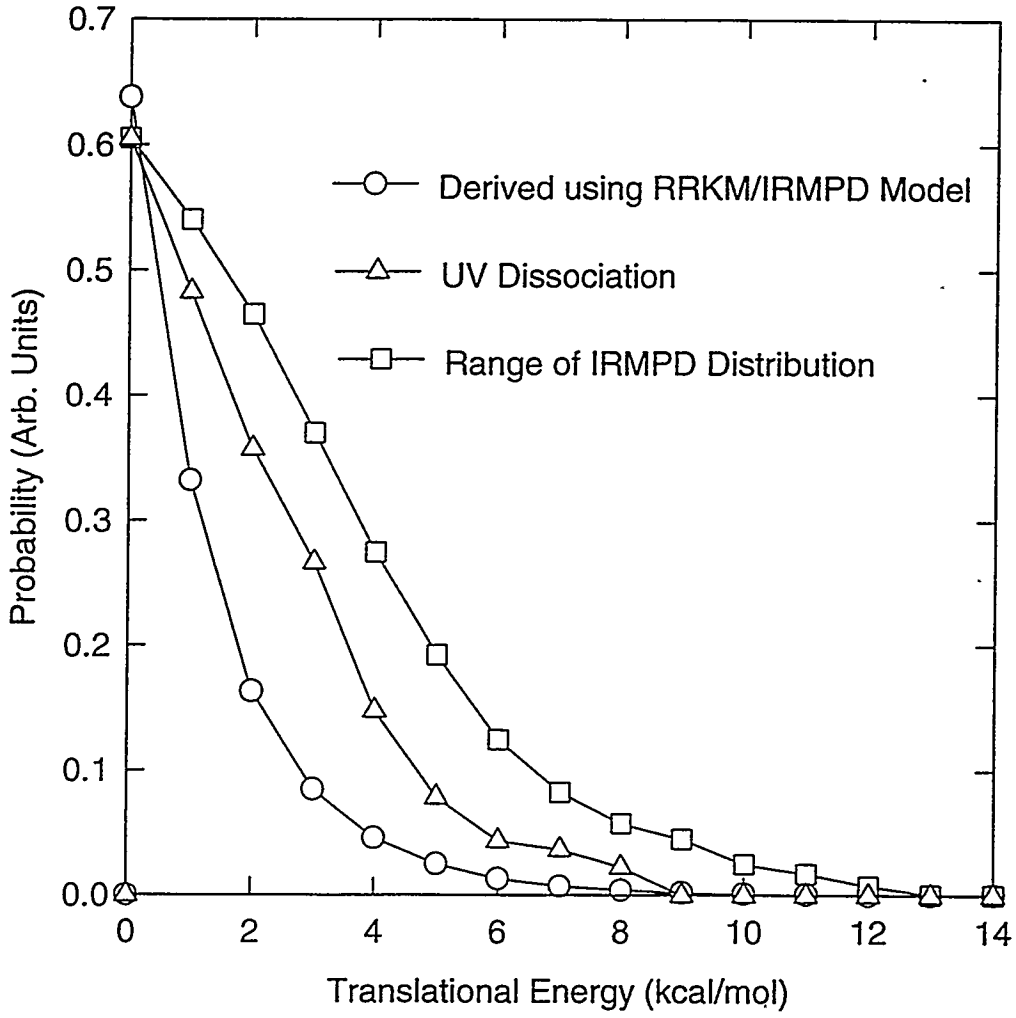

Figure 4-6. Translational energy distributions from IRMPD and UV experiments for CF_3 + C_2F_3. The open circles are from the RRKM/IRMPD calculation in Chapter Three. The open triangles represent the translational energy distribution from Figure 4-2. The open squares represent the limiting translational distribution obtained from the IRMPD experiments.

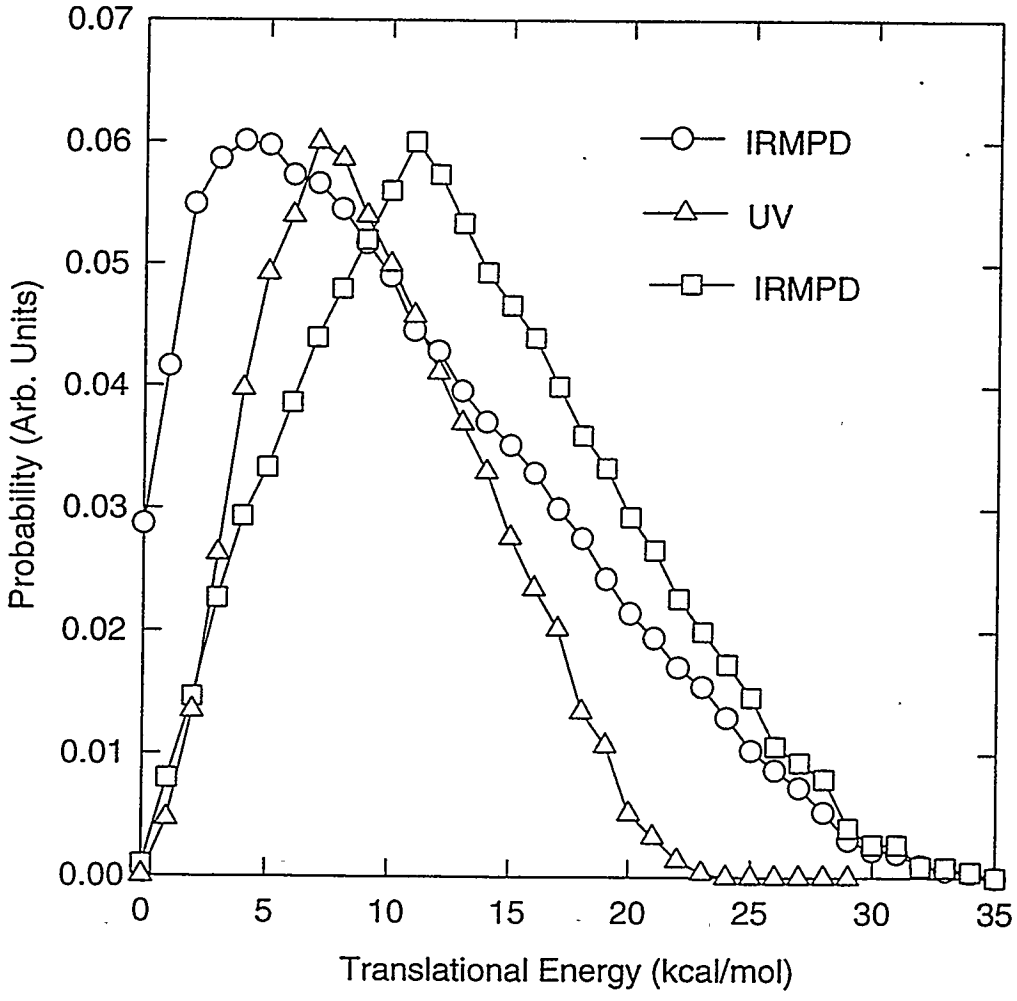

Figure 4-7. Similar to Figure 4-6, the translational energy distributions for CF_2 loss from the IRMPD and UV experiments are plotted together. The open circles and open squares represent the range determined by the IRMPD experiment. The open triangles are the translational energy distribution from Figure 4-2.

Chapter 5

Infrared Multiphoton Dissociation of Two Perfluorobutenes

5.1. Introduction

The fluorocarbon series of tetrafluoroethylene, hexafluoropropene and octafluorobutene all have in common a single unsaturated site and complete fluorination. It is of fundamental chemical interest to examine whether this series of compounds exhibits similar chemical behavior when exposed to heat, light, or other perturbations. Our focus is on elucidating the possible chemical pathways in thermal-type dissociations under collisionless experiments. No successful IRMPD experiments have been carried out on tetrafluoroethylene because it does not absorb IR radiation within the range of the CO_2 laser (9-11μm). In Chapter Three of this thesis IRMPD experiments on hexafluoropropene were described. The major dissociation products were CF_2, CF_3, C_2F_3 and C_2F_4.

Although tetrafluoroethylene has not been investigated using IRMPD, its thermal decomposition has generated a great deal of speculation as to the identity of the intermediate species involved. According to its Materials Safety and Data Sheet, combustion of tetrafluorethylene without oxygen, produces carbon and carbon tetrafluoride.[1] This cannot be ascribed to a unimolecular reaction. Figure 1-2 in Chapter One illustrates how C_2F_4 polymerization can lead to the formation of either octafluoro-1-butene or octafluoro-2-butene. CF_4 elimination from the pyrolysis of one or both of these compounds could explain the C_2F_4 combustion products. The focus of this study is to

investigate these compounds by IRMPD coupled with photofragment translational spectroscopy to determine the primary reaction channels.

An early study on the pyrolysis of tetrafluoroethylene found reaction products such as perfluorocyclobutane, perfluoropropene, perfluoroisobutene, and perfluoroethane.[2] This same experiment found in the pyrolysis of hexafluoropropene that perfluoroisobutene and octafluorocyclobutane were also produced. Another study on the pyrolysis of hexafluoropropene identified octafluoro-2-butene and perfluoroisobutene as the major reaction products with traces of octafluoro-1-butene also present.[3] The production of a white dust, presumably polytetrafluoroethylene, was another product.

An adiabatic compression study of tetrafluoroethylene and hexafluoropropene examined the formation and decomposition of some perfluorobutene compounds in more detail.[4] After compressing either tetrafluoroethylene or hexafluoropropene, the compounds containing four carbon atoms were identified as perfluoroisobutene, perfluorocyclobutane, perfluoro-1-butene, and perfluoro-2-butene. From the rate of formation at different compression values, activation energies for two decomposition reactions of perfluoro-2-butene were obtained. Figure 5-1 shows these possible reaction pathways.

$$C_4F_8 \rightarrow 2\ C_2F_4 \qquad (5\text{-}1)$$

For reaction 5-1, cleavage of the C-C double bond, an activation energy of 99.6 kcal/mol was obtained. This indicates an exit barrier of ~ 35 kcal/mol based on the enthalpy values for these compounds.[5] A second reaction, 5-2, producing CF_2 and hexafluoropropene, requires an activation energy of 90.8 kcal/mol.

$$C_4F_8 \rightarrow C_3F_6 + CF_2 \qquad (5\text{-}2)$$

An exit barrier of 23.8 kcal/mol is predicted for this reaction.

An additional complication is that octafluoro-2-butene can be in either its cis or trans form. The activation energy for trans-cis isomerization of octafluoro-2-butene is 56.4 kcal/mol.[6] The activation energies necessary for reactions 5-1 or 5-2 to take place are well above this isomerization barrier. This implies that the thermal decomposition of these species should be independent of which isomer is initially excited. From the adiabatic compression study,[3] activation energies for these reactions initiated from octafluoro-1-butene were not determined. The barrier to isomerization from octafluoro-1-butene to octafluoro-2-butene is not known. If the dissociation pathways are similar in both octafluoro-1-butene and octafluoro-2-butene this would imply that the barrier to isomerization is less than the barrier for dissociation.

This chapter discusses the use of photofragment translational spectroscopy coupled with IRMPD to identify the major reaction products of octafluoro-1-butene and octafluoro-2-butene. From the measured translational energy distributions, reaction mechanisms can be suggested. The isomerization of octafluoro-1-butene to octafluoro-2-butene or vice versa would confirm that fluorine migration plays a role in these large fluorocarbon systems. In addition, the elimination of CF_4 from either of these compounds would support the hypothesis that C_2F_4 polymerizes to a four carbon species before decomposing to CF_4 and carbon.

5.2. Experimental Section

These experiments were performed on the Berkeley rotating source molecular beam machine that has been described in Chapter One. A 5% mixture of the perfluorobutene[7] of interest in He was passed through a Trickl type pulsed valve.[8] A Lumonics TEA-820 pulsed CO_2 laser was tuned to the P(20) line of the 10.6-μm branch (944 cm^{-1}) and crossed the molecular beam at the interaction region. The laser was typically focused with a 25 cm focal length ZnSe lens to a 2×1.5 mm^2 spot with a laser fluence from 7 to 75 J/cm^2. The fluence was varied by placing a copper screen in the laser path. The fragments created by IRMPD traveled 36.7 cm to the universal detector described in Chapter One. A multichannel scaler triggered by the laser collected the detector counts as a function of the time taken for the fragments to travel from the interaction region to the detector.

A 0.020" nozzle with stagnation pressures ranging from 250 to 600 torr was used to create a supersonic expansion with mean velocity of 900-1000 m/s and a full width at half-maximum (FWHM) spread of ~5 to 6% (speed ratio of 14 to 17). The velocity distribution of molecules in the beam was measured using standard time-of-flight techniques with a spinning slotted wheel.[9] The molecular beam was collimated with two skimmers resulting in an angular divergence slightly less than three degrees. The wide range in backing pressure was used to control the formation of dimers. At lower backing pressures the dimer contribution decreased significantly as will be discussed further in Section 5.3.1.

In a slightly different configuration a heated source identical to that described in Chapter 2 (Figure 2-3) was also used. Because of the lower throughput of the source, the distance between the pulsed valve and the laser was decreased by removing the first skimmer and moving the pulsed valve closer to the interaction region. This created a more intense beam at the interaction region but resulted in a broader angular spread (~4 degrees). The source temperature was varied from 30 to 350°C. A backing pressure of 600 torr was commonly used and the mean velocity of the molecular beam ranged from 1000-1200 m/s with a FWHM of 7 to 10% (s.r. of 14 to 10). The speed ratio at high source temperatures tended to be lower than that for the room temperature source.

5.3. Results and Analysis

Measurements were taken at detector to source angles of 15, 20, 30, 40, and 50 degrees. Dissociation signal was observed at a large number of m/e ratios. The fragmentation of fluorocarbon species in the electron impact ionizer was significant. In a typical experiment, the time-of-flight spectra of all fragments are measured and the conservation of linear momentum is used to identify which products belong to the same channel. This assignment becomes more difficult if each m/e ratio contains contributions from numerous products. In addition, there are fluorocarbons that fragment so extensively in the electron impact ionizer that no parent survives. CF_4 is one such example.[10] The next few sections describe one possible interpretation of the dissociation pathways of octafluoro-1-butene and octafluoro-2-butene, within the limitations described here.

5.3.1. Dimers

In both octafluoro-2-butene and octafluoro-1-butene, dissociation signal at the parent mass showed the presence of dimers in the molecular beam. This was rather unexpected as no dimers were observed in the hexafluoropropene experiments (Chapters Three and Four). In Figure 5-2a is shown a time-of-flight spectrum taken at 10 ° at the parent mass (*m/e* = 200) for octafluoro-2-butene. The signal comes at the same time as the molecular beam background; therefore, it can only be observed by careful shot-to-shot background subtraction. It is also necessary to collimate the molecular beam with two skimmers to observe this signal, which occurs at small source to detector angles. Figure 5-2b is the center-of-mass translational energy distribution resulting from dissociation assuming *m/e* = 400 produces two *m/e* = 200 species. This distribution is peaked at zero and rapidly decreases as would be expected in the dissociation of a very weak van der Waals type bond.

The signal at m/e = 200 for both octafluoro-1-butene and octafluoro-2-butene is identical. For octafluoro-2-butene decreasing the backing pressure from 550 torr to 380 torr caused the dimer signal to be eliminated. However, for octafluoro-1-butene it was necessary to decrease the backing pressure to 200 torr before the signal resulting from dimer dissociation was significantly reduced. This suggests that the dimer bond in octafluoro-1-butene is stronger than in octafluoro-2-butene. Octafluoro-2-butene is a very symmetrical molecule while octafluoro-1-butene may have a larger dipole moment resulting in a stronger dimer bond.

5.3.2. Power Dependence

There is a dramatic difference between the signal observed at low power (25 J/cm^2) and high power (60 J/cm^2) for the lower weight fluorocarbon fragments. An example of this is shown in Figure 5-3 where the signal at *m/e* = 62 (CFCF) increases substantially at higher powers in octafluoro-2-butene dissociation. At the lower power, the signal was collected for twice as long and still was less intense by a factor of 10. In addition to the intensity difference, the shapes of the two peaks are quite different. This indicates that at high laser fluences another reaction channel begins to dominate in the dissociation of octafluoro-2-butene.

In the IRMPD of octafluoro-1-butene the laser fluence again has a dramatic effect on the shape and intensity of the fluorocarbon products. The signal measured for this compound is relatively high compared to octafluoro-2-butene so that it is possible to observe signal not only at 60 J/cm^2 and 25 J/cm^2 but also at 7 J/cm^2. In Figure 5-4 the signal at m/e = 62, CFCF, is shown at these three laser fluences. Again, the dramatic difference in shape and intensity is observed. Any explanation of the dissociation processes in either of these two compounds must account for the remarkable difference in signal intensity and shape at this m/e ratios at higher powers. Besides CFCF, the signal resulting from fluorine atom also increased dramatically with a power increase.

5.3.3. Octafluoro-1-butene

The time-of-flight spectra shown in Figures 5-5, 5-6, 5-7, and 5-8 were taken at 25 J/cm^2 with the one skimmer setup. The signal obtained at *m/e* = 131 ($C_3F_5^+$) shown in Figure 5-5a, is attributed completely to reaction 5-3.

$$C_4F_8 \rightarrow C_3F_5 + CF_3 \qquad (5\text{-}3)$$

A similar time-of-flight distribution is observed for m/e = 112 ($C_3F_4^+$) and is shown in Figure 5-5b, indicating that C_3F_4 results only from fragmentation of C_3F_5 in the ionizer. The momentum matched component to *m/e* = 131 is *m/e* = 69 (CF_3^+), which is shown in Figure 5-7a. The signal at m/e = 69 can be explained assuming contributions from only reaction 5-3.

In Figure 5-6 the time-of-flight spectra for m/e = 100 ($C_2F_4^+$) and m/e = 81 ($C_2F_3^+$) are shown. It is at m/e =100 that the presence of another reaction channel becomes apparent. Initially, the fast edge in Figure 5-6a was taken as evidence for reaction 5-1. However, another possibility is that the products of reaction 5-4 undergo secondary dissociation (5-5).

$$C_4F_8 \rightarrow C_2F_5 + C_2F_3 \qquad (5\text{-}4)$$

$$C_2F_5 \rightarrow C_2F_4 + F \qquad (5\text{-}5)$$

The formation of fast, unique (not from fragmentation) fluorine atoms, Figure 5-8b, supports this hypothesis. The signal at m/e = 81 results solely from fragmentation of m/e = 100. No direct evidence for reaction 5-4 is seen at the m/e ratio of either of its primary

products, C_2F_5 and C_2F_3. However, as illustrated in Figure 5-7b there is a fast component at m/e = 62 ($C_2F_2^+$) that can be attributed to the secondary dissociation of m/e = 81 (5-6)

$$C_2F_3 \rightarrow C_2F_2 + F \qquad (5\text{-}6)$$

The one mass not discussed is m/e = 50 ($CF2^+$) shown in Figure 5-8a, the signal from which can be readily explained as fragmentation of m/e = 69 and m/e = 131.

The translational energy distributions derived from the time-of-flight spectra are shown in Figure 5-9. For the simple bond rupture reaction (5-3) the distribution peaks at zero and slowly decays. The average translational energy release is 3.6 kcal/mol. The translational energy distribution for reaction 5-4 is peaked away from zero at 4.5 kcal/mol and averages 4.0 kcal/mol. There is a high degree of uncertainty in this distribution owing to the complete dissociation of both the primary products. The secondary distribution used to fit both reactions 5-5 and 5-6 peaks at zero with an average of 1.8 kcal/mol. If a less energetic distribution is used for reaction 5-4 the secondary translational energy distribution used to fit m/e = 100 and m/e = 62 creates fluorine atoms faster than observed experimentally.

5.3.4. Alternative Explanations in the Octafluoro-1-butene Dissociation

A large number of dissociation schemes were considered and discarded. In the next few paragraphs a discussion of the more likely possibilities will be presented along with the reasons for rejecting them. First, there is no evidence for reaction 5-2 at this fluence (25 J/cm^2) in the dissociation of octafluoro-1-butene. No signal was observed at m/e = 150, and the signal at m/e = 50 could be fully explained without any contributions from reaction 5-2. Furthermore, if the assumption is made that m/e = 131 results from

fragmentation of m/e = 150, the signal at m/e = 50 does not momentum match, which gives further evidence that reaction 5-2 does not take place. The existence of reaction 5-1 entails a more complicated explanation. Although the fast edge at m/e = 100 can be fit as resulting from two m/e =100 components there is no other evidence to substantiate this claim. If the assumption is made that reaction 5-1 occurs, the origin of the fast signal observed at m/e = 62 and m/e = 19 has to be addressed.

One initial attempt to explain the data observed from octafluoro-1-butene was to assume that both reactions 5-1 and 5-3 were occurring. The m/e = 131 fragment then undergoes further dissociation to m/e = 69 and m/e = 62. This assumption requires that the fast edge of m/e = 62 momentum match to the fast edge of m/e = 69. In order to force the signal at m/e = 62 to be fast and that at m/e 69 to be slow (similar to the data) an anisotropic secondary angular distribution is necessary. This is not a realistic assumption, as the m/e = 131 fragment survives to the detector; this type of anisotropy requires an intermediate with a lifetime much less than its rotational period.[11] In addition, these reactions, 5-1, 5-3, and the secondary dissociation of C_3F_5 cannot explain the fast fluorine atom signal observed.

Another way of explaining the data was to assume that the fast fluorine atoms originated from the secondary dissociation of C_3F_5. This dissociation scheme includes only reactions 5-1 and 5-3. The very front edge of the m/e = 112 time-of-flight spectrum is momentum matched to the fluorine atom signal. However, for m/e = 112 to have a fast edge, the fit to m/e = 131 must be necessarily slightly slower. This leaves the fast edge at m/e = 50 unexplained, as is the fast dissociation signal observed at m/e = 62. If C_3F_4

undergoes further dissociation (tertiary!) the fast edges at m/e = 62 and m/e = 50 can be qualitatively explained.. There are two linear closed shell isomers of m/e = 112, perfluoropropylene and perfluoroallene. To our knowledge, tertiary dissociation in photofragment translational spectroscopy experiments has not been observed before. The reason this fit was rejected is primarily because of the suspicion that tertiary dissociation is highly unlikely.

From the discussion above it should be apparent that the most consistent fit was presented in Section 5.3.4. As mentioned earlier, the initial interest in examining these perfluorobutenes was to determine if CF_4 loss takes place (5-7).

$$C_4F_8 \rightarrow C_3F_4 + CF_4 \qquad (5\text{-}7)$$

As expected no signal was observed at m/e = 88 (CF_4^+) owing to its extensive fragmentation. The predominant fragmentation product of m/e = 88 is m/e = 69,[9] however, no unexplained signal at m/e = 69 was observed. Therefore, the concerted elimination of CF_4 from octafluoro-1-butene does not take place under collisionless conditions.

5.3.5. Octafluoro-2-butene

The signal from octafluoro-2-butene dissociation is much weaker than that from octafluoro-1-butene, consequently the time-of-flight spectra taken at 25 mJ/pulse are not very useful. At m/e ratios such as 131, 69, and 19 the signal/noise is very poor and the spectra cannot be used to ascertain the dissociation pathways. All the time-of-flight spectra discussed below were collected at a fluence of 60 J/cm^2. The time-of-flight

spectrum in Figure 5-10a results from reaction 5-2. The product formed at m/e = 150 ($C_3F_6^+$) cannot completely explain the m/e = 131 ($C_3F_5^+$) time-of-flight spectrum (Figure 5-10b); a contribution from reaction 5-3 is necessary. In Figure 5-13b the fast edge from the m/e = 50 (CF_2^+) spectrum momentum matches with m/e =150. Also, in Figure 5-12b the bulk of the signal observed can be attributed to m/e = 69 (CF_3^+), the momentum matched species to m/e = 131.

In Figure 5-11a the m/e = 112 ($C_3F_4^+$) time-of-flight spectrum can be completely explained as resulting from fragmentation of m/e = 131 and m/e = 150. At m/e = 100 (Figure 5-11b) an additional fast component is evident. This is attributed to reaction 5-1. The signal at m/e = 81 (C_2F_3), shown in Figure 5-12a, is from the fragmentation of m/e = 100, m/e = 131, and m/e = 150. Significant contributions from reaction 5-1 are also observed at m/e = 62 ($CFCF^+$) shown in Figure 5-13a, m/e = 50, and m/e = 19 (F^+) shown in Figure 5-14. In addition, the m/e = 19 time-of-flight spectrum contains fragmentation from m/e = 50.

The translational energy distributions for these three reactions are shown in Figure 5-15. For reaction 5-3, a simple bond rupture, the distribution peaks near zero and averages 2.8 kcal/mol. The average translational energy release for reaction 5-1 is 16.3 kcal/mol while for reaction 5-2 a value of 14.0 kcal/mol is obtained. There is a broad internal energy distribution for the excited molecules formed above the dissociation threshold that depends on the number of photons absorbed. Because of the uncertainty in the total energy absorbed, the maximum translational energy release cannot be used to obtain any bond dissociation energy estimates for either reaction 5-1 or reaction 5-2.

5.3.6. Alternative Explanations in the Octafluoro-2-butene Dissociation

A painstaking effort to impose the octafluoro-1-butene reaction pathways suggested in Section 5.3.3 upon octafluoro-2-butene was made and vice versa. One significant difference (besides the presence of reaction 5-2) was that the signal at m/e = 50 from octafluoro-2-butene dissociation could not be explained as fragmentation from m/e = 69. If the fast contribution at m/e = 100 was assumed to be from secondary dissociation (5-5) instead of from reaction 5-1, forcing this component to be momentum matched with m/e = 19 resulted in unexplained signal at m/e = 50. However, similar to octafluoro-1-butene the presence of reaction 5-7 was not observed.

5.3.7 Branching Ratios and Fluence Dependence

In the dissociation of octafluoro-1-butene at 25 J/cm^2 the predominant channel is CF_3 loss (reaction 5-3). The branching ratio of CF_3:C_2F_3 is 1.0:0.08. At 7 J/cm^2 there is no evidence for any other reaction than 5-3. It was observed that at higher fluences (60 J/cm^2) reaction 5-2 and reaction 5-1 become measurable contributions in the IRMPD of octafluoro-1-butene. However, a unique fit incorporating reactions 5-1, 5-2, 5-3 and 5-4 with secondary dissociation is not possible. A rough branching ratio, C_2F_4:C_3F_5:C_3F_6, estimated from the contributions at the parent masses only (Figure 5-16), is 0.05:1.0:0.01. A distinct fast peak at m/e = 100, the isolated m/e = 150 spectrum, and the assumption that m/e = 131 is completely from reaction 5-3 allows this estimate. The contribution from reaction 5-4 cannot be quantified.

In the octafluoro-2-butene dissociation, the branching ratio C_2F_4:CF_3:CF_2 is 1.0:0.9:0.8. The uncertainty in this branching ratio is on the order of ± 0.3. This large

uncertainty results from the difficulty in assigning fragmentation products. The signal at certain m/e ratios, i.e., m/e = 50, m/e = 62, and m/e = 69, is very intense and changing the proportion of fragmentation at these masses can change the branching ratio significantly. As mentioned earlier, the signal at 25 J/cm^2 is quite weak for this compound. However, judging by the lower weight fragments observed all three reactions are again present at this fluence. Figure 5-17 shows contributions from all three reactions in the time-of-flight spectra of m/e = 69, m/e = 62, and m/e = 50. A rough branching ratio, C_2F_4:CF_3:CF_2, of 0.06:1.0:0.47 is obtained. At this low fluence, reaction 5-3 appears to dominate in the IRMPD of octafluoro-2-butene.

5.4. Discussion

In the IRMPD of octafluoro-1-butene, reaction 5-3 is the only channel observed at low fluences (7 J/cm^2), and continues to be the predominant channel (>90%) at high fluences (25 and 60 J/cm^2). This is markedly different from the IRMPD of octafluoro-2-butene. At 7 J/cm^2 no signal is observed, while at 25 J/cm^2 reactions 5-1, 5-2 and 5-3 are detected. Reaction 5-3 accounts for roughly 65% of the observed signal but this decreases to ~33% at 60 J/cm^2, with reaction 5-1 accounting for 37 % and reaction 5-2 the remainder. In the following sections the reasons for these differences will be explored.

5.4.1. Resonance Stabilization

The loss of CF_3 from octafluoro-1-butene results in the formation of the fluorinated allyl radical (Figure 5-18a). The fluorinated allyl radical is formed in a single step by

simple bond rupture, as evidenced by the slow translational energy distribution (Figure 5-9). The π molecular orbitals overlap in this allyl-like radical, resulting in stronger bonds and greater stabilization than in a system without such overlap. In octafluoro-2-butene the loss of CF_3 results in the formation of a fluorinated propene radical. A 1,3 fluorine migration would be required to form the presumably more stable fluorinated allyl radical. An explanation for the signal observed at such low fluences in the dissociation of octafluoro-1-butene is that it requires much less energy to directly form the resonance stabilized radical than it does to form the fluorinated propene radical. As CF_3 loss continues to dominate the octafluoro-1-butene dissociation at increasingly higher fluences, it must also have a large A-factor, as would be expected in a simple bond rupture reaction.

5.4.2. Octafluoro-2-butene Reaction Mechanisms

Besides CF_3 loss (reaction 5-3) two other reactions occur significantly in octafluoro-2-butene dissociation. Cleavage of the C-C double bond is the most prevalent channel at a fluence of 60 J/cm^2. The translational energy distribution obtained from the reaction products (Figure 5-15) is peaked away from zero at 10 kcal/mol, with an average translational energy release of 16.3 kcal/mol. As discussed in Chapter Three, it requires energy for the excitation of each singlet species to form covalent bonds.[12] The energy gained from electron pairing upon dissociation of the double bond can result in a translational energy distribution peaked away from zero. The singlet-triplet splitting for $CFCF_3$ has been calculated to be 9.2 kcal/mol with the singlet lying lower in energy.[13] If two $^1CFCF_3$ species are formed when the double bond is broken, a translational energy

distribution peaked at 10 kcal/mol would be reasonable. A concerted reaction in which two tetrafluoroethylene molecules are formed is also possible. The repulsion between two closed-shell species would likewise result in a translational energy distribution peaked away from zero.

The third channel present in the IRMPD of octafluoro-2-butene is reaction 5-2, which results in the loss of CF_2. Again the translational energy distribution is peaked well away from zero at ~ 10 kcal/mol. Shown in Figure 5-18c is a possible reaction mechanism for CF_2 loss from this fluorocarbon. A 1,2 fluorine migration followed by rearrangement to form the closed shell species hexafluoropropene takes place. The repulsion between the closed-shell species, hexafluoropropene, and $^1CF_2$ explains the observed translational energy distribution peaked away from zero..

5.4.3. Overall Energetics

From the reactions observed at the varying fluences in octafluoro-1-butene and octafluoro-2-butene, a rough energy level diagram can be sketched. Figure 5-19 is a revised picture of perfluorobutene dissociation. From the extensive signal at low fluence the initial dissociation products of octafluoro-1-butene (CF_3 and the perfluoroallyl radical) must lie lower in energy than those of octafluoro-2-butene. Also the differences in the dissociation pathways indicate that the barrier for isomerization between octafluoro-1-butene and octafluoro-2-butene requires more energy than reaction 5-3. The rough branching ratios from octafluoro-2-butene dissociation indicate that the activation energies increase from reaction 5-3 to reaction 5-2 to reaction 5-1. That reaction 5-1 has a higher activation energy than reaction 5-2 agrees with the previous adiabatic compression experiments.[3] Reaction 5-

4 in the IRMPD of octafluoro-1-butene was primarily proposed because reaction 5-2 was not observed and the fast fluorine atoms could be explained in no other rational manner. If reaction 5-4 takes place, it represents only a small fraction of the reaction products and appears to be insignificant at higher fluences. The relatively small contribution of reaction 5-4 observed at low fluence suggests a small A-factor and an activation energy slightly greater than that for forming CF_3 and the perfluoroallyl radical.

5.4.4. Unsaturation and Perfluorobutenes

As discussed in the introduction to this chapter and in Chapter One, one goal in these fluorocarbon experiments was to explain the explosive decomposition of C_2F_4 to the products CF_4 and carbon. From the IRMPD experiments, no evidence of the direct elimination of CF_4 was observed. Rather, the predominant reaction process in these compounds is CF_3 loss. It is possible that CF_4 can be formed if CF_3 abstracts a fluorine atom from other species in its surroundings. Another possibility is that a different polymerization product of C_2F_4 decomposes to give CF_4. Chapter Three eliminates this possibility for hexafluoropropene as CF_4 was not a dissociation product of hexafluoropropene. In addition, extensive experiments of octafluorocyclobutane have shown the only decomposition products to be C_2F_4 and CF_2.[14] However, perfluoroisobutene has yet to be studied, as its extremely toxic nature makes it difficult to obtain.

Although these experiments did not observe CF_4 elimination, a significant amount of new information was obtained. Of great interest is that not only does an unsaturated site enhance reactivity, but its placement within the molecule is also important. In addition,

direct evidence for a fluorine migration was observed in the loss of CF_2 from octafluoro-2-butene. Finally, at high fluences the time-of-flight spectra for these two molecules begin to share similar characteristics, indicating that the activation barrier for isomerization from octafluoro-1-butene to octafluoro-2-butene is greater than the activation energy for CF_3 loss but close to the activation energy for CF_2 loss.

5.5. Conclusions

Extensive fragmentation of the reaction products was seen in the IRMPD of both octafluoro-1-butene and octafluoro-2-butene. The predominant reaction in octafluoro-1-butene at moderate laser fluences is cleavage of a carbon-carbon single bond to give the products CF_3 and C_3F_5. These products are observed at very low fluences owing to allylic resonance stabilization of the C_3F_5 fragment. In octafluoro-2-butene CF_2 loss and cleavage of the carbon-carbon double bond compete with CF_3 loss. No evidence for the loss of CF_4 was observed in either perfluorobutene.

References and Notes

[1] In addition, the procedure for handling tetrafluoroethylene at the Experimental station for Du Pont discusses the decomposition of tetrafluoroethylene to CF_4 and carbon.

[2] B. Atkinson and V. A. Atkinson, J. Chem. Soc., 2086 (1957).

[3] R. A. Matula, J. Phys. Chem. **72**, 3054 (1968).

[4] N. N. Buravtsev, A. S. Grigor'ev, and Y. A. Kolbanovskii, Kinetics and Catalysis, **30**, 386 (1989).

[5] See Chapters Three and Four for the heats of formation for C_3F_6, CF_2, and C_2F_4. The value for octafluoro-2-butene is from reference 3.

[6] E. W. Schlag and E. W. Kaiser, J. Am. Chem. Soc. **87**, 1171 (1965).

[7] The octafluoro-2-butene purchased from PCR Inc. contained a 50-50 mixture of cis and trans octafluoro-2-butene. Twenty-five grams of octafluoro-1-butene was generously supplied by Dr. M. H. Hung of Du Pont.

[8] D. Proch and T. Trickl, Rev. Sci. Instrum. **60**, 713 (1989).

[9] See, for example, B. A Balko, Ph.D. Thesis, University of California, Berkeley, (1991).

[10] From the *Atlas of Mass Spectral Data*, E. Stenhagen, S. Abrahamsson, and F. W. McLafferty, Eds; John Wiley: NewYork, 1969, Vol. 1, p.153.

[11] S. W. North, C. A. Longfellow, and Y. T. Lee, J. Chem. Phys. **99**, 4423 (1993).

[12] E. A. Carter and W. A. Goddard, J. Phys. Chem. **90**, 998 (1986).

[13] D. A. Dixon, J. Phys. Chem. **90**, 54 (1986).

[14] A. Yokoyama, K. Yokoyama, and G. Fujisawa, Chem. Phys. Lett. 237, 106 (1995). S. M. Lin and Y. R. Lee, Institute of Atomic and Molecular Sciences, Taipei, Taiwan, To be published.

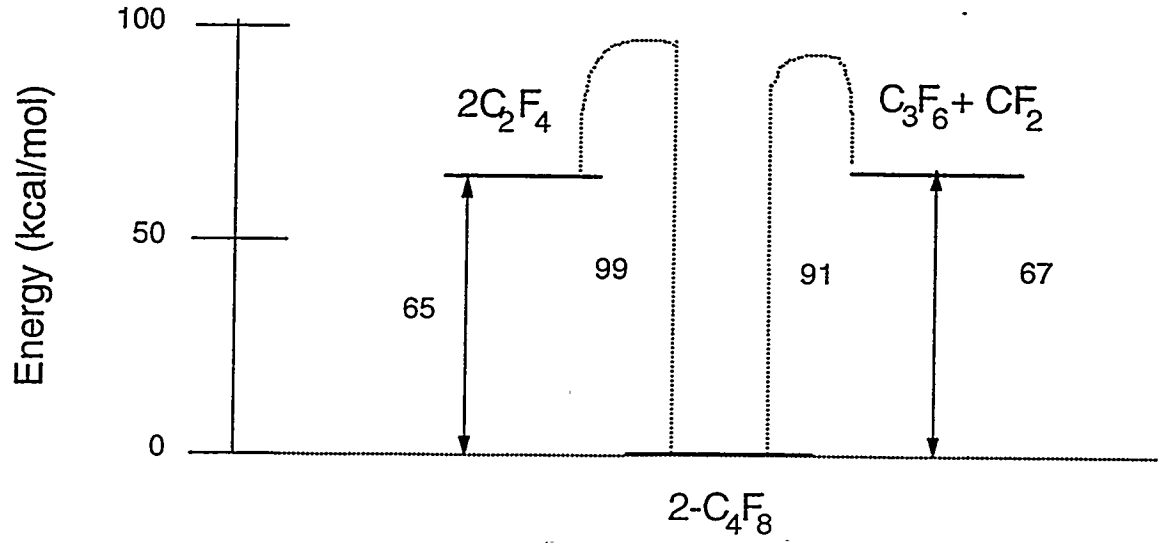

Figure 5-1. Energy level diagram for octafluoro-2-butene. Reactions 5-1 and 5-2 are predicted to have significant exit barriers.

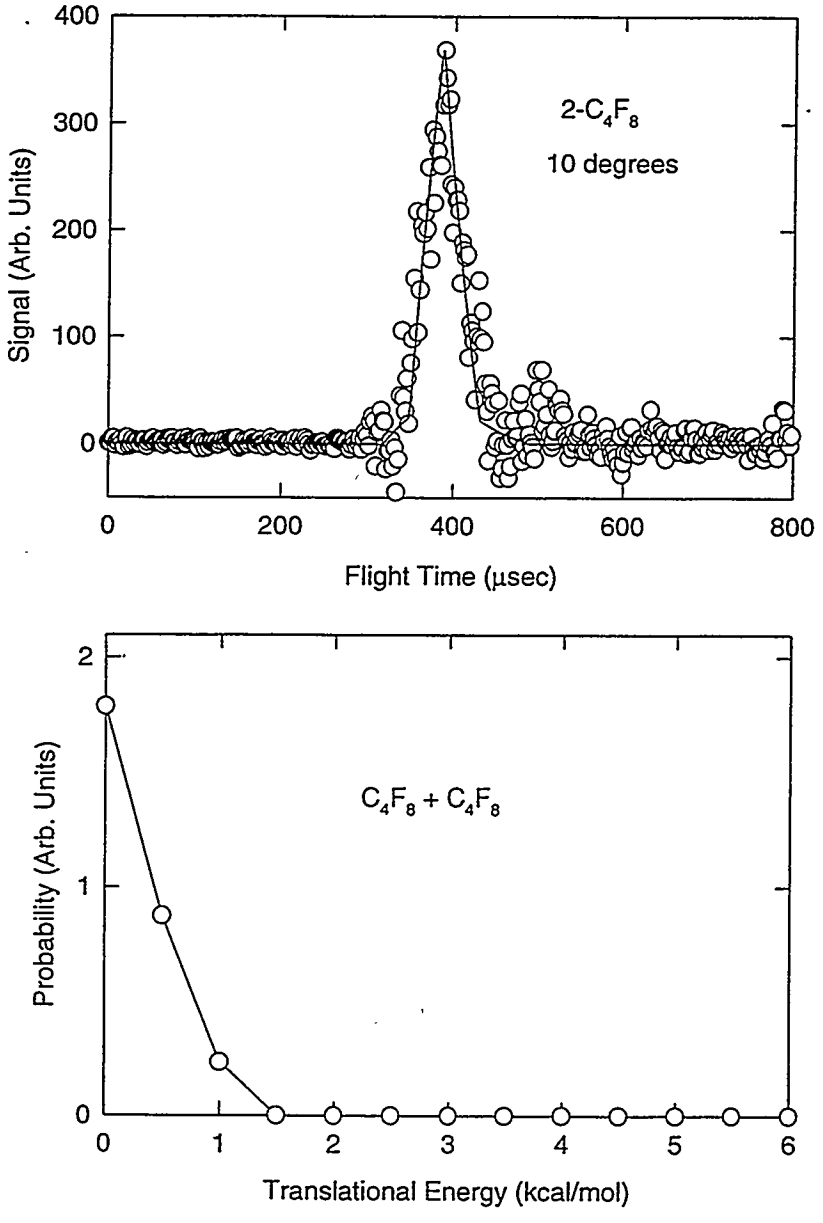

Figure 5-2. (a) Time-of-flight spectrum of octafluoro-2-butene at its parent mass at 10°. (b) Center-of-mass translational energy distribution assuming the parent mass signal results from dissociation of the dimer.

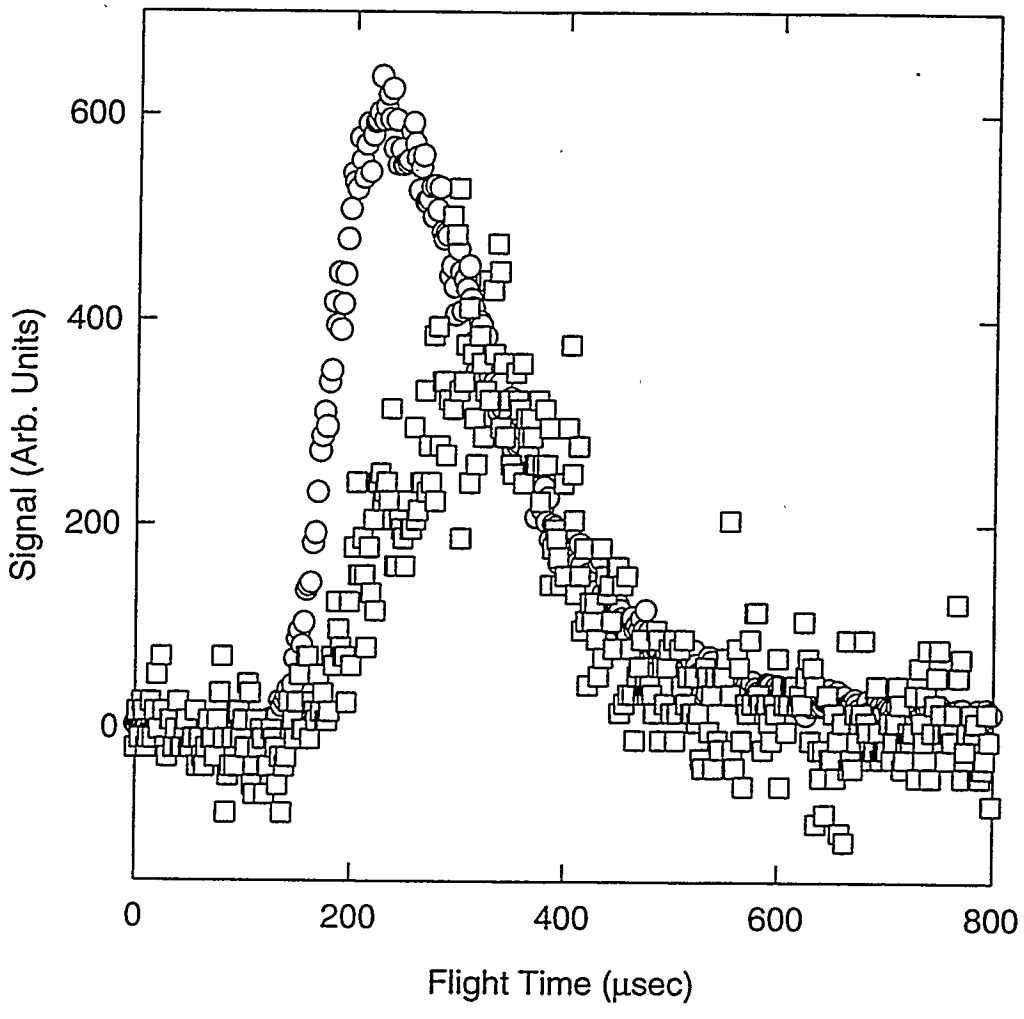

Figure 5-3. Comparison of *m/e* = 62 ($C_2F_2^+$) at two different fluences in octafluoro-2-butene dissociation. The open squares represent the spectrum taken at a 25 J/cm^2 which is displayed with the 60 J/cm^2 spectrum (open circles).

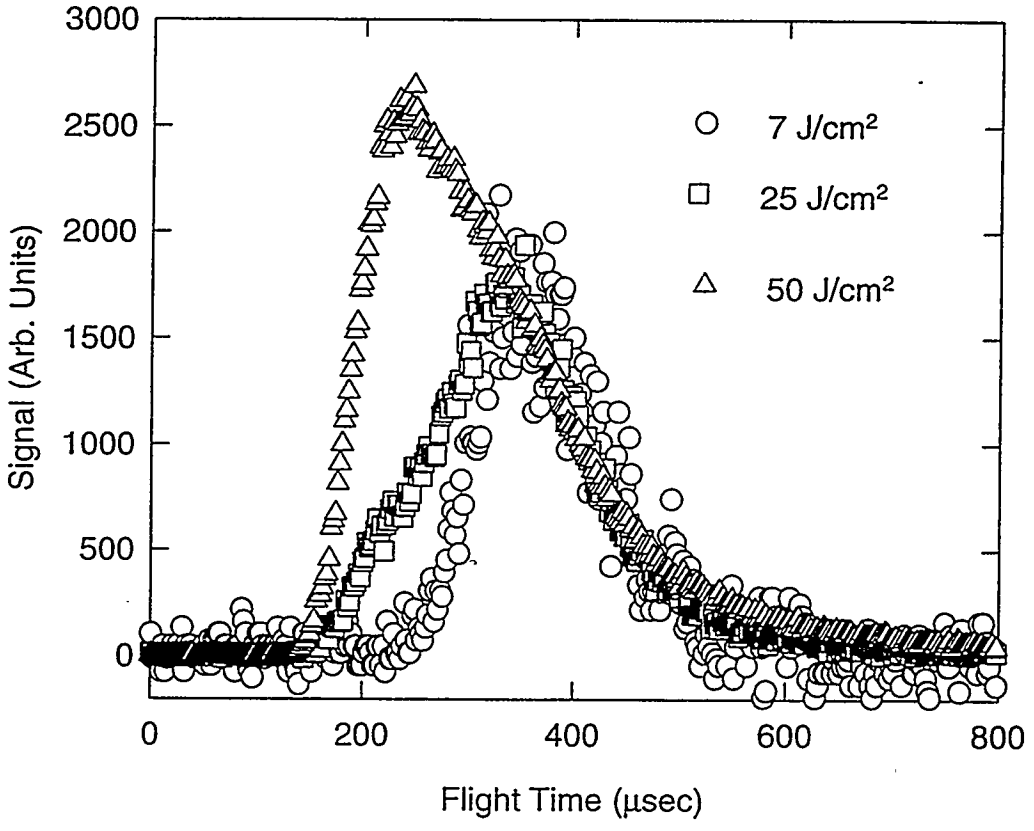

Figure 5-4. Time-of-flight spectra of $C_2F_2^+$ from the IRMPD of octafluoro-1-butene at three fluences.

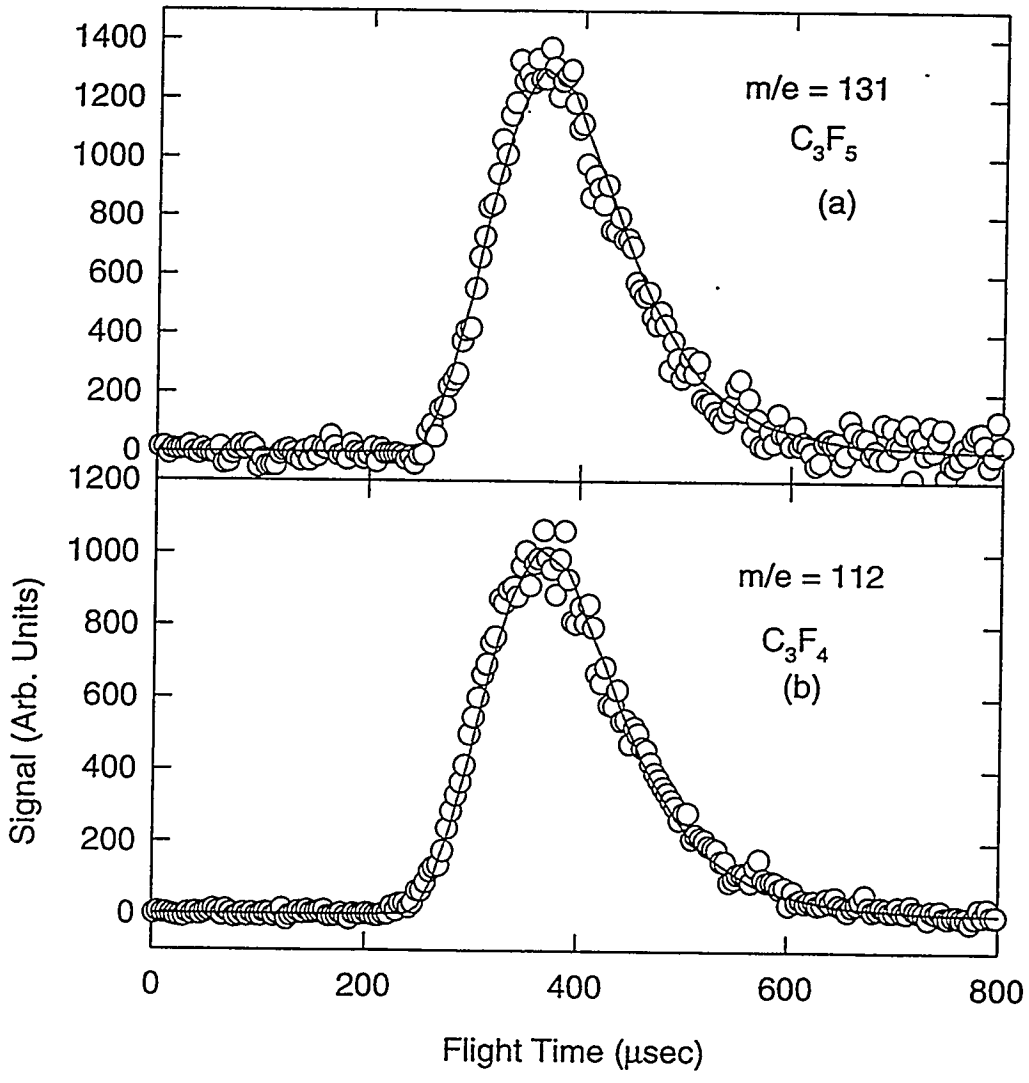

Figure 5-5. Time-of-flight spectra from the dissociation of octafluoro-1-butene at 20°.

(a) The solid line represents the fit to the data at m/e = 131 at 25 J/cm^2 from reaction 5-3.

(b) The signal at m/e = 112 can be completely explained as fragmentation of m/e = 131.

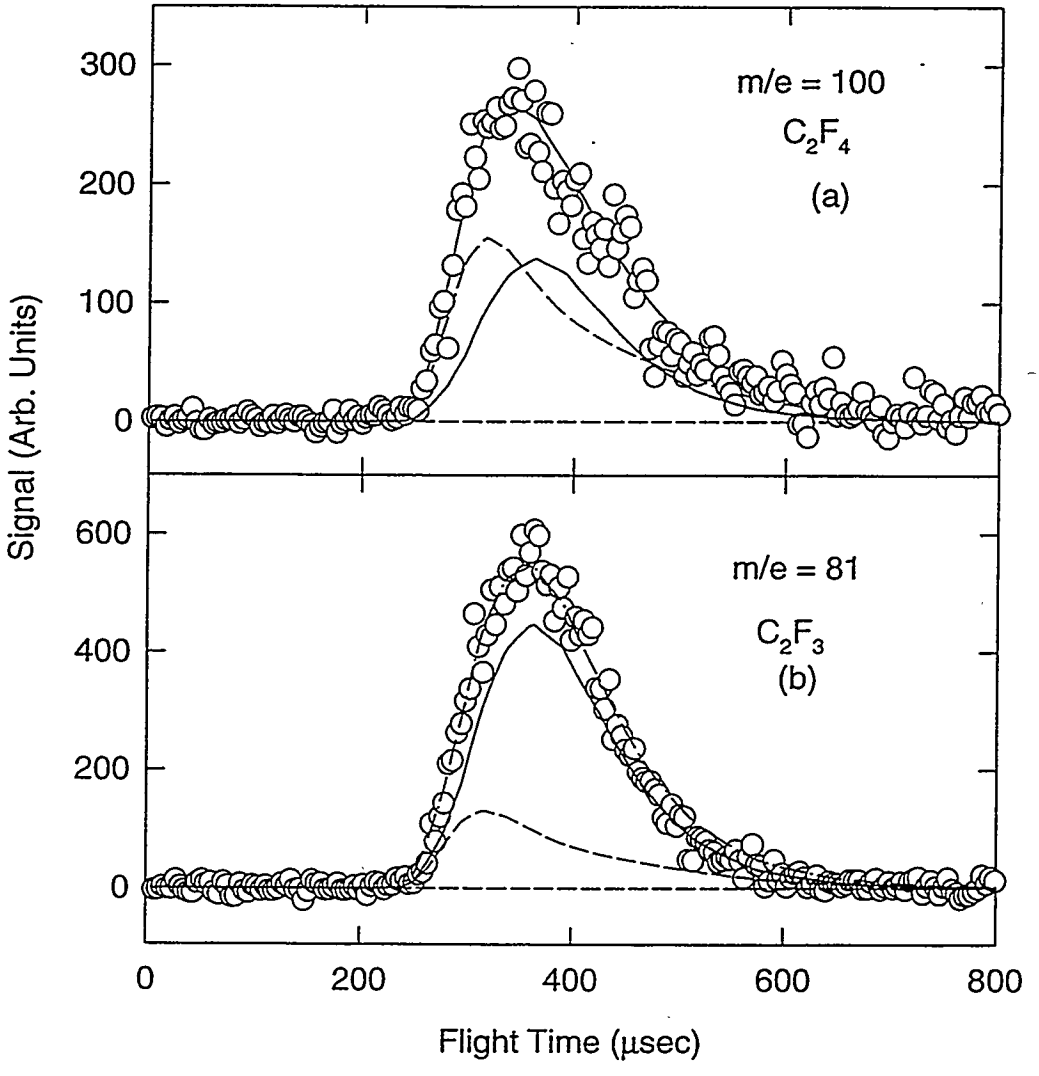

Figure 5-6. Time-of-flight spectra from the dissociation of octafluoro-1-butene at 20°. (a) The solid line in the m/e = 100 spectrum results from fragmentation of m/e = 131. The dashed line is a fit assuming the secondary dissociation of m/e = 119. (b) The time-of-flight spectrum for m/e = 81 results from fragmentation of m/e = 131 (solid line) and m/e = 100 (dashed line).

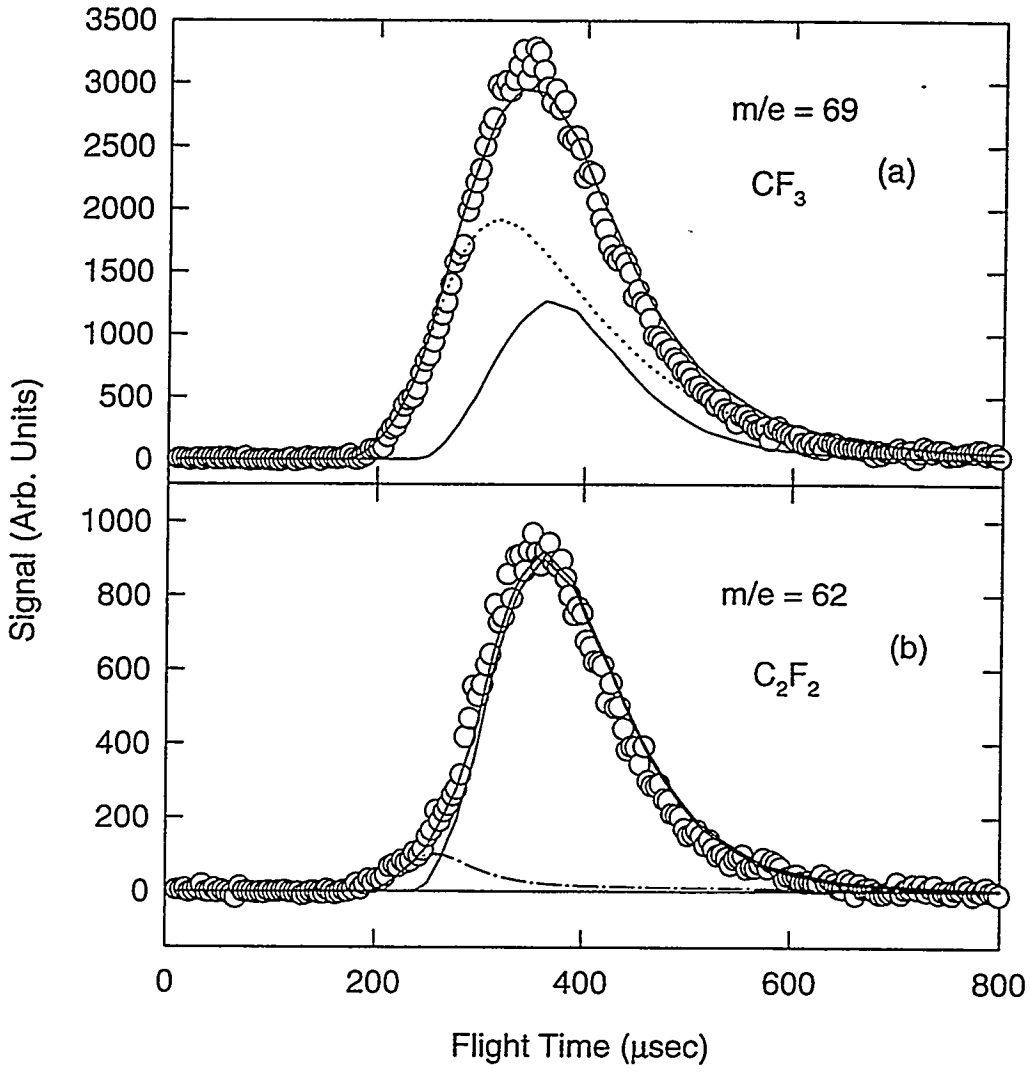

Figure 5-7. Time-of-flight spectra for the lower weight fragments in the IRMPD of octafluoro-1-butene at 25 J/cm^2. (a) The dotted line represents the contribution from m/e = 69, which is formed as a complimentary fragment to the solid line, m/e = 131. (b) CFCF, m/e = 62, contains fragmentation from m/e = 131 (solid line) and m/e = 62 produced from the secondary dissociation of m/e = 81 (dash-dot-dash line).

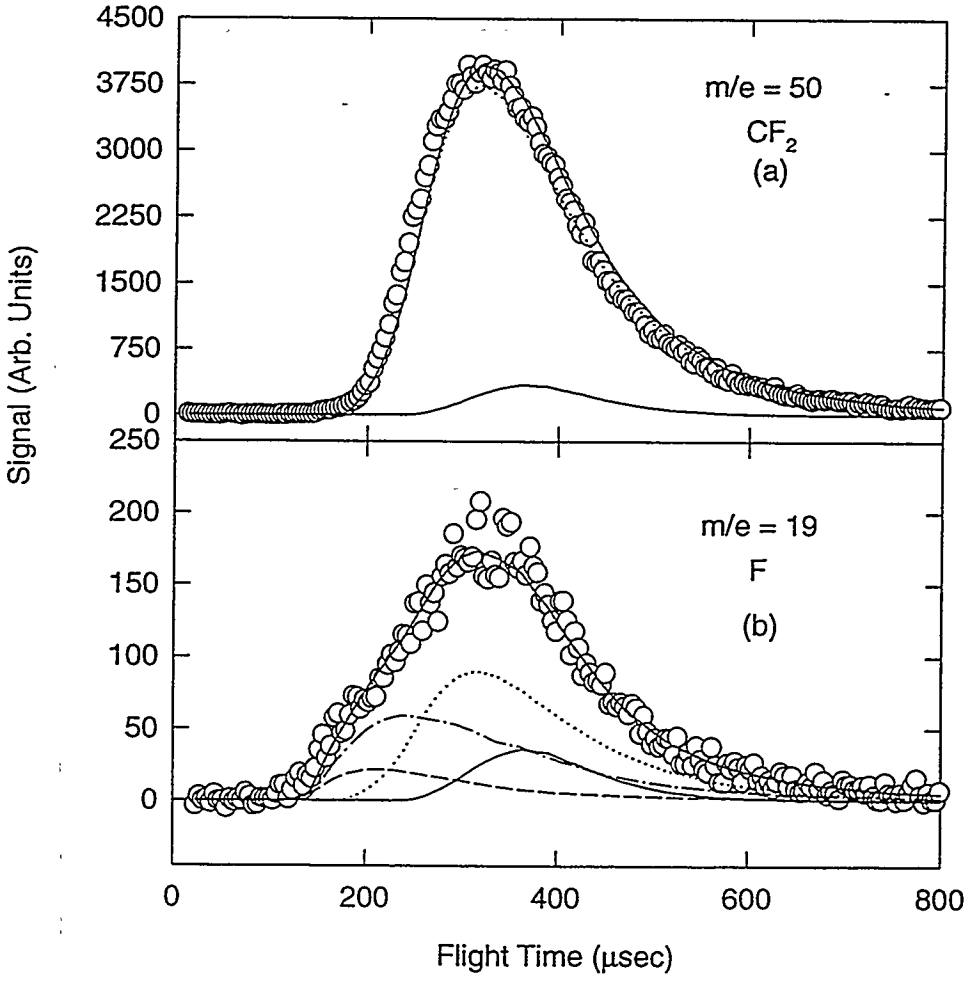

Figure 5-8. Time-of-flight spectra at 25 J/cm^2 for octafluoro-1-butene dissociation. (a) The signal at m/e = 50 can be completely explained by fragmentation of m/e = 69 and a slight contribution from m/e = 131. (b) At m/e = 19 significant fast unique fluorine atom signal is observed. Two contributions from secondary dissociation are shown. The dashed line is momentum matched to m/e =100 while the dash-dot-dash line is momentum match to m/e = 62. Other contributions include fragmentation of m/e = 69 (dotted line) and m/e = 131 (solid line).

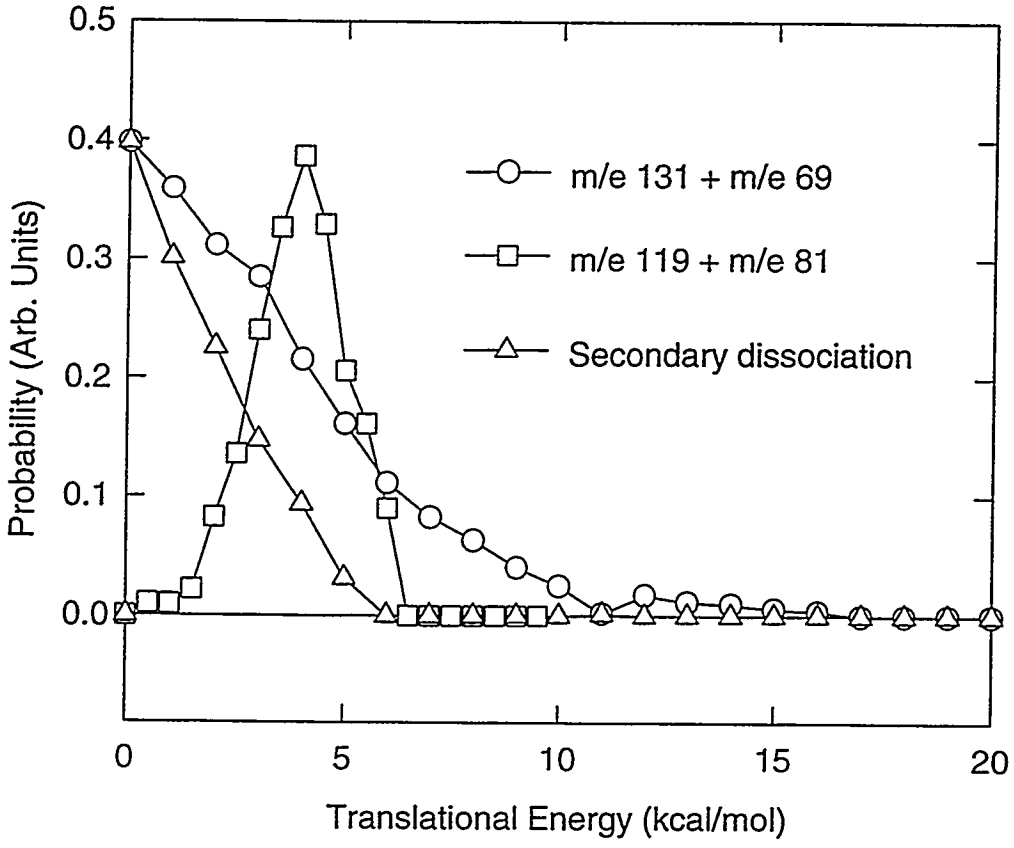

Figure 5-9. Center-of-mass translational energy distributions for reactions 5-3, 5-4, 5-5, and 5-6. The same translational energy distribution was used for reactions 5-5 and 5-6.

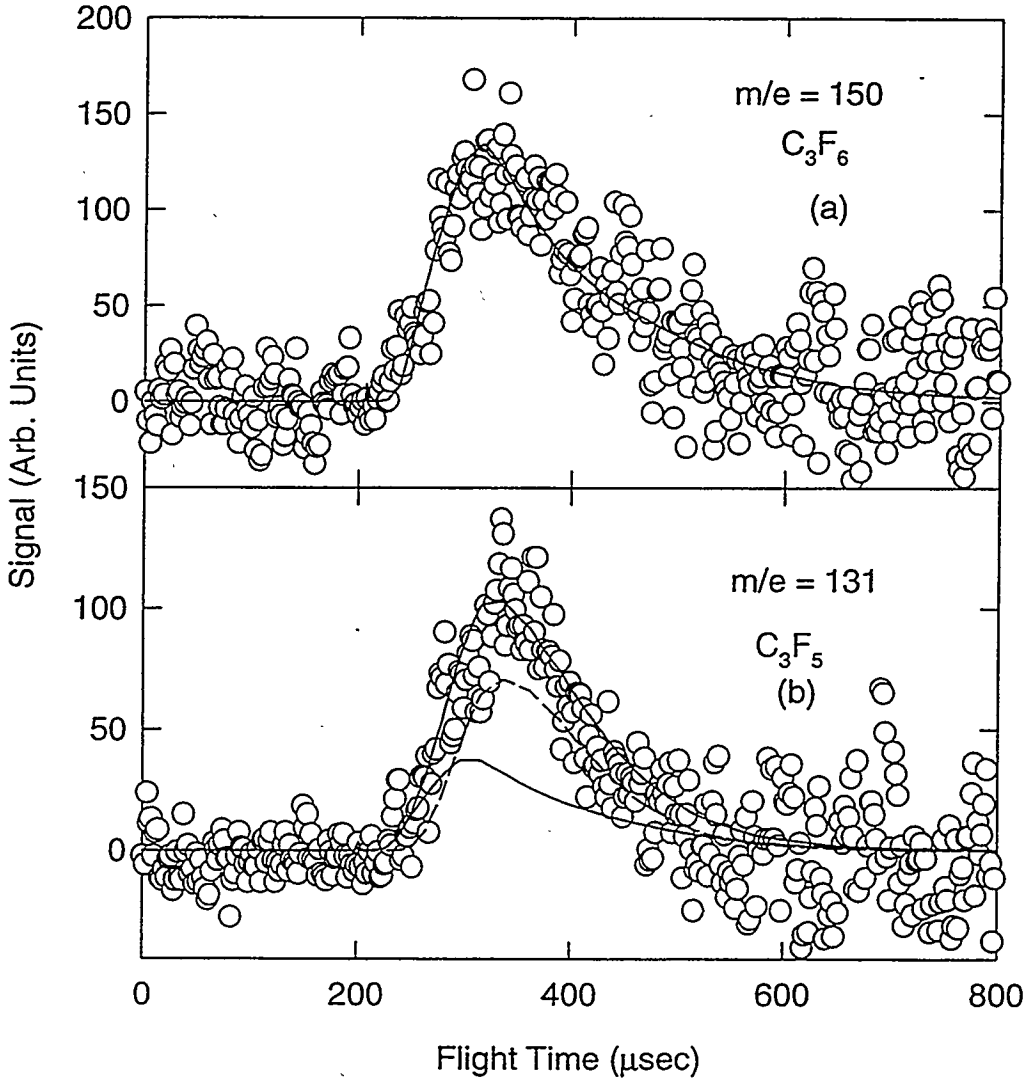

Figure 5-10. Time-of-flight spectra from the dissociation of octafluoro-2-butene at 20°.

(a) The solid line represents the fit to the data at m/e = 150 at 60 J/cm^2 from reaction 5-2.

(b) The signal at m/e = 131 results from fragmentation of m/e = 150 (solid line) and from reaction 5-3 (dashed line).

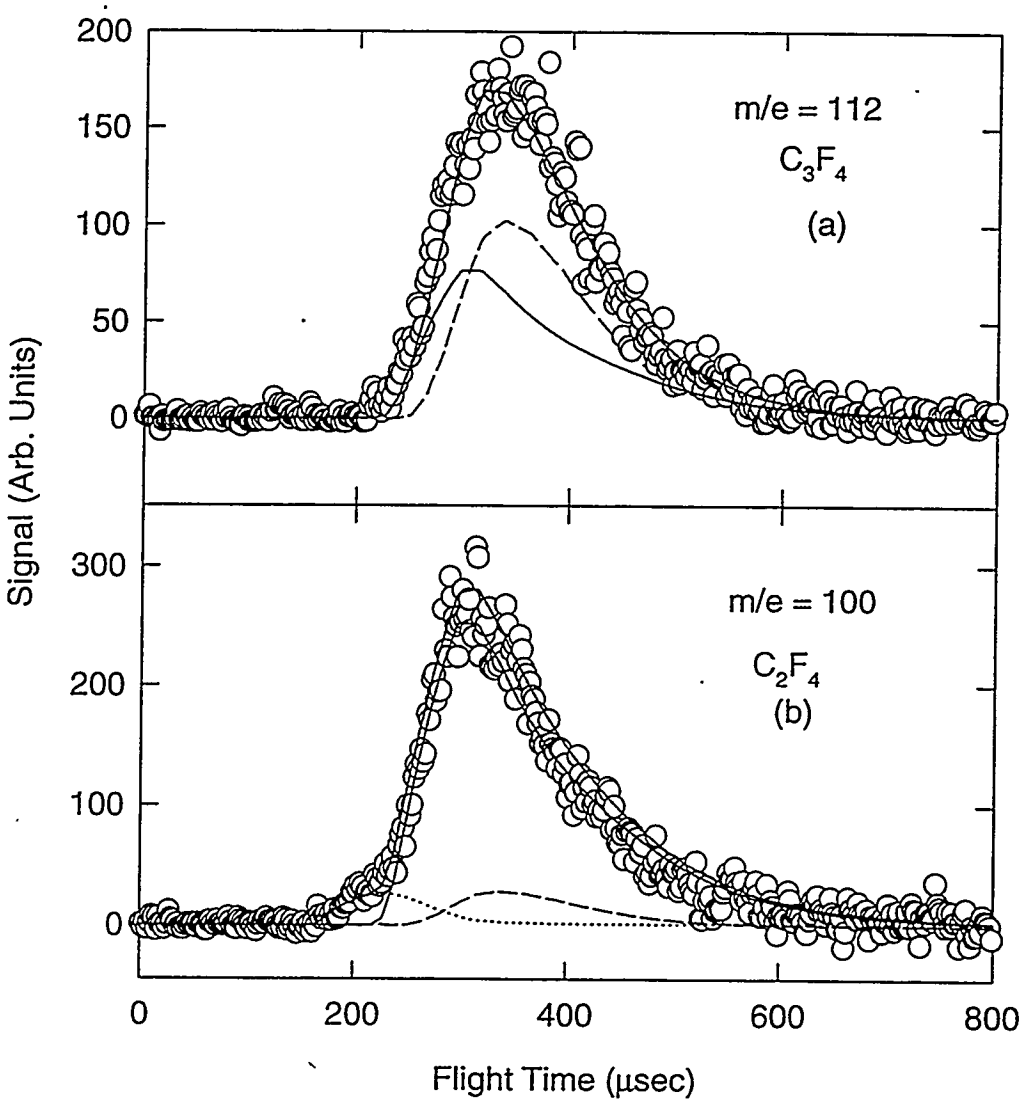

Figure 5-11. Time-of-flight spectra from the dissociation of octafluoro-2-butene at 20°. (a) The signal at m/e = 112 can be explained as fragmentation from m/e = 150 (solid line) and from m/e = 131 (dashed line). (b) A new feature at m/e = 100 is attributed to reaction 5-1 (dotted line) while fragmentation from m/e = 150 (solid line) and m/e = 131 (dashed line) is also evident.

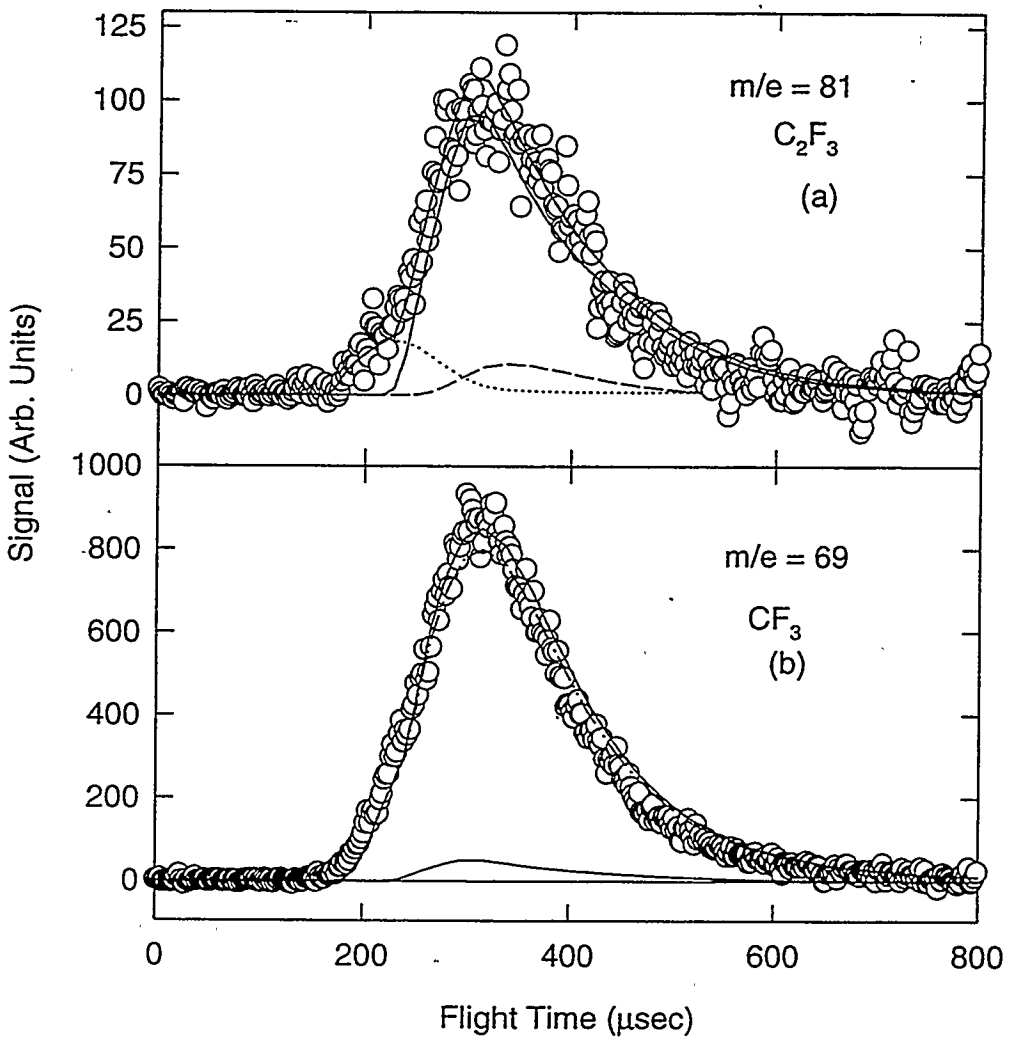

Figure 5-12. Time-of-flight spectra for some lower weight fragments in the IRMPD of octafluoro-2-butene at 60 J/cm^2. (a) At m/e = 81, fragmentation from m/e = 150 (solid line) m/e = 131 (dashed line) and m/e = 100 (dotted line) is present. (b) A major portion of the time-of-flight spectrum at m/e = 69 is attributed to CF_3 (dash-dot-dash line), the complimentary fragment to m/e = 131. A small portion is attributed to m/e = 150 fragmentation (solid line) although an equal amount could be attributed to m/e = 131.

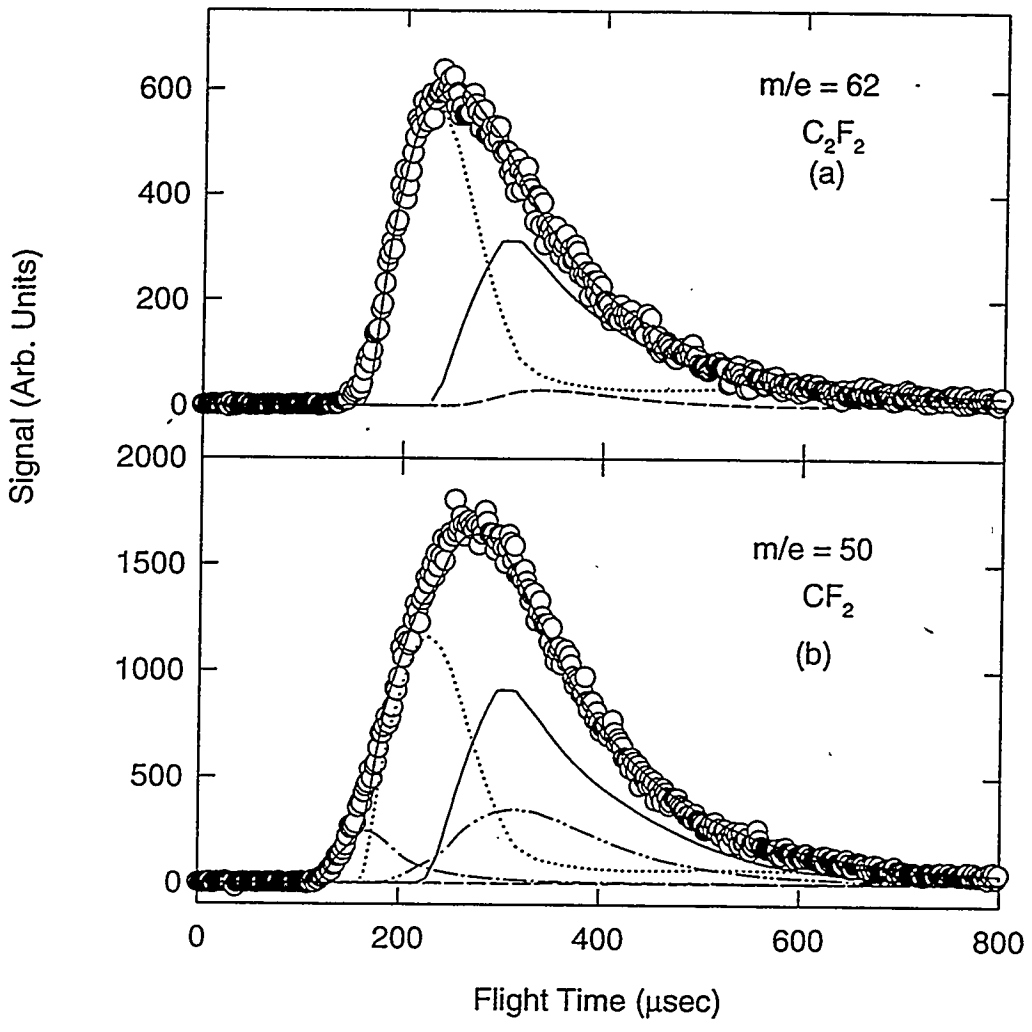

Figure 5-13. Time-of-flight spectra at 60 J/cm^2 for octafluoro-2-butene dissociation. (a) The signal at m/e = 62 is attributed to fragmentation from m/e = 150 (solid line), m/e = 131 (dashed line), and m/e = 100 (dotted line). (b) At m/e = 50, the fast edge has a contribution from the momentum matched partner to m/e = 150 (dash-dot-dash line). Other contributions include fragmentation from m/e = 100 (dotted line), m/e 69 (dash-dot-dot line), and m/e = 150 (solid line).

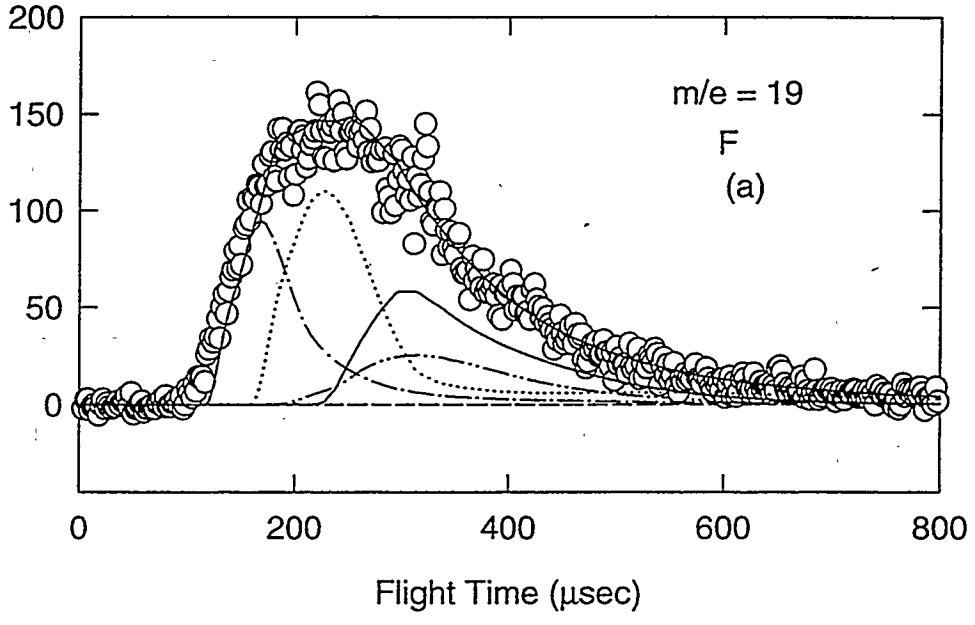

Figure 5-14. Time-of-flight spectrum of m/e = 19 in the IRMPD of octafluoro-2-butene. Contributions include fragmentation from m/e = 50 (dash-dot-dash line), m/e = 100 (dotted line), m/e = 69 (dash-dot-dot line) and m/e = 150 (solid line).

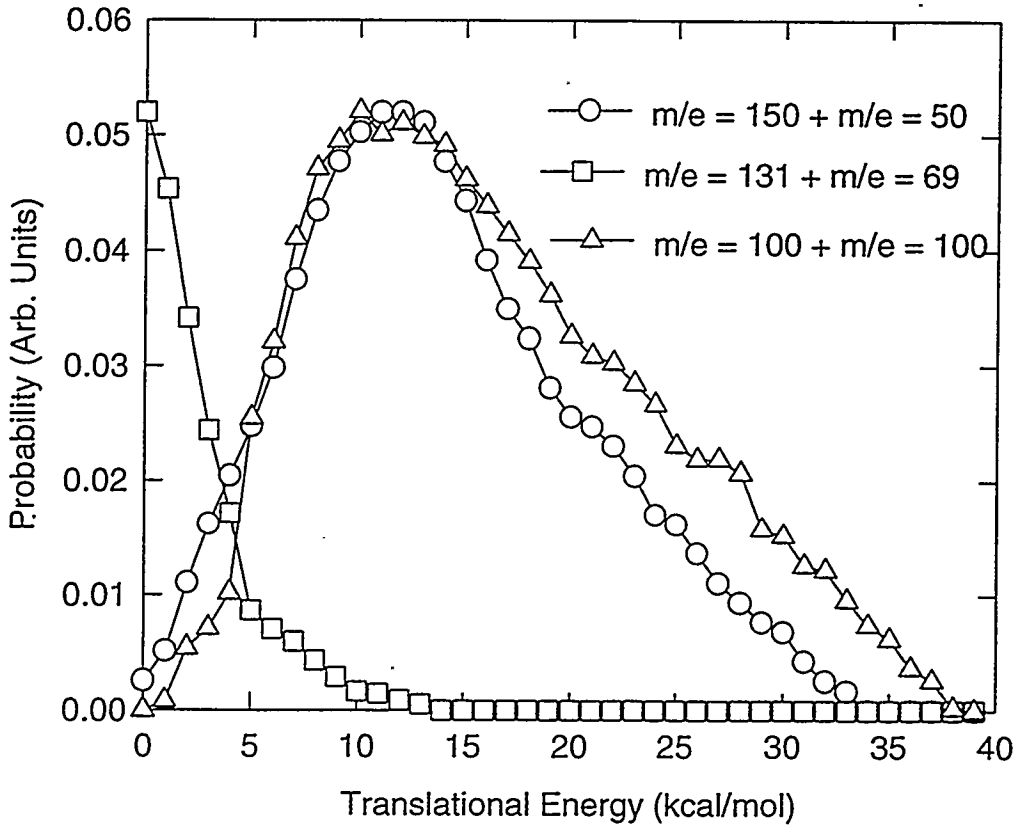

Figure 5-15. Center-of-mass translational energy distributions for reaction 5-1, 5-2 and 5-3 found from the IRMPD of octafluoro-2-butene at 60 J/cm^2.

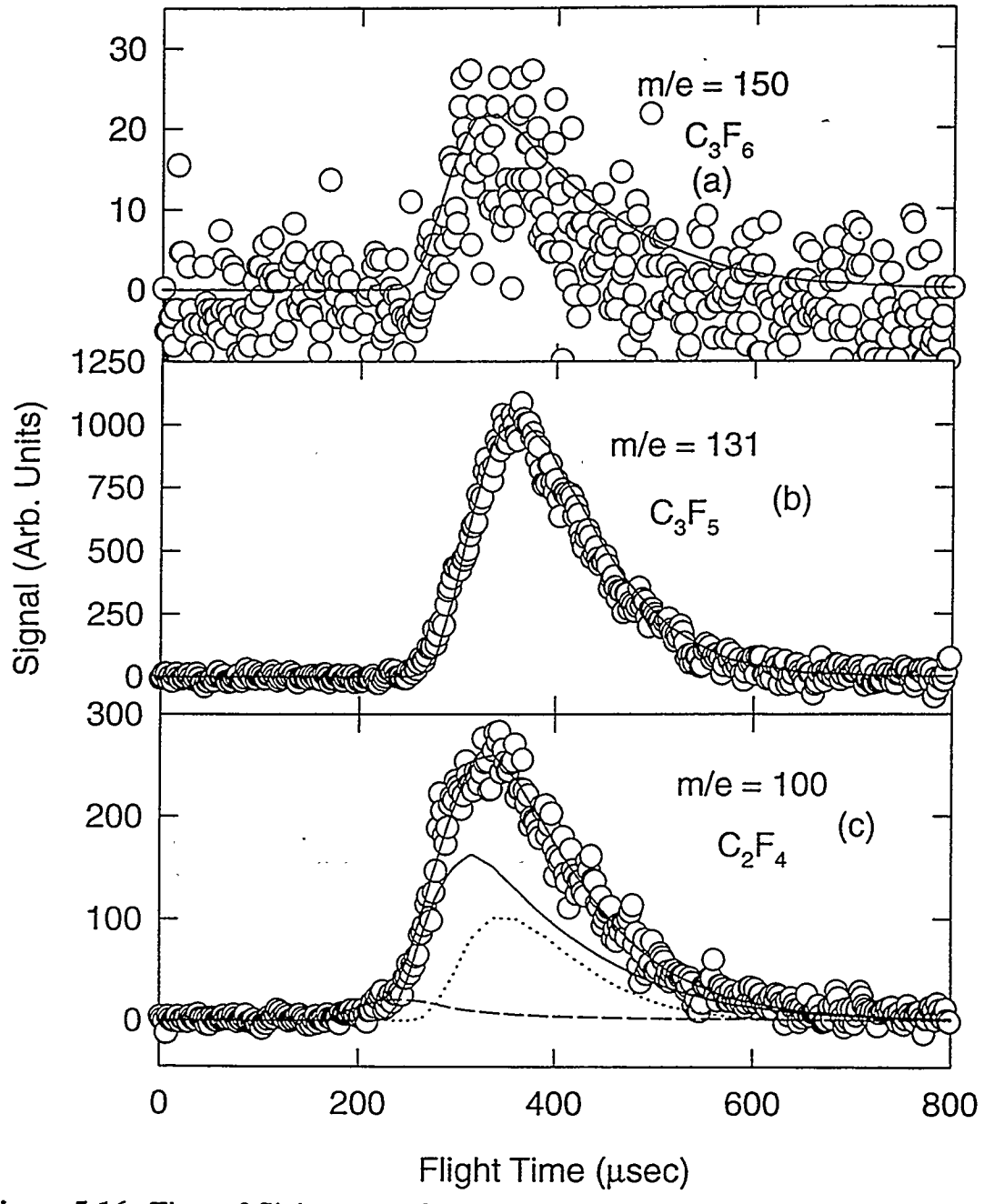

Figure 5-16. Time-of-flight spectra from the IRMPD of octafluoro-1-butene at 60 J/cm^2. Each spectrum was collected for the same number of laser triggers. (a) Evidence of reaction 5-2. (b) All the signal is attributed to reaction 5-3. (c) Contributions from m/e 150 (solid line), m/e = 131 (dotted line) and m/e = 100 (dashed line) are evident in the m/e = 100 time-of-flight spectrum.

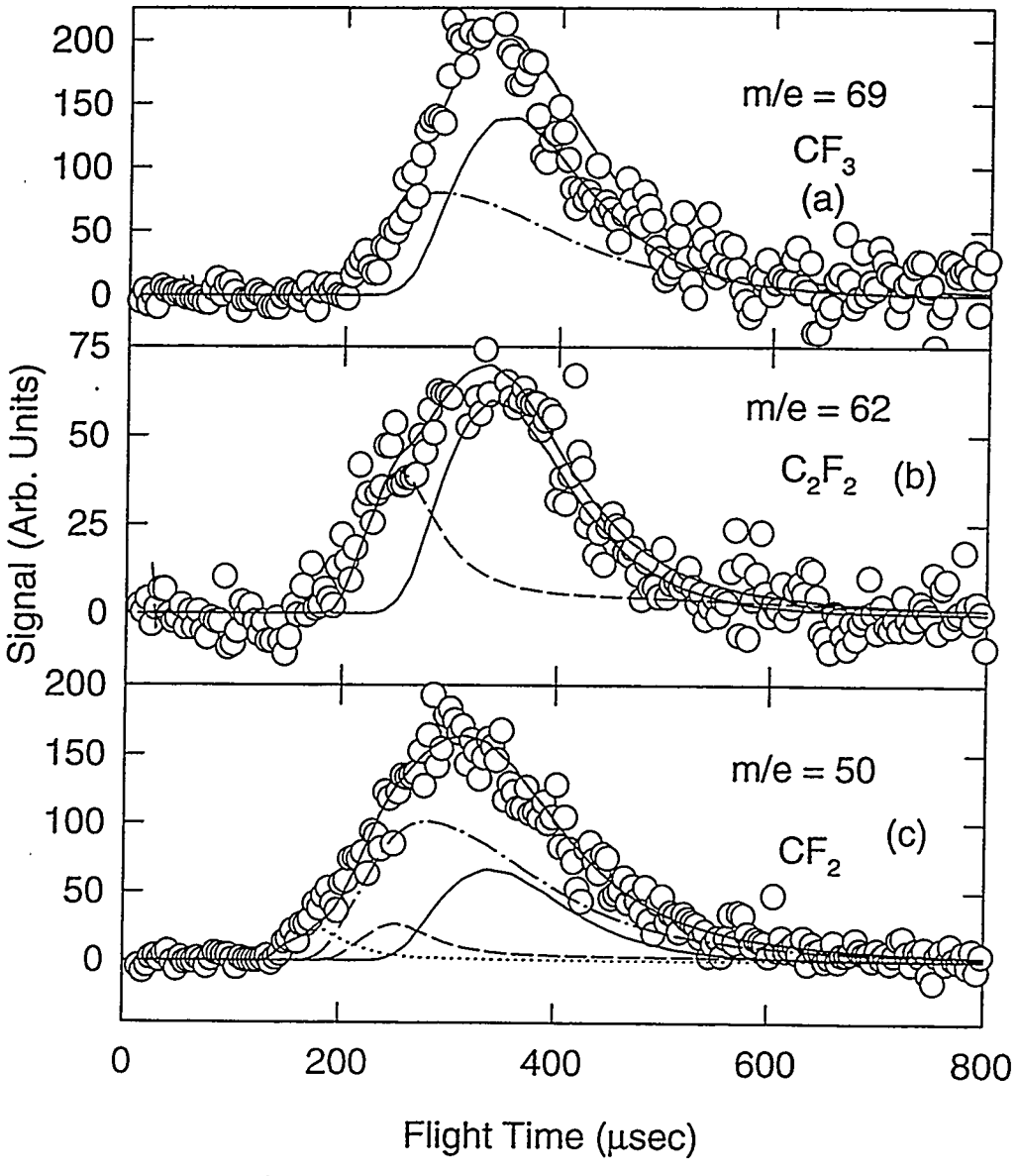

Figure 5-17. Time-of-flight spectra for the IRMPD of octafluoro-2-butene at 25 J/cm^2. (a) At m/e = 69 contributions from m/e = 131 (solid line) and m/e 69 (dash-dot-dash line) are evident. (b) At m/e = 62 there is fragmentation from m/e = 150 (solid line) and m/e = 100 (dashed line). (c) A fast contribution from m/e = 50 (dotted line), and fragmentation from m/e = 100 (dashed line), m/e = 69 (dash-dot-dash), and m/e = 150 (solid line) are present.

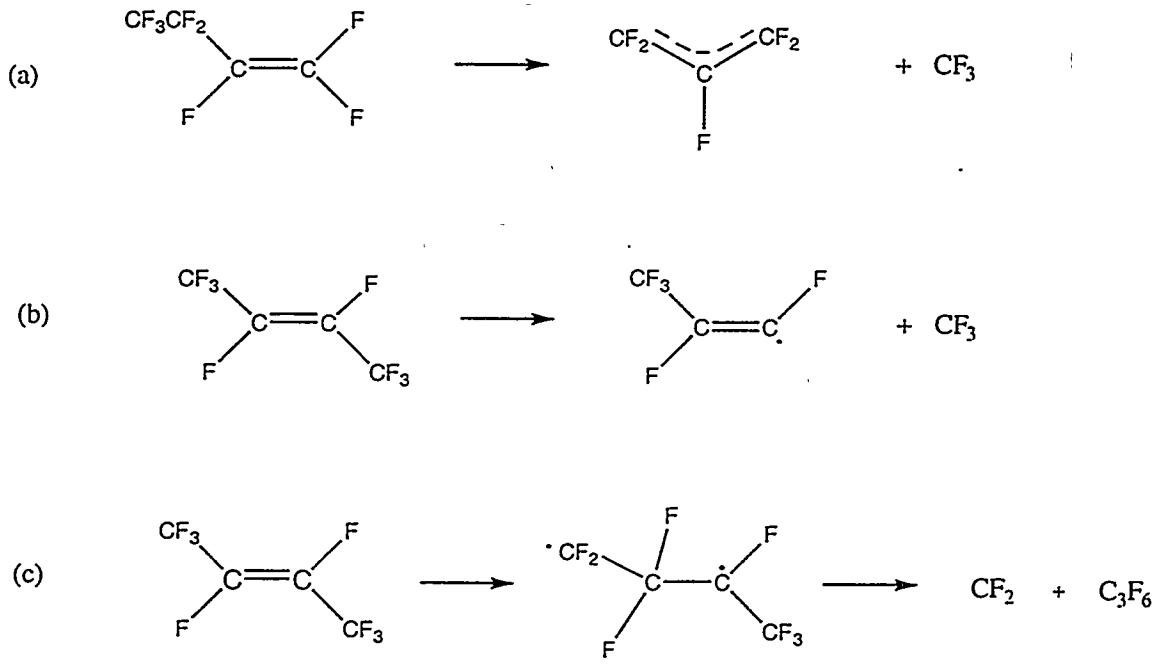

Figure 5-18. Reaction products/mechanisms in the IRMPD of octafluoro-1-butene and octafluoro-2-butene. (a) Loss of CF_3 from octafluoro-1-butene leads to the formation of an allyl-like radical. (b) In octafluoro-2-butene simple bond rupture results in a fluorinated propene radical. (c) A proposed pathway in which a fluorine migration takes place in octafluoro-2-butene before dissociation to hexafluoropropene and the difluorocarbene radical.

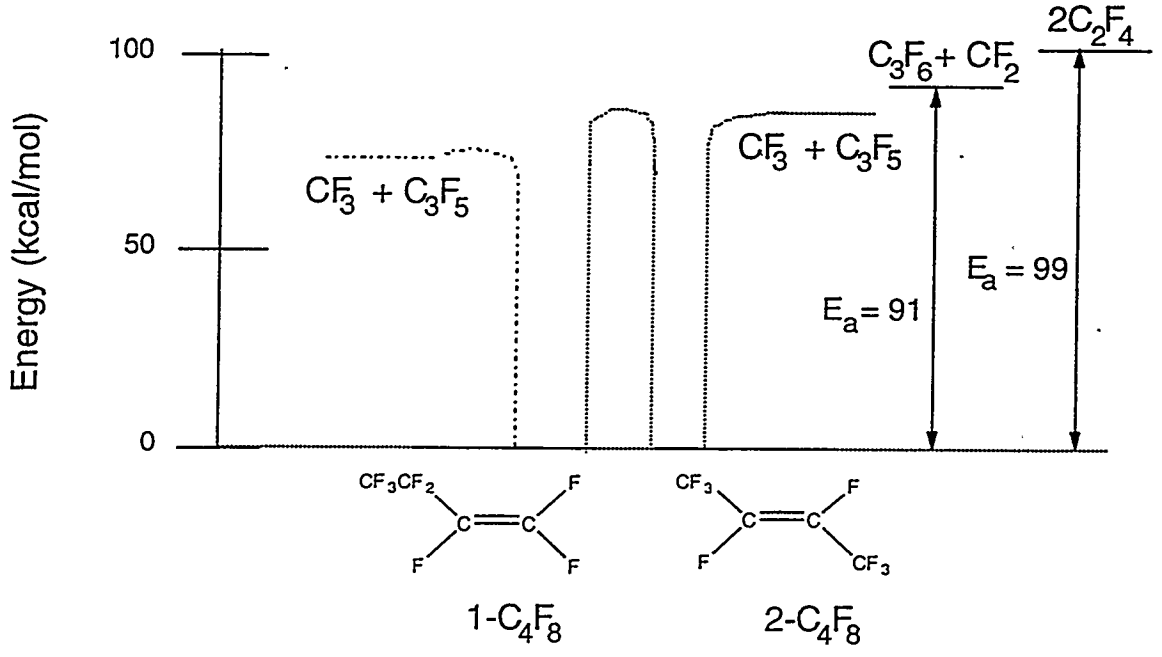

Figure 5-19. Energy level diagram for octafluoro-1-butene and octafluoro-2-butene. The heats of formations for the perfluorobutenes are unknown and assumed to be similar. The lowest lying reaction is the formation of CF_3 and the perfluoroallyl radical (- — - line). This pathway is initially only available to octafluoro-1-butene. Based on the observed dissociation channels, the barrier to isomerization from octafluoro-1-butene to octafluoro-2-butene is higher than the activation energy for reaction 5-3 in octafluoro-1-butene (dotted line). The next available reaction channel is the formation of CF_3 and the propene-like radical (dotted line) from octafluoro-2-butene. The activation energies for reactions 5-2 and 5-1 are higher than for CF_3 loss in either compound and the activation energies shown are from reference 3.

Appendix A

A Comparison Between the Berkeley Rotating Source Machine and the Taiwan Rotating Source Machine

A.1. Physical Differences

Some significant differences exist between the detectors in the two otherwise similar rotating source machines. One of the most crucial differences is that the quadrupole rods in the Taiwan Rotating Source Machine (TRSM) are mounted directly in the detector and the quadrupole can has been removed. Thus the ionizer cannot be mounted on the quadrupole as in the Berkeley Rotating Source Machine (BRSM) and is instead mounted on a flange in region 2 of the detector. This is important as it changes slightly the geometry of the detector.

A.2. Detector Settings

The respective settings for the two machines as of September 1994 are shown in Table 1. The first difference to notice is that the filament current used is significantly lower for the TRSM. A 10 mA filament will ionize considerable more signal as well as background. The extractor voltages are also different. The extraction voltage determines the width of the ionizer, the greater the voltage the smaller the ionizer region, which results in greater resolution. However, too high an extractor voltage and the electrons will be pushed out of the ionizer and the ions formed will not be able to enter the detector. The extractor voltage will also have some affect on the ion flight constant as the

higher the voltage the more the ions are accelerated. A typical ion flight constant experimentally determined on the machine at Berkeley is 3.5 while with the TRSM settings shown in Table 1 an ion flight constant of approximately 5 was commonly found.

The third lens on the TRSM has a positive voltage applied to it while the third lens in the BRSM has been disconnected. In the TRSM this lens is used to help focus the ions from the ionizer to region 2 of the detector since the ionizer is not directly mounted on the quadrupole. An ion energy range of 10 - 20 volts has been found to result in the maximum transmission through the quadrupole while avoiding space-charge effects.[1] In the case of the TRSM settings there was some concern that allowing only a 5 V ion energy range into the quadrupole was limiting the transmission. Also, the positive voltage on this lens is somewhat unconventional. In order to focus ions it is best not to decelerate them with a positive voltage as this can introduce a spread in the ions accepted.

A.3. Standard Calibration Experiment

An initial attempt was made to use the BRSM detector settings on the TRSM. The standard Cl_2 photodissociation experiment at 351 nm was used to calibrate the flight length and also the ionizer width.[2] However, it was quickly found that the third lens was necessary. The value of the voltage on the third lens is crucial as illustrated by the time-of-flight peaks measured on axis (Figure A-1). A bimodel distribution such as illustrated in Figure A-1 has been observed before with a Brink-type ionizer operating above 4 mA.[3] Thirty-five volts was the optimum lens voltage that allowed acceptance of a reasonable ion energy spread as well as time-of-flight measurements without artifacts. A comparison

of the photodissociation signal from the Cl^+ ion illustrates that the time-of-flight spectra are broader when the BRSM settings were used (Figure A-2). The ion flight constant for the BRSM settings was calculated to be ~ 6 indicating that ions were possibly being trapped after they were formed and contributing to the spread of the signal.

To reduce this broadening the filament was lowered to 7 mA and a wide range of extractor and lens settings were tried. At detector settings which resulted in a acceptable time-of-flight spectrum on axis, the photodissociation signal was still broad. The end result was that the original TRSM detector settings (Table A-1) were found to work best with this detector to eliminate broadening effects. One difference in the settings was that the voltage on Lens Three remained at 35 to 40 V for the remainder of the experiments. This allowed a wider range of ions to be accepted and is close to the optimum ion energy.[1] In addition, it was found that previously a different speed ratio had to be used for each mass measured. For example, using the Settings in Table A-1 for m/e = 70 a speed ratio of 11.5 was obtained, while for m/e = 35 a value of 9.6 was measured. Using the lower value for Lens Three of 35 V, consistent speed ratios (within ± 0.5) between all m/e ratios were obtained.

The lesson here is that even "identical" machines can be dramatically different due to slight geometry changes in sensitive areas. The third lens on the TRSM is crucial whereas it is not necessary on BRSM. In addition, the detector settings maximized for signal on the BRSM induce artifacts when applied to the TRSM.

References and Notes

[1] Y. T. Lee, J. D. McDonald, P. R. LeBreton, and D. R. Herschbach, Rev. Sci. Instrum. **40**, 1402 (1969).

[2] G. E. Busch, R. T. Mahoney, R. L. Morse, and K. R. Wilson, J. Chem. Phys. **51**, 449 (1969).

[3] D. J. Krajnovich, Ph. D. Thesis, University of California, Berkeley (1983) Appendix C.

Table A-1. Comparison of Detector Settings.

	Taiwan RSM	Berkeley RSM
Filament	4 mA	10 mA
Electron Energy	-120 V	-200 V
Ion Energy	70 V	73.9 V
Extractor	-250 V	-524 V
Lens 1	-750 V	-1500 V
Lens 2	-150 V	-87.8 V
Lens 3	+ 65 V	---
Exit Lens 1	-50 V	0 V
Exit Lens 2	-1000 V	-503 V
HV (Doorknob)	20 kV	27.5 kV
PMT	2,150 V	2320 V

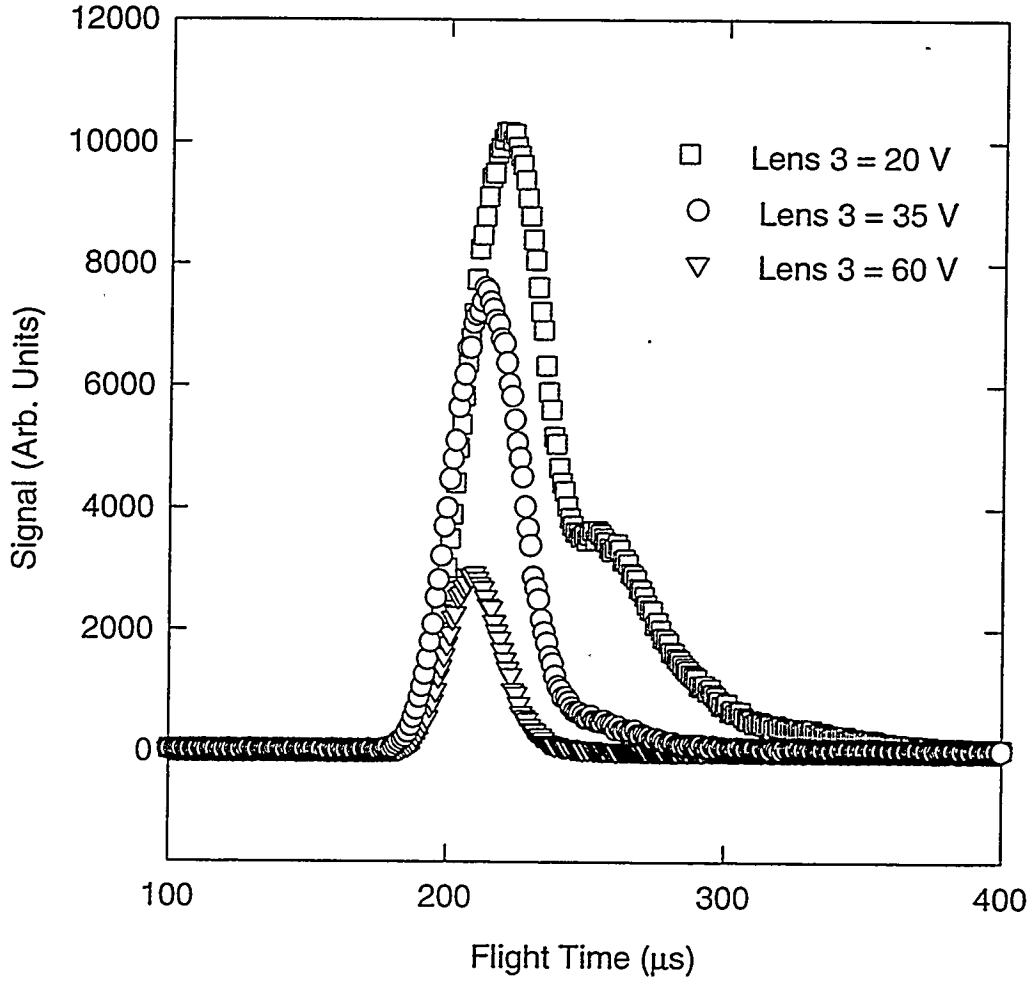

Figure A-1. Time-of-flight spectra of m/e = 70 (Cl_2^+) on axis. Spectra were obtained on the TRSM using the normal BRSM detector settings. The voltage on Lens Three dramatically affects the shape and intensity of the spectra.

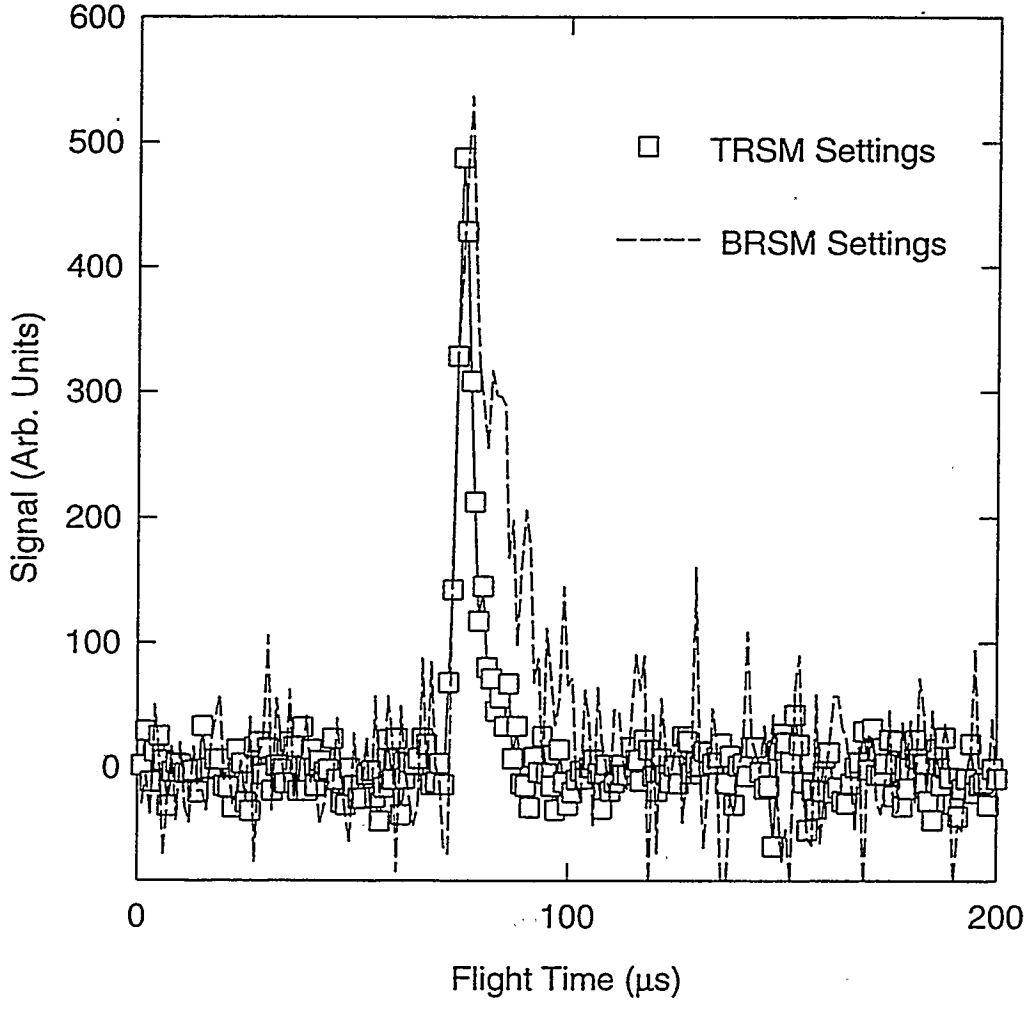

Figure A-2. Time-of-flight spectra of m/e 35 (Cl^+) at 20° from the photodissociation of Cl_2. The open square represent the data taken using the orignial TRSM settings while the dashed line illustrates the signal taken using the BRSM settings.